

---

Bisphosphonates: From Bone-Targeted Therapies to Molecular  
Imaging Agents of *In Vivo* Bone Metabolism

---

Dissertation submitted to the Faculty of Mathematics and Natural Sciences  
Christian Albrechts University, Kiel, Germany

For the Degree of  
Doctor of Natural Sciences (Dr. rer. nat.)

Presented by

**Robert J. Tower**

Section Biomedical Imaging  
Department of Radiology and Neuroradiology  
University Hospital Schleswig-Holstein

Kiel, Germany 2014





Primary supervisor: Prof. Dr. Stanislav N. Gorb

Co-supervisor: Prof. Dr. Claus C. Glüer  
Co-supervisor: Prof. Dr. Holger Kalthoff

Committee chair: Prof. Dr. Matthias Leippe

Oral examination: March 16, 2015

Approved for print: \_\_\_\_\_

Signed \_\_\_\_\_, Dean

## **i. Declaration**

I hereby declare that this PhD thesis entitled “Bisphosphonates: from bone-targeted therapies to molecular imaging agents of *in vivo* bone metabolism” is a presentation of my original work. All sections or passages that refer to existing literature are pointed out by the according citations.

The work was done under the guidance of Prof. Claus C. Glüer at the University of Kiel, Germany, and has not been previously submitted for the award of any degree, diploma or its equivalent to any other university or institution.

I commit myself to adhering to the standards of Good Scientific Practice of the German Research Foundation valid at the time of my research-related activities at the university.

A portion of this work has previously been published by the “Journal of Bone and Mineral Research” and by “Bone”. Additionally, a portion of this work was contributed to as a part of a medical dissertation project by Anna- Christina Rambow and Philipp Kniessl, supervised by Dr. Christian Schem from the department of gynecology, UKSH.

---

Place, Date, Signature

## ii. Abstract

Bisphosphonates are a class of drugs that show high affinity for the bone and act to inhibit bone resorption mediated by osteoclasts. As a therapeutic, bisphosphonates are currently prescribed to patients with osteoporosis or with primary cancers, which have a high probability of metastasizing to the bone (eg. breast cancer). More recently, the bisphosphonate's ability to target the bone with high efficiency has been exploited to develop novel targeted molecules. These drugs provide the possibility of increased drug delivery to the bone while minimizing systemic toxicity. Several new conjugate drugs, combining the anti-tumor effects of chemotherapeutics and bisphosphonates have been developed for the treatment of bone metastases. In this thesis, the initial *in vivo* characterization of the drug 5-FdU-ale, a new conjugated drug between the anti-metabolite 5-fluoro-2'-deoxyuridine (5-FdU) and the bisphosphonate alendronate is presented. Initial toxicity studies indicate no signs of necrosis or inflammation at the site of injection, no induced weight loss and no impaired renal function for doses up to 200 mg/kg. Next, 5-FdU-ale was assessed for its anti-tumor effects in a mouse model of breast cancer bone metastases. Mice treated with 5-FdU-ale showed a significant reduction in the number of tumors compared to untreated controls and showed a significant reduction in tumor size compared to untreated mice or mice treated with either 5-FdU or alendronate alone. Mice treated with 5-FdU also showed significantly greater bone volume and mineral content, and a significant inhibition in osteoclast number, without negatively impacting normal osteoblast function.

Along with their uses in novel targeted therapeutics, fluorescently-labeled bisphosphonates have been used to characterize bisphosphonate localization, distribution, cellular uptake and penetration into bone. Radiological assessments of the bone provide site-specific analyses of changes in bone morphology, but require significant changes over weeks or even months before they could be detected. In contrast, serum analyses provide an assessment of the current overall bone metabolic status, but fail to localize aberrant changes to a specific site. In this thesis, fluorescently-labeled bisphosphonate binding kinetics were used to characterize and monitor the site-specific changes in bone metabolism. Binding kinetics were applied to animal models of osteoporosis (ovariectomy) (OVX) and in mice treated with an anabolic bone agent (parathyroid hormone) (PTH). Binding

kinetics revealed significant decreases in both the rate constant and plateau binding values in response to OVX and a significant increase in rate constant values in response to PTH in the proximal tibia region. Co-registration of fluorescence and micro-computed tomography (micro-CT) scans of *ex vivo* bone sections revealed a preferential uptake of bisphosphonates shortly after injection to regions of less dense, newly deposited bone mineral. Additionally, the uptake of bisphosphonates at the spine was compared and was found that changes in binding kinetic parameters were consistent between sites and correlated with time-lapse micro-CT analyses which supported active, mineralizing surfaces as being high bisphosphonate uptake regions and also demonstrated an intermediate uptake by regions associated with newly exposed minerals resulting from bone resorption. An additional correction factor was then generated to monitor changes in unbound bisphosphonates in the blood pool allowing for multi-compartment kinetic analyses to be conducted.

Overall, bisphosphonates hold great promise, not just as anti-resorptive agents, but as targeting molecules for the delivery of therapeutics. Preclinical evaluations of the novel conjugate drug 5-FdU-ale suggests significant improvements in the reduction of tumor size and metastatic frequency as well as a reduction in the lytic activity of the osteoclasts induced by the bone lesions without negatively impacting bone formation. As an imaging probe, binding kinetics of fluorescently-labeled bisphosphonates is a highly sensitive, site-specific assay for changes in bone metabolism and could have great implications for the monitoring of skeletal lesions in patients and potentially contribute to the development of new conjugate therapies.

### **iii. Zusammenfassung**

Bisphosphonate gehören einer Medikamentengruppe an, die eine hohe Affinität zur Anlagerung am Knochen besitzt und die dazu beiträgt, die Knochenresorption durch Osteoklasten zu verhindern. In der Behandlung werden Bisphosphonate Patienten mit Osteoporose oder mit Primärkrebsarten verschrieben, bei denen eine hohe Wahrscheinlichkeit zur Bildung von Metastasen im Knochen vorliegt (wie z.B. bei Brustkrebs). In jüngerer Zeit wurde die Eigenschaft der Bisphosphonate, sich am Knochen anzulagern, verstärkt genutzt, um zielgerichtete Moleküle zu entwickeln. Verschiedene neue konjugierte Wirkstoffe wurden zur Behandlung von Knochenmetastasen entwickelt, die Tumoren entgegenwirkende Effekte aus Chemotherapie und dem Einsatz von Bisphosphonaten vereinen. In der vorliegenden Arbeit wird die *in vivo* Charakterisierung des Medikaments 5-FdU-ale, eines neuen Präparats, das das Antimetabolit 5-fluoro-2'-deoxyuridine (5-FdU) und das Bisphosphonats Alendronat vereint, vorgenommen. Erste Studien zur Toxizität in Mäusen lassen keine Zeichen von Nekrosis oder Entzündungen an der Injektionsstelle erkennen, ebenso konnte kein Gewichtsverlust und keine gestörte Nierenfunktion bei Dosierungen von bis zu 200 mg/ kg beobachtet werden. Im nächsten Schritt wurde der tumorreduzierende Effekt von 5-FdU-ale in einem Mausmodell bei Knochenmetastasen Brustkrebs untersucht. Mäuse, die mit 5-FdU-ale behandelt wurden, zeigten eine signifikante Reduktion in der Anzahl der Tumoren mit Vergleich mit der unbehandelten Kontrollgruppe und zeigten außerdem einen signifikanten Rückgang der Größe der Tumoren im Vergleich mit unbehandelten Mäusen oder Mäusen, die nur mit entweder 5-FdU oder Alendronat allein behandelt wurden. Mäuse, die mit 5-FdU behandelt wurden, wiesen zudem eine signifikante Verbesserung der Knochenqualitätsparameter bei signifikanter Hemmung der Osteoklasten, jedoch ohne negative Wirkung auf die normale Funktion der Osteoblasten, auf.

Parallel zu ihrer Anwendung in neuen zielgerichteten Therapien wurden fluoreszenzmarkierte Bisphosphonate eingesetzt, um ihren Verbleib zu lokalisieren und ihre Verteilung, sowie die Aufnahme in unterschiedliche Zellarten und die Eindringtiefe der Bisphosphonate in den Knochen zu untersuchen. In dieser Arbeit wird die Bindungskinetik fluoreszenzmarkierter Bisphosphonate genutzt, um orts-spezifische Veränderungen im Knochenstoffwechsel zu charakterisieren und im Verlauf zu beobachten. Die Bindungskinetik wurde in Tiermodellen aus der Osteoporoserecherche (Ovariectomie, OVX) und in Mäusen, die mit einem knochen-anabolischen Präparat (Parathormon,



PTH) behandelt wurden, untersucht. Bindungskinetische Studien im Bereich der proximalen Tibia zeigten signifikante Abnahmen, sowohl in den Bindungsratenkonstanten als auch in den Plateaubindungswerten als Reaktion auf die OVX und eine signifikante Zunahme der Bindungsratenkonstanten als Reaktion auf PTH. Aufnahmen von Schnitten des *ex vivo* Knochens nach Co-Registrierung von Fluoreszenz und hochauflösender Mikrotomographie ließen eine bevorzugte Aufnahme der Bisphosphonate in Bereichen mit neu angelagertem und damit weniger dichten Knochenmaterial kurz nach Injektion erkennen. Zusätzlich wurde die Aufnahme der Bisphosphonate an unterschiedlichen Stellen des Skeletts verglichen. Veränderungen der bindungskinetischen Parameter an verschiedenen Messorten waren konsistent und korrelierten mit den Ergebnissen, die aus Zeitrafferserien von Mikrotomographieaufnahmen gewonnen wurden. Dies unterstützt die These, nach der aktive, neu mineralisierte Oberflächen als hochgradige Aufnahmeeregionen für Bisphosphonate fungieren und gleichzeitig eine nur mäßige Aufnahme in Regionen, die mit freiliegenden, mineralischen Oberflächen in Verbindung gebracht werden, die beim Knochenabbau freigelegt werden. Anschließend wurde ein zusätzlicher Korrekturfaktor entwickelt, um die Veränderung der Konzentration ungebundener Bisphosphonate im Gefäßsystem zu beobachten, die somit eine Kinetik-Analyse für multiple Kompartimente erlauben.

Insgesamt zeigen Bisphosphonate sehr vielversprechende Ergebnisse, nicht nur als antiresorptive Wirkstoffe, sondern auch als zielgerichtete Trägermoleküle für die Zuführung von Wirkstoffen. Präklinische Untersuchungen des neuen konjugierten Wirkstoffs 5-FdU-ale deuten auf signifikante Verbesserungen, sowohl in Bezug auf die Tumorgröße und die Anzahl der Metastasen, als auch auf eine Reduktion der lytischen Aktivität der Osteoklasten, ohne dass dabei die Knochenbildung negativ beeinflusst würde. Als bildgebendes Verfahren ist die Bindungskinetik fluoreszenzmarkierter Bisphosphonate ein hochsensitives, ortsspezifisches Analyseverfahren, um Veränderungen des Knochenstoffwechsels zu erfassen und sie besitzt ein enormes Anwendungspotenzial für die Kontrolle der Entwicklung von Skelett Läsionen bei Patienten und könnte möglicherweise zur Entwicklung neuer Therapien mit konjugierten Substanzen beitragen.

## iv. Content

i.	Declaration .....	i
ii.	Abstract .....	ii
iii.	Zusammenfassung .....	iv
v.	List of tables .....	vii
vi.	List of figures .....	viii
1.	Introduction .....	1
	1.1 Biology of the bone .....	1
	1.2 Diseases of the bone .....	4
	1.3 Bone assessments .....	5
	1.4 The bisphosphonates .....	6
2.	Results .....	10
	2.1 5-FdU-alendronate a new bone-seeking duplex drug: Studies of its <i>in vitro</i> cytotoxicity and systemic <i>in vivo</i> toxicity .....	10
	2.2 Inhibition of osteolytic tumor growth by 5-FdU-Alendronate, a bisphosphonate conjugate that maintains bone formation: implications for treatment of bone metastases .....	38
	2.3 Binding kinetics of a fluorescently-labeled bisphosphonate as a tool for dynamic monitoring of bone mineral deposition <i>in vivo</i> .....	64
	2.4 Utilizing time-lapse micro-CT-correlated bisphosphonate binding kinetics and soft tissue-derived input functions to differentiate site-specific changes in bone metabolism <i>in vivo</i> .....	92
3.	Discussion and future directions .....	122
4.	Conclusions .....	126
5.	Additional published works .....	127
6.	References .....	128

**v. List of tables**

Table 1	Bisphosphonate structures and relative affinities .....	8
Table 2	Evaluation of 5-FdU-ale toxicity <i>in vitro</i> .....	21
Table 3	Rate constant values reflect changes in forming surfaces while plateau values reflect changes in bone formation and resorption volumes .....	113
Table S1	Treatment with alendronate of 5-FdU-ale results in significantly greater BMD values than untreated mice or mice treated with 5-FdU .....	62
Table S2	Treatment with 5-FdU-ale results in significantly greater BV/TV values than untreated mice or mice treated with 5-FdU or alendronate .....	63
Table S3	Two-way ANOVA comparison of time-lapse micro-CT parameters from short-term and long-term OVX mice .....	107
Table S4	Two-way ANOVA comparison of time-lapse micro-CT parameters from OVX+PTH and OVX+long-term PTH-treated mice .....	110

**vi. List of figures**

Figure 1 The bone remodeling process ..... 3

Figure 2 Structure formula of 5-FdU-ale ..... 15

Figure 3 Growth inhibition of the stromal cell line KM105 incubated with 5-FdU, ale or 5-FdU-ale at concentrations from 6.25-100  $\mu$ M after 120 h ..... 23

Figure 4 Growth inhibition of the stromal cell line HS27A incubated with 5-FdU, ale or 5-FdU-ale at concentrations from 6-25-100  $\mu$ M ..... 25

Figure 5 Selected inhibition of malignant cells by 5-FdU-ale ..... 27

Figure 6 Embryotoxicity ..... 29

Figure 7 Weight effects in a mouse model ..... 31

Figure 8 Treatment with 5-FdU-ale shows no impaired renal function ..... 33

Figure 9 Nephrotoxicity ..... 34

Figure 10 5-FdU-ale toxicity in breast cancer is mediated by cell cycle arrest *in vitro* ..... 47

Figure 11 Treatment with 5-FdU-ale reduces the frequency and size of bone metastases *in vivo* ..... 49

Figure 12 Mice treated with 5-FdU-ale show significant reductions in tumor burden ..... 50

Figure 13 Mice treated with 5-FdU-ale results in significantly greater osteoblast activity than mice treated with 5-FdU or alendronate ..... 52

Figure 14 Treatment with 5-FdU-ale significantly reduces the number of tumor-associated osteoclasts ..... 53

Figure 15 Mice treated with 5-FdU-ale show increased bone quality ..... 54

Figure 16 5-FdU-ale is detectable on the bone several weeks after injection at levels significantly greater than 5-FdU alone ..... 56

Figure 17 Study design overview ..... 71

Figure 18 Kinetic distribution of fluorescent bisphosphonate ..... 76

Figure 19 Ovariectomy results in decreased rate constant and binding plateau values of fluorescently-labeled bisphosphonate ..... 78

---

Figure 20	Ovariectomized mice treated with PTH showed increased rate constants and plateau-weighted rate constants .....	80
Figure 21	Bisphosphonates preferentially bind to bone regions associated with new bone formation .....	82
Figure 22	Bisphosphonates preferentially bind to regions of low bone density .....	84
Figure 23	Ovariectomy and treatment with PTH results in significantly altered binding kinetic parameters of fluorescently-conjugated bisphosphonate .....	102
Figure 24	Spine and knee regions show differential changes in bisphosphonate binding kinetics in response to ovariectomy and PTH treatment .....	104
Figure 25	Bone loss associated with ovariectomy preferentially affects the spine .....	106
Figure 26	Treatment with PTH results in significant changes in bone microstructure .....	109
Figure 27	Linear correlations between binding kinetic and time-lapse micro-CT parameters .....	112
Figure 28	Abdominal soft tissue fluorescence correlates with serum bisphosphonate levels and shows altered clearance in OVX and PTH-treated mice .....	115
Figure 29	Binding kinetic parameters correlate with tumor progression .....	124
Figure S1	Treatment with 5-FdU, alendronate or 5-FdU-ale results in altered bioluminescence <i>in vitro</i> .....	61

## 1. Introduction

### 1.1 Biology of the bone

Formed primarily from the mineralization of cartilage through endochondral ossification, bone has the ability to absorb incredible loads without fracturing, while at the same time remaining light weight<sup>43</sup>. The skeleton provides structural support, protects sensitive internal organs, serves as a signaling reservoir of growth factors and minerals as well as forms the environment for hematopoiesis<sup>139</sup>. There are two major forms of bone, trabecular and cortical, comprising ~20% and ~80% of the overall bone, respectively<sup>35</sup>. Trabecular bone, also known as cancellous or spongy bone, is usually of lower density with a higher surface area to volume ratio than cortical bone, giving it a more flexible characteristic<sup>105</sup>. It is present primarily within the ends of the long bones and makes up the majority of the vertebra where it functions to distribute and dissipate impact<sup>16, 48</sup>. Trabecular bone is also known to be highly porous and vascularized<sup>23</sup>. In contrast to trabecular bone, cortical bone is denser, more rigid and less porous and is found primarily in the long bones and forms the outer shell around the trabecular bone of the vertebra and near the joints<sup>105</sup>. Cortical bone provides the main support of the body, as well as serves as attachment sites for muscles, providing levers for movement.

Bone is primarily comprised of type I collagen<sup>10</sup> which provides flexibility and serves as the scaffold for bone mineralization. Type I collagen is synthesized in the osteoblast, a bone-specific cell derived from mesenchymal stem cells (MSCs) which functions as the primary bone builders in the body<sup>14</sup>. Collagen fibers form as a braided triple helix and are then secreted outside the cells where they form fibrils<sup>143</sup>. These fibril networks, in coordination with osteoblast secretion of the enzyme alkaline phosphatase and small vesicles, are then mineralized by hydroxyapatite, an insoluble crystal comprised primarily of calcium and phosphorus<sup>54, 65</sup>. This mineralized collagen network forms the basis of both cortical and trabecular bone. During development, new bone formation is essential for normal growth and is under constant modulation to help the body adapt to changing mechanical loads and other physiological influences<sup>29</sup>. This process, termed bone modeling, is an uncoupled process involving, primarily, the function of osteoblasts. After maturity is reached, the skeleton is constantly being renewed to maintain the integrity of the bones and repair microfractures which occur during

normal life<sup>20</sup>. Termed bone remodeling, this process is tightly regulated and primarily involves the resorption of old bone by osteoclasts and the subsequent formation of new bone by the osteoblasts (Figure 1). Osteoclasts are large, multi-nucleated cells of hematopoietic stem cell (HSC) origin which secrete H<sup>+</sup> ions, tartrate-resistant acid phosphatase (TRAP), cathepsin K, matrix metalloproteinases and gelatinases which digest bone, resulting in the formation of resorption pits<sup>140</sup>. The bone surfaces of these resorbing pits are next lined by osteoblasts which refill these cavities with newly mineralized bone equal to that resorbed<sup>129, 159</sup>, thereby maintaining the skeletal homeostasis. Bone remodeling is regulated by several factors including parathyroid hormone (PTH), the only currently prescribed anabolic therapy for bone<sup>59, 103</sup>. The primary role of circulating PTH is the regulation of plasma calcium levels<sup>118</sup>, modulated by its regulation of both osteoblasts and osteoclasts, to regulate the flow of calcium from the bone to the blood stream and back again. Although all the mechanisms are not fully understood, PTH has been shown to promote commitment of MSCs to the osteoblast lineage and inhibit osteoblast and osteocyte apoptosis resulting in increased osteoblast number, bone mineral deposition and overall bone mass<sup>66</sup>. However, because of the coupled nature of bone remodeling, continuous treatment with PTH can result in increased bone resorption as well<sup>44, 100</sup>, and as such, is administered intermittently to induce overall bone gain in patients<sup>80</sup>.

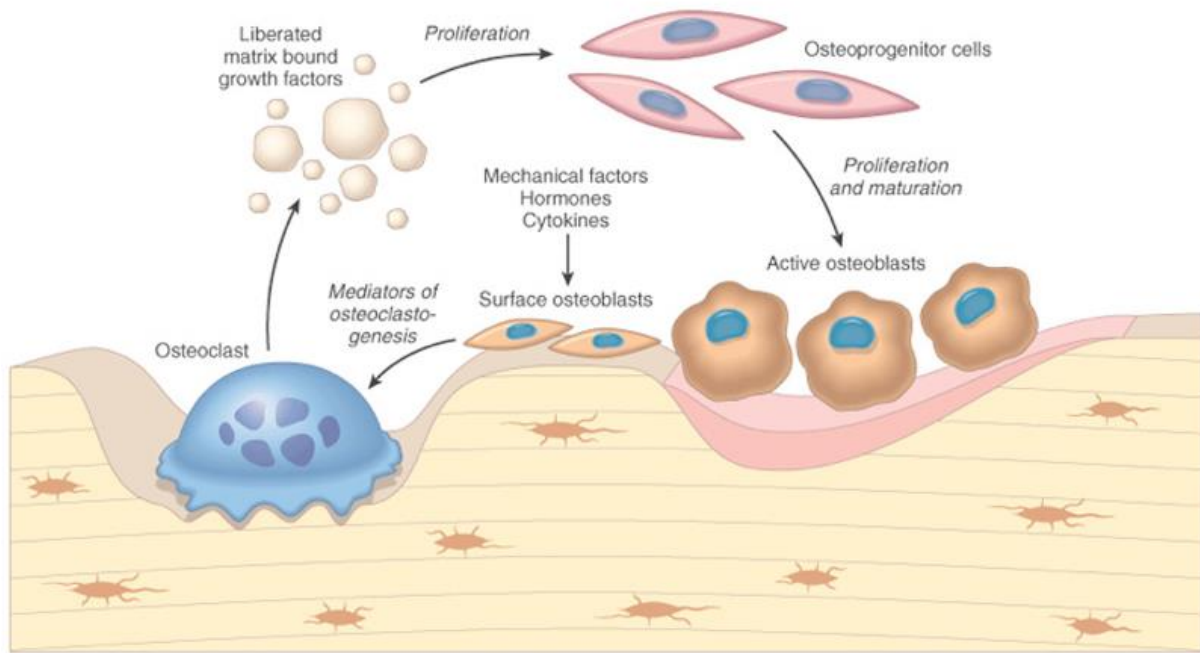


Figure 1 **The bone remodeling process**<sup>128</sup>. Bone is continuously being remodeled in a highly coordinated process to maintain the integrity of the tissue. During this process, old bone is removed by osteoclasts and replaced with newly deposited minerals secreted by active osteoblasts derived from osteoprogenitor cells. This process is regulated both by cross-talk between the osteoblasts and the osteoclasts, as well as other secreted and mechanical factors.



## 1.2 Disease of the bone

A careful balance of osteoclast and osteoblast activity is required to ensure the homeostasis of the skeleton<sup>84</sup>. However, a common byproduct of aging is the disruption of this balance, tipping the scales in favor of excessive bone resorption leading to osteopenia or osteoporosis<sup>129</sup>. Osteoporosis affects more than 200 million people worldwide<sup>90</sup> and is the result of excessive bone loss, often resulting in fractures<sup>67</sup>, the most common of which are fractures of the hip and femoral neck<sup>69</sup>. Due to our aging population, combined with sedentary lifestyles, the frequency of osteoporosis, and subsequently bone fractures, is expected to increase. Though many factors may contribute to the development of osteoporosis, the most common form of this disease is in postmenopausal women and is linked to a reduction in estrogen production<sup>19</sup>. Among its many roles in the body, estrogen has been shown to inhibit the formation of osteoclast precursors and activity of active osteoclasts by modulating the expression of interleukin 1 (IL-1) and tumor necrosis factor alpha (TNF- $\alpha$ ), by inducing expression of osteoprotegerin (OPG), a decoy receptor for receptor activator of nuclear factor-kappaB ligand (RANKL), by osteoblasts and by inducing expression of transforming growth factor beta (TFG- $\beta$ ) which induces osteoclast apoptosis<sup>60, 84, 95, 107, 137</sup>.

While osteoporosis represents a systemic loss of bone, other conditions result in highly localized changes on bone metabolism. In the case of Paget's disease, initial stages of excessive osteoclast-mediated bone loss are followed by induction of robust osteoblast activity and deposition of disorganized, hypervascularized lamellar bone<sup>46, 117</sup>. This results in weakened, misshapen bones associated with an increased occurrence of fractures<sup>158</sup>. Paget's disease is typically confined to only a few skeletal regions, primarily in the pelvis, femur and lower vertebra. While the causative agent of Paget's disease remains elusive, both viral and genetic components have suggested as contributors to disease formation.

Another form of localized bone defect is the result of various cancers metastasizing to the bone, forming osteolytic (excessive bone loss) or osteosclerotic (excessive bone gain) lesions. With its supply of stem cell niches, high level of vascularization and abundance of growth factors, the bone marrow makes an ideal location for clusters of tumor cells, which have been released into the blood

stream from the primary tumor, to take hold. These clusters of tumors home to the bone, typically in the spine or long bones, and colonize along the bone surfaces disrupting the established homeostasis between bone formation and bone resorption<sup>149</sup>. In the case of breast cancer, 60-80% of patients will develop secondary osteolytic bone lesions causing severe morbidity, an increased risk of fractures, compression of the spine and hypercalcemia<sup>21, 22</sup>. Tumor-derived osteolytic factors such as RANKL, interleukins and growth factors stimulate osteoclast activity and excessive bone resorption. This excessive bone resorption in turn releases growth factors and bone morphogenic proteins (BMPs) stored within the bone matrix which feedback to the tumor, inducing further metastatic growth<sup>18, 52, 53, 73</sup>. This feedback loop between tumor cells and osteoclasts has been termed “the vicious cycle” and results in severe osteolytic lesions.

### 1.3 Bone assessments

To evaluate changes in bone resulting from altered formation and resorption, a variety of techniques have been developed to quantify changes in bone parameters. For structural assessment and mineral content analyses, several radiological approaches have been developed<sup>9, 47, 68</sup>. Radiographs, bone densitometry and computed tomography (CT) rely on the attenuation of electromagnetic radiation as it passes through a sample. Because of the high attenuation coefficient of bone mineral, radiological approaches are well suited at providing high resolution imaging of bone structure and mineral density. These methods have the benefit of having high tissue penetration properties, but provide only a static assessment of bone and rely on follow-up scans to monitor any changes in bone structure. As well, secondary consideration must be given to radiation dosing, limiting the number and frequency of follow-up scans, the size of region imaged and the scan time (and correspondingly, the resolution)<sup>88</sup>.

In contrast to radiological techniques, which provide site-specific assessment of bone structure and mineral content, analyses of serum markers can provide insight into overall levels of bone metabolism<sup>130</sup>. In preclinical mouse models, the most common serum markers are osteocalcin, a protein secreted solely by osteoblasts and indicative of osteoblast bone-forming activities, and TRAP.

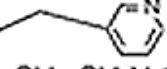
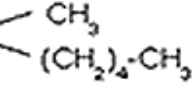
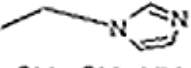
Serum markers have the benefit of repeated, long-term measurements without negative side effects associated with repeated radiation doses and of providing a current quantitative measure of bone metabolic status without the requirements of structural changes. However, because sampling occurs from circulating blood, abnormalities observed in serum markers cannot be localized to a specific site and are relatively insensitive to conditions such as newly formed breast cancer bone metastases<sup>131</sup>, which result in highly localized increases in osteoclast activity, but do not show any major changes on the skeletal bone metabolism as a whole. For this reason, serum markers provide greater use in monitoring systemic changes in bone metabolism while radiological approaches are better suited for monitoring of diseases resulting in site-specific changes in bone microstructure. An *in vivo* tool which would allow the site-specific assessment of the bones current metabolic status could bridge the gap between these two existing methods and could prove useful in locating potential skeletal events, as well as monitoring in the context of disease spread and the evaluation of therapeutic interventions.

#### 1.4 The bisphosphonates

Bisphosphonates are a class of drug commonly prescribed to patients with excessive bone loss<sup>119</sup>. Bisphosphonates contain a backbone similar to pyrophosphates which show a very high affinity for the bone, stably binding to hydroxyapatite crystals on the bone surface for long periods of time. As bone is resorbed, bound bisphosphonates are taken up by the osteoclasts inducing apoptosis and thereby inhibiting further bone resorption<sup>30</sup>. Bisphosphonates can be divided into nitrogen-containing and non-nitrogen-containing groups and act to inhibit osteoclasts in different ways. Non-nitrogenous bisphosphonates, such as etidronate and clodronate, are converted in the cell to products which are incorporated into non-functional ATP molecules, disrupting cellular energy metabolism and inducing apoptosis<sup>91, 114</sup>. Nitrogen-containing bisphosphonates such as zoledronate and alendronate inhibit the activities of the enzyme farnesyl diphosphate synthase which is involved in the post-translational prenylation of proteins such as small G-proteins including Ras, Rac and Rho<sup>32, 70</sup>. Bisphosphonate-mediated inhibition of this enzyme results in the accumulation of proteins with aberrant function leading to induction of apoptosis. Several nitrogen-containing bisphosphonates

currently exist which vary primarily in the R<sub>2</sub> side chain. These side chain modifications have been shown to affect not only their affinity for bone mineral (Table 1), but also their efficacy in inhibiting osteoclast activity<sup>77</sup>. While both bisphosphonate groups preferentially inhibit osteoclast activity, the nitrogen-containing bisphosphonates have been shown to have increased antiresorptive potency, and as such, have become the bisphosphonates of choice for patient care<sup>120</sup>.

Table 1 Bisphosphonate structures and relative affinities<sup>77</sup>

Bisphosphonate	R <sub>1</sub> Side Chain	R <sub>2</sub> Side Chain	Relative Affinity (μM)
Clodronate	-Cl	-Cl	806
Etidronate	-OH	-CH <sub>3</sub>	90.7
Risedronate	-OH		84.6
Ibandronate	-OH	-CH <sub>2</sub> -CH <sub>2</sub> N 	116
Alendronate	-OH	-(CH <sub>2</sub> ) <sub>3</sub> -NH <sub>2</sub>	60.9
Zolendronate	-OH		80.8
Pamidronate	-OH	-CH <sub>2</sub> -CH <sub>2</sub> -NH <sub>2</sub>	82.7

Because of their high affinity for bone, bisphosphonates are also under intensive research as targeting molecules for pharmaceuticals or as imaging agents. Recently, a drug conjugate was described in which the anti-tumor agent gemcitabine was conjugated with a bisphosphonate which showed a reduction in the number and size of bone metastases in a preclinical model for breast cancer bone metastases<sup>34</sup>. Additional complexes between bisphosphonates and platinum(II)<sup>93</sup> or the anti-metabolite 5-fluoro-2'-deoxyuridine (5-FdU)<sup>124</sup> have also been described to have anti-tumor effects *in vitro*. In addition to targeting drugs to the bone, bisphosphonates have also been conjugated to fluorescent dyes to be used as *in vivo* imaging markers. This has led to new insights into bisphosphonate binding distribution, retention and penetration. Previous work has shown a preferential binding of low affinity bisphosphonates to resorbing pits while high affinity bisphosphonates tend to bind less discriminately<sup>113</sup>. It was also noted that lower affinity bisphosphonates were able to penetrate deeper into the bone surface compared to higher affinity bisphosphonates<sup>113</sup>. These studies additionally identified macrophages and monocytes as cell types which demonstrate bisphosphonate uptake, owing to their high endocytic nature<sup>25, 112</sup>. More recently, bisphosphonate binding has been used as an *in vivo* tool to monitor changes in bone characteristics. A model of bone gain stimulated by mechanical loading showed increased binding of fluorescently-labeled bisphosphonate, though large intra-group variations resulted in no correlation with bone formation rates assessed by micro-CT<sup>76</sup>.

The goal of this thesis was to explore the use of bisphosphonates as bone-targeting agents in the context of new pharmaceutical drug conjugates in the treatment of breast cancer bone metastases and as a site-specific, *in vivo* imaging marker for monitoring changes in bone metabolism using a binding kinetics approach. By developing new, targeted therapeutics using bisphosphonates, we can increase the local drug concentrations at sites of disease while minimizing off-target toxic effects associated with systemically administered treatments. As imaging agents, bisphosphonates have the ability to bridge the gap between systemic metabolic markers and site-specific, radiological assessments of changes in bone morphology.

## **2. Results**

### Chapter 2.1

Modified from:

Schott S, Valett S, Tower RJ, Noor S, Tiwari S, Schem C and Busch C. (2014). *In vitro* and *in vivo* toxicity of 5-FdU-alendronate, a novel bone-seeking duplex drug. *Invest New Drugs, submitted*

**Title Page**

*In vitro* and *in vivo* toxicity of 5-FdU-alendronate, a novel bone-seeking duplex drug

Sarah Schott<sup>1,2</sup>, Sonia Valett<sup>2</sup>, Robert J. Tower<sup>3</sup>, Seema Noor<sup>4</sup>, Sanjay Tiwari<sup>3</sup>, Christian Schem<sup>5</sup>,  
Christian Busch<sup>4</sup>

<sup>1</sup>Department of Gynecology and Obstetrics, University of Heidelberg, Heidelberg, Germany, Im  
Neuenheimer Feld 440 69120 Heidelberg

<sup>2</sup>The National Centre of Tumor Disease (NCT), University of Heidelberg, Heidelberg, Germany, Im  
Neuenheimer Feld 410 69120 Heidelberg

<sup>3</sup>Section Biomedical Imaging, Department of Radiology and Neurology, University Hospital  
Schleswig-Holstein, Kiel, Germany

<sup>4</sup>Section of Dermato-Oncology, Department of Dermatology and Allergology, University of  
Tuebingen, Liebermeisterstr.25, 72076 Tuebingen, Germany

<sup>5</sup>Department of Gynecology, University Hospital Schleswig-Holstein, Campus Kiel, Germany

Key words:

Bone targeting, Bone disease, Polychemotherapy, Antimetabolite-bisphosphonate



**Abstracts**

Bone metastases remain one of the most common sites for metastatic cancer and its limited therapeutic options aggravate cancer-related morbidity and mortality in multiple malignancies. The covalent conjugation of the amino-bisphosphonate alendronate (ale) with the antimetabolite 5-FdU results in the generation of 5-FdU-ale, an effective new bone-seeking duplex drug against osseous cancer manifestations.

Method: *In vitro*, cytotoxicity was evaluated with the Aleamar Blue and MUH cell viability assays in different, highly proliferative malignant melanoma or multiple myeloma cells, as well as in osteoblast and stromal cell lines. *In vivo* systemic toxicity was addressed with the chick embryo assay and nephrotoxicity in Balb/c nude mice.

Results: A cell-specific, dose-related cell death was observed for 5-FdU-ale in all cancer cell lines, though significant less toxic than 5-FdU. Cell assays revealed a higher tumor cell-specific cytotoxicity in comparison to osteoblast or stromal cells. The embryotoxicity of 5-FdU-ale was significant less than that of the parental drugs ale or 5-FdU. The duplex drug did not reveal any signs of side effects such as inflammation at the site of injection, weight loss or nephrotoxicity in mice.

Conclusion: The coupling of amino-BPs with antimetabolite via a N-alkyl-bonding is a new synthesis route for the preparation of amino-BPs with a high cytotoxic bone-seeking potential along with a reduced systemic toxicity. This innovative duplex drug warrants further *in vivo* investigation to determine its potential use as an anti-bone metastatic agent.

## Introduction

Bone metastases remain a frequent occurrence in patients with metastatic cancers, aggravating cancer-related morbidity and mortality in multiple malignancies with limited therapeutic options. Breast cancer, for example, which remains the leading cancer among women worldwide, causes metastasis in over 20 % of patients with bone manifestation in 80 % in patients at late stages of systemic disease. Beside solid tumours with a known increased propensity for bone metastasis and bone marrow involvement, it often remains underestimated e.g. for malignant melanoma<sup>135, 138</sup>. In addition, multiple myeloma is characterized as a systemic disease with osteolytic lesions up to 80 % among newly diagnosed patients<sup>141</sup>. The osteolytic, bone destructive properties cause skeletal-related events through bone pain, pathological fractures, cord compression or hypercalcemia, that deteriorate quality of life and limit survival<sup>149</sup>. Since Paget's hypothesis of "seed and soil", the occurrence of metastasis is now seen as part of the multi-stage carcinogenesis<sup>138</sup>. The tumor microenvironment and interaction with bone marrow-derived cells, the pre-metastatic niche formation and dissemination of tumor cells gained predominant attention in this process and demand novel therapeutic approaches beyond the treatment of losses in bone mass in order to overcome the elusive metastatic disease<sup>2, 122</sup>. For a successful therapy of bone metastasis, an effective therapeutic dose of systemically applied antitumor agents should be localized in the microenvironment of bone with minimal systemic adverse effects. An increased cytotoxicity with simultaneous boosted systemic toxicity by any drug does not gain therapeutic advance or superiority.

Bisphosphonates (BPs) are a class of anti-resorptive agents, approved to treat multiple skeletal disorders and are effective against malignancy-related bone diseases<sup>27, 51, 58</sup>. The ability to prevent progression of bone metastasis with the available BPs is limited and therefore combinations that could enhance efficacy are highly sought after. Cytotoxic drugs linked with BP represent bone-seeking conjugates that could improve the cytotoxic potential of BPs and allow a bone targeting for chemotherapeutics due to the osseous-seeking properties of the BP-residue. The challenge for such bone-seeking conjugates is on the one hand, to provide high stability for the *in vivo* delivery process avoiding systemic toxicity, but on the other hand, it must inhibit bone destruction as well as metastatic

growths once it has targeted to sites of increased osteolysis. The chemical linkage of the compounds is the determining factor for the stability, pharmacokinetic and pharmacological properties of such bone-seeking conjugates. Several previously synthesized BPs-conjugates linking antitumor agents to the terminal amino group of amino-BP showed modest activities in animal models<sup>36, 61, 136, 152</sup>.

Recently, a new synthesis route was developed for the linking of amino-BPs with cytotoxic pyrimidine nucleoside analogues via their nucleobases<sup>124</sup>. Using this concept of BPs-based anti-tumor agents, Figure 2 shows the structure of 5-FdU-alendronate (5-FdU-ale) in which the well-known antimetabolite 5'-fluoro-2'-deoxyuridine (5-FdU) is linked via an N-alkyl bonding with alendronate (ale). The unnatural N-alkyl linkage increased the enzymatic and hydrolytical stability of the whole conjugate in respect to previously used natural amide or anhydride bondings. This new drug was then assessed for its chemosensitivity of several tumor cell lines as well as osteoblasts and stromal cell lines. *In vivo* studies about its systemic toxicity were performed. These investigations address if 5-FdU-ale could improve the therapeutic potential of antitumor drugs against bone metastasis via bone-targeting while reducing its systemic toxicity.

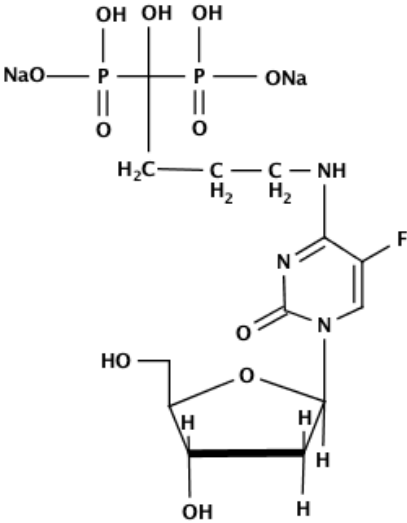


Figure 2 Structure formula of 5-FdU-ale

## Material and methods

### *Cells and cell culture*

Human metastatic melanoma cell lines BLM, MEWO, SKMel19, SKMel28, SKmel5, 1205LU, MDA-MB-435, MALME-3M, LOXIMV, UACC62, SKMel2, UACC257, M14, 451LU were purchased from ATCC. Multiple myeloma (MM) green fluorescent protein (GFP)-positive MM1S and its parental cell line have been received from Dr. S. T. Rosen, Northwestern University, Chicago, IL, USA. The human bone marrow stromal cell lines (BMSC) HS27A was obtained from ATCC/LGC Standards GmbH, Wesel Germany, and the KM105 was kindly provided by Dr. Kenichi, Chiba University Graduate School of Medicine, Chiba, Japan<sup>56</sup>. Osteoblasts (OB) were obtained by differentiating KM105 cells under osteogenic conditions. Mature cells were analysed for cell viability and function as previously described<sup>33, 147</sup>. The cells were cultured in RPMI 1640 medium supplemented with 10 % fetal bovine serum (FBS), penicillin, and streptomycin and maintained at 37°C in a 95 % air / 5 % CO<sub>2</sub> atmosphere at 100 % humidity. All cell culture reagents were from PAA, Pasching, Austria. Media was changed at 48 h intervals and cells were passaged upon confluence for a maximum of four passages (short term culture) or 20 passages (long term culture).

### *Drugs and treatment*

5-FdU and ale were commercially available from the local University hospital pharmacy. 5-FdU-ale was a gift from H. Schott. Drugs were dissolved in sterile PBS resulting in a stock solution and stored at -20°C. Dilutions of the stock solution were prepared shortly before administration. The drug concentrations for each cytotoxic agent were either determined as a set of test experiments or by our previous results<sup>125, 126</sup>. The agents were dissolved in PBS then added directly to the culture medium of cell lines in monolayer after 24 h and then incubated for 72 h. Control cells grew in PBS without drug. The intensity of fluorescence indicates the number of viable cells in the wells and their percentages were calculated by normalization between background of cultures without cells and the control.

*Drugs cytotoxicity assay on melanoma cell lines*

Since plasma peak concentrations of 5-FdU-ale are not known for those test systems, the starting concentration was set at 0.5  $\mu\text{M}$  for the first cell viability in malignant melanoma cell assay. For the determination of melanoma cell viability the MUH [4-methylumbelliferyl heptanoate] assay was used in triplicates for each cell line. Briefly, 5000 cells in 100  $\mu\text{l}$  or 2500 cells in 50  $\mu\text{l}$  ( $5 \times 10^5$  cells per ml) were plated in flat-bottomed 96-well plates (Nunc, Wiesbaden, Germany)<sup>125</sup>. After 24 h, medium was replaced with medium containing PBS as control or with 5-FdU or 5-FdU-ale at concentrations of 0.5, 1.0 or 2.0  $\mu\text{M}$  and incubated for 72 h. Medium was discarded, each well was washed two times with PBS and 100  $\mu\text{l}$  of a solution containing 100 mg MUH [4-methylumbelliferyl heptanoate] (Sigma-Aldrich, Munich, Germany) per ml PBS was added. Plates were then incubated at 37°C for 1 h. The number of viable cells in the wells was measured in a Fluoroskan II (Labsystems, Helsinki, Finland), with a  $\lambda_{\text{ex}}$  of 355 nm and a  $\lambda_{\text{em}}$  of 460 nm.

*Drugs cytotoxicity assay on stromal, multiple myeloma and osteoblast*

For the cytotoxicity assays, drug concentrations ranged from 6.25 to 100  $\mu\text{M}$ . The cell viability was assessed for the multiple myeloma and stromal cells as well as the osteoblast under normoxic and hypoxic conditions (1%  $\text{O}_2$ ) as described previously<sup>146</sup>. In brief, a short-term culture was analysed after 48 h whereas a long-term culture was analysed after 120 h following drug incubation with 0.125 to 20  $\mu\text{M}$ . Cell number was quantified using the AlamarBlue assay (BioSource International, Camarillo, CA), pulsing the cells with AlamarBlue (10  $\mu\text{L}$ ) and incubating for 4 hours at 37°C. Cell viability was assessed measuring absorption at a wavelength of 570 nm (with correction at 600 nm) on a spectrophotometer (Infinite™ 200, Tecan).

*Embryotoxicity testing*

For embryotoxicity testing, 45 eggs were obtained and prepared as described previously<sup>125 13</sup>. After 50 h of incubation, the eggs, approximately equal to stage 13 according to Hamburger and Hamilton (HH), which corresponds to approximately six human gestational weeks<sup>37</sup>, received the cytostatic treatment. The drugs 5-FdU-ale (30  $\mu\text{M}$ ), ale (10 or 30  $\mu\text{M}$ ) or 5-FdU (30  $\mu\text{M}$ ) dissolved in 50  $\mu\text{l}$

sterile ddH<sub>2</sub>O were applied on top of the blastoderm (n=9 embryos per treatment group). The control group received 50 µl sterile ddH<sub>2</sub>O. The eggs were sealed with adhesive tape (Super88, 3 M, St. Paul, MN) and replaced in the incubator. 8, 12, 24 and 32 h after application of the drugs, viability of the embryos was monitored by viewing the heart. No animal approval was required for the local animal care guidelines as chick embryos were used in very early stage.

#### *In vivo toxicity study*

Animal experiments and care were in accordance with the guidelines of institutional authorities and approved by the Ethics Committee for Animal Experiments at Christian-Albrechts-Universität zu Kiel (V312-72241.121-10). Four female, nude Balb/c mice, 5-6 week old were purchased from Charles River (Wilmington, MA, USA). All animals were kept in a temperature and humidity-controlled environment, with a 12 h light/dark cycle, and access to food and water ad libitum. Mice were injected intraperitoneally (ip) with 5-FdU-ale 4, 2, 1 or 0.5 mg, corresponding to a dose of 200, 100, 50 or 25 mg/kg, dissolved in 100 µl sterile PBS. Mice were monitored daily for 5 days for signs of weight loss, inflammation at the sight of injection or general signs of suffering such as lethargy, lack of water and food intake and loss of righting reflex.

#### *Functional and histomorphological nephrotoxicity study*

To determine short and long-term drug effects, 9 mice were injected with 4 mg (corresponding to 191 mg/kg) 5-FdU-ale dissolved in 100 µl sterile PBS. The short-term drug effects on glomerular filtration were evaluated in 5 mice treated with a single dose of 5-FdU-ale to check for impaired renal clearance of inulin. This was assessed using the fluorescent inulin conjugate GFR-Vivo 680 (PerkinElmer, MA, USA) on day 1 and day 4 post injection. Mice were analysed using a two-phase decay (Prism version 5, GraphPad Software, CA, USA) with the equation:  $Y = \text{plateau} + \text{SpanFast} * \exp^{-K_{\text{Fast}}t} + \text{SpanSlow} * \exp^{-K_{\text{Slow}}t}$ , where  $\text{SpanFast} = (Y_0 - \text{plateau}) * \% \text{Fast} * 0.01$  and  $\text{SpanSlow} = (Y_0 - \text{plateau}) * (100 - \% \text{Fast}) * 0.01$ .  $Y_0$  was constrained to 170 RFU (based on average predicted  $Y_0$  values for control mice of non-constrained regression) and plateau was constrained to  $>0$ .

For long-term kidney toxicity, 4 mice received weekly doses of 5-FdU-ale for 5 weeks. For histopathologic changes of kidney injury, such as focal cellular necrosis or increased tubular degeneration, the kidneys were excised at the end of the experiment. Kidneys were fixed in 4% buffered formalin overnight and embedded in paraffin. 5 µm sections were generated, stained with hematoxylin and eosin (H&E) and Periodic acid-Schiff reaction (PAS) assessed microscopically with NIKON Eclipse Ti and digitalized with NIS Element imaging Software (Version 3.2. NIKON) .

#### *Statistical analyses*

Statistics were calculated either using the GraphPad Prism software Version 5 (GraphPad Prism Software Inc, California, US), or using SPSS (Version 18). Results were analyzed using an unpaired t test with Welch's correction to avoid the assumption of equal variance for *in vivo* studies and the Student's two-tailed t test for *in vitro* evaluation (95% CI,  $p < 0.05$  was considered significant). Error bars represent standard deviation. *In vivo* embryotoxicity assays were depicted as Kaplan Meier plots and analysed using log rank test (95% CI,  $p < 0.05$  was considered significant).



## Results

### *Different chemosensitivity of melanoma cell against 5-FdU and 5-FdU-ale*

The cytotoxicity of 5-FdU and 5-FdU-ale expand with increasing drug concentrations (Table 2). The chemosensitivities of cell lines against 5-FdU and 5-FdU-ale differ clearly and are generally markedly higher for 5-FdU in comparison to 5-FdU-ale. The applied concentration of 5-FdU-ale in the range of 0.5-2.0  $\mu\text{M}$  did inhibit the growth of 8 cell lines only marginally. However, under corresponding conditions with 5-FdU, the growth of 6 cell lines was inhibited (21-52% cell death). The highest chemosensitivity measured as cell death among melanoma cells against 5-FdU-ale shows the LOXIMVI (52 %) and MDA-MB-435 (35%) whereby 5-FdU caused a cell death of 77% and 43% respectively.

Table 2 Evaluation of 5-FdU-ale toxicity *in vitro*

% Cell Death		Conc. ( $\mu\text{M}$ )		
Cell Type	Drug	0.5	1	2
BLM	5-FdU	65	72	80
	5-FdU-ale	-2	10	27
SKMel5	5-FdU	58	67	75
	5-FdU-ale	4	6	21
1205LU	5-FdU	61	65	63
	5-FdU-ale	14	17	32
MDA-MB435	5-FdU	22	31	43
	5-FdU-ale	5	18	35
MALME-3M	5-FdU	20	22	33
	5-FdU-ale	7	9	22
LOXIMVI	5-FdU	65	70	77
	5-FdU-ale	17	34	52
Mewo	5-FdU	49	57	67
	5-FdU-ale	5	3	11
UACC62	5-FdU	38	43	51
	5-FdU-ale	6	2	2
SEKmel28	5-FdU	28	30	34
	5-FdU-ale	-2	-5	-3
SKMel2	5-FdU	22	30	30
	5-FdU-ale	-3	1	-1
UACC257	5-FdU	33	41	47
	5-FdU-ale	1	-4	3
SKMel19	5-FdU	36	43	58
	5-FdU-ale	1	-1	9
M14	5-FdU	46	56	63
	5-FdU-ale	-11	-8	-4
451LU	5-FdU	29	35	43
	5-FdU-ale	-1	3	9

*5-FdU- ale shows less stromal cell toxicity than ale or 5-FdU alone*

After 48 h of treatment with 5-FdU-ale up to 100  $\mu\text{M}$  there was no significant toxicity for KM105 stromal cells. The growth inhibitory effect of ale alone occurred dose-dependent from a concentration of 25  $\mu\text{M}$  onwards ( $p < 0.05$  compared to untreated cells). Whereas 5-FdU showed growth inhibition already at a concentration starting from 6.25  $\mu\text{M}$ , which was significant ( $p < 0.05$ ) compared to untreated cells. 120 h after drug incubation there was a concentration-dependent effect for all drugs (Fig. 3). 5-FdU showed the strongest and significant toxicity in respect to ale and 5-FdU-ale, starting at 6.25  $\mu\text{M}$  onwards. 12.5  $\mu\text{M}$  ale was significantly more toxic than the untreated control after 5 days of incubation and, compared to the results received after 2 days of incubation, revealed a significant higher toxicity.

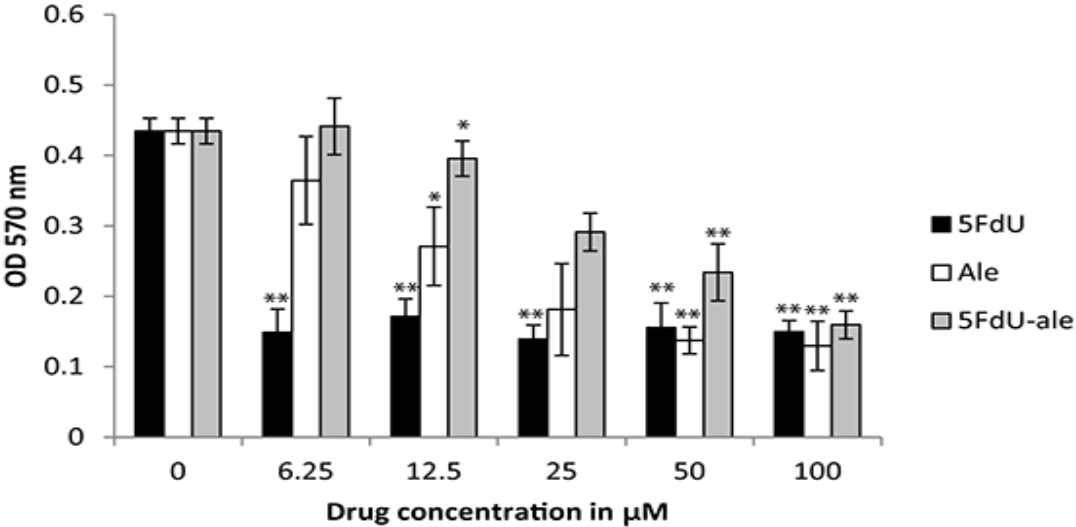


Figure 3 Growth inhibition of the stromal cell line KM105 incubated with 5-FdU, ale or 5-FdU-ale at concentrations from 6.25-100  $\mu\text{M}$  after 120 h.

In HS27A stromal cells, 5-FdU killed all cells starting from 6.25  $\mu\text{M}$  and remained significantly more toxic than 5-FdU-ale after 2 days and at all subsequent observation times (Fig. 4). After 120 h of incubation, a similar effect was observed for the KM105 stromal cell. Ale, as well as 5-FdU, showed a higher cytotoxicity than 5-FdU-ale at 6.25 $\mu\text{M}$  ( $p < 0.05$  compared to untreated control). A significant dose-dependent cytotoxic effect was observed with 5-FdU-ale at 50 and 100  $\mu\text{M}$  after 120 h of incubation.

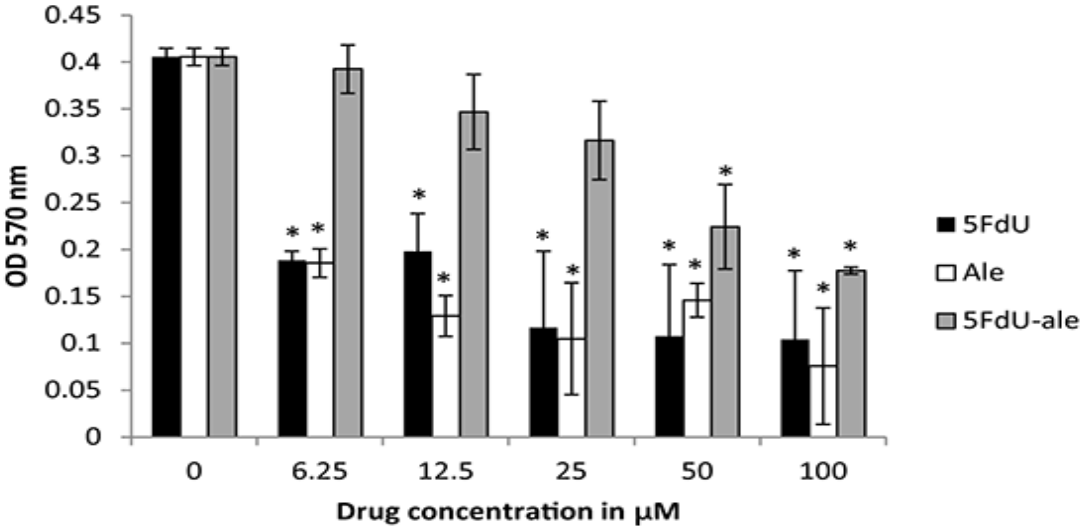


Figure 4 Growth inhibition of the stromal cell in HS27A incubated with 5-FdU, ale or 5-FdU-ale at concentrations from 6-25-100  $\mu\text{M}$

*Dose-dependent and cell specific cytotoxicity of 5-FdU-ale in highly proliferative MM1S cell lines*

5-FdU-ale, along with its parent single drugs 5-FdU and ale, inhibited in a time and dose-dependent manner the growth of MM1S cell lines (Fig. 5a). The assay revealed an MM1S cytotoxicity of 5-FdU-ale at concentrations starting from 1  $\mu$ M, in comparison to ale and 5-FdU with cytotoxic effects at 0.5  $\mu$ M. Compared to osteoblasts (OB) and stroma cell lines (BMSC) the cytotoxic effect of 5-FdU was more pronounced in MM1S cells (Fig. 5b). Indeed, OB and BMSC cells were not affected at concentration up to 20  $\mu$ M 5-FdU-ale (Fig. 5b).

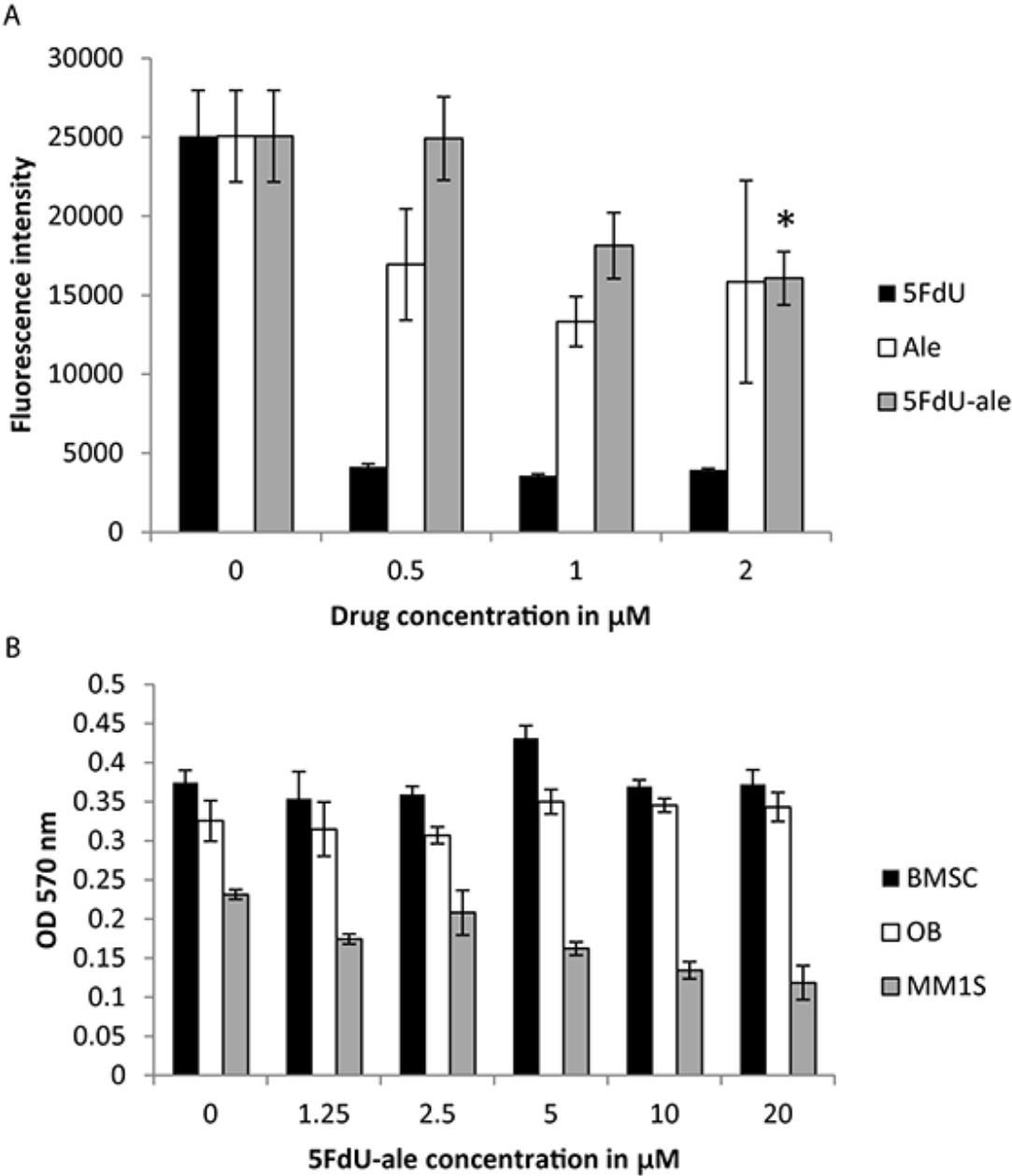


Figure 5 **Selected inhibition of malignant cells by 5-FdU-ale.** a)MM1S cell growth inhibition after 120 h by 5-FdU, ale or 5-FdU-ale at concentrations from 0.5-2 μM. b)The MM1S, OB and BMSC cell growth inhibition by 5-FdU-ale at concentrations from 1.25-20 μM.



*5-FdU-ale shows significant lower embryotoxicity than 5-FdU or ale*

The *in vivo* toxicity of 5-FdU-ale, in comparison to the single agents 5-FdU and ale and the solvent ddH<sub>2</sub>O as control, was evaluated in the embryotoxicity assay on stage 13 HH chick embryos. The survival of chick embryos were monitored over 32 h after treatment with different concentrations (Fig. 6). Ale at 10  $\mu$ M or 30  $\mu$ M proved lethal for 8/9 or 5/9 embryos respectively after 8h and was significantly more toxic than 5-FdU-ale at 10 or 30  $\mu$ M ( $p < 0.000004$ ;  $p = 0.01$  respectively) which showed no embryo death. After 16 h, 1/9 embryos of 10  $\mu$ M ale and 30  $\mu$ M 5-FdU groups each survived whereas 6/9 of the 30  $\mu$ M 5-FdU-ale were still alive. 5-FdU-ale being therefore significant less toxic than 5-FdU or ale ( $p = 0.013$ ). 100% lethality occurred in all treatment groups after 24 h post treatment.

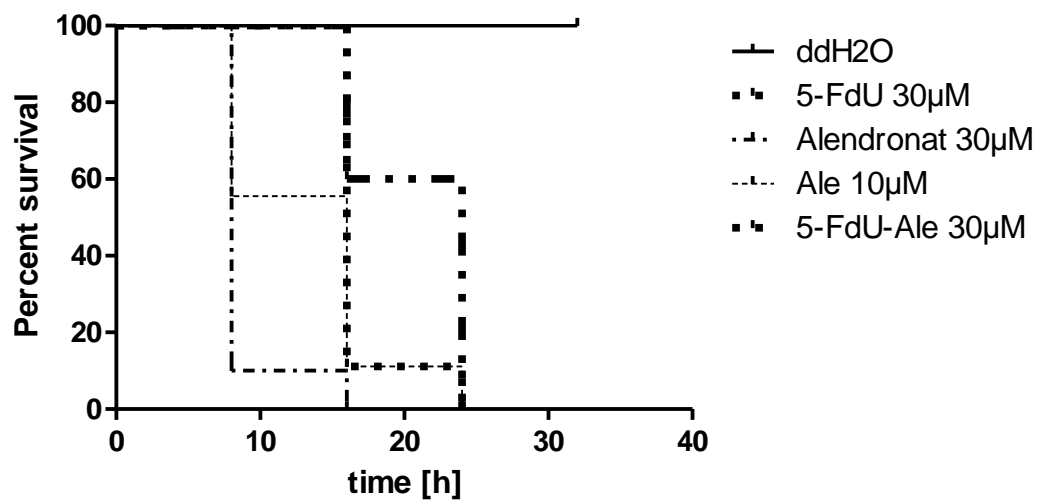


Figure 6 **Embryotoxicity.** Survival rates of chick embryos exposed to 5-FdU, ale, 5-FdU-ale after 8, 16, 24 h are depicted in a Kaplan-Meier plot. 30 µM 5-FdU-ale is less embryotoxic than 10 or 30 µM ale after 8 h and 30 µM 5-FdU after 16 h.

*5-FdU-ale has no signs of short or long-term systemic toxicity in a mouse model*

4 Mice were injected with 25, 50, 100 or 200 mg/kg 5-FdU-ale and monitored for 5 days. Mice showed no signs of toxicity, inflammation at the site of injection or increased sensitivity to touch resulting from pain. Mice showed no deviation in weight gain (Fig. 7A), nor were any signs of inflammation or suffering detected. The long-term effects of repeated drug exposure were also assessed in 6 mice treated with 191 mg/kg 5-FdU-ale weekly for 5 weeks. No difference in weight gain was found in mice treated with 5-FdU, relative to untreated controls, over the observation period of 5 weeks (Fig. 7B).

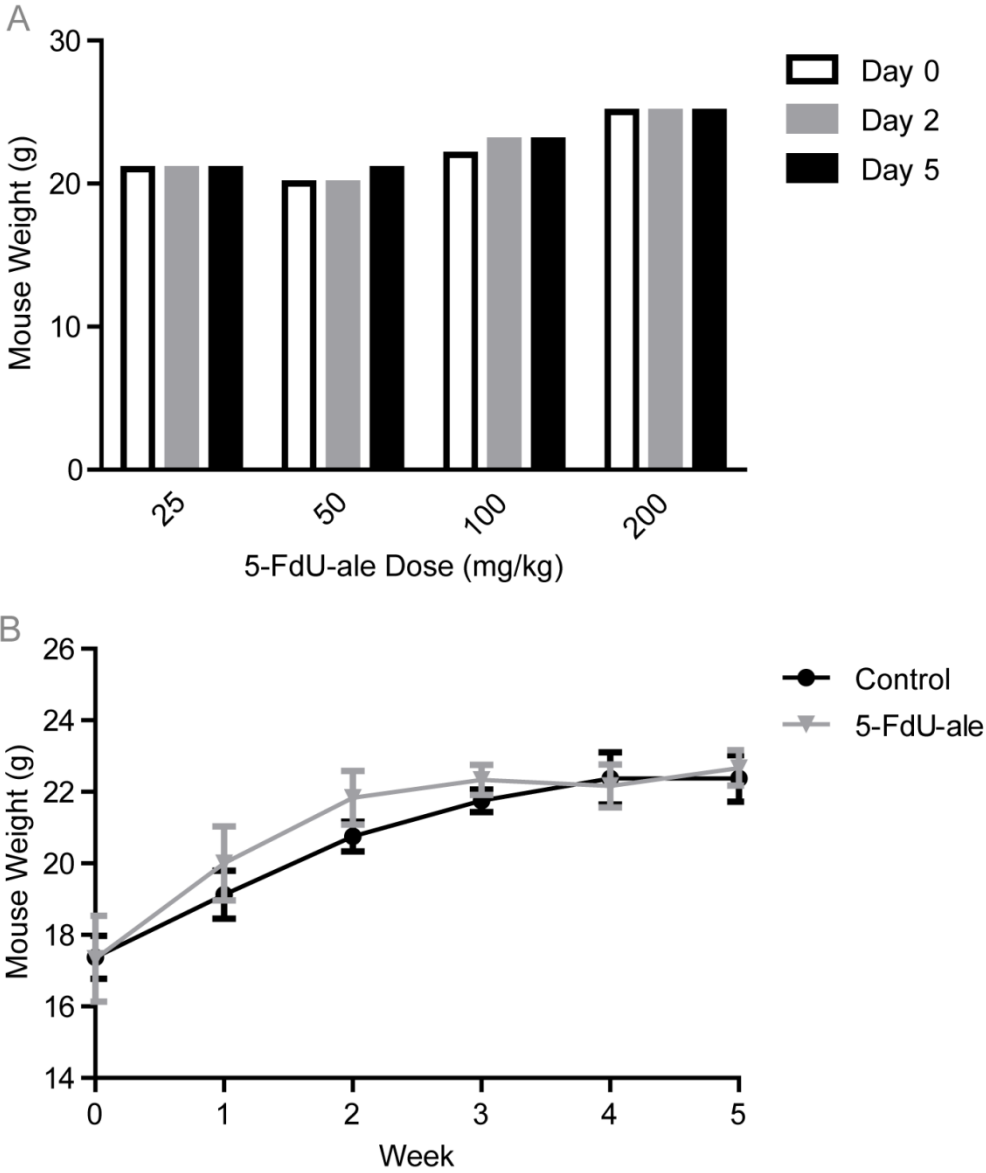


Figure 7 **Weight effects in a mouse model.** a) 5-FdU-ale shows no weight reduction in Balb/c nude mice when administered i.p. at 25-200 mg/kg, monitored for 5 days. b) A weight gain of all mice was observed over the 5 day period.

*5-FdU-ale shows no signs of functional or morphological nephrotoxicity*

Untreated control mice and mice treated with a single dose of 191mg/kg 5-FdU-ale were analysed for impaired renal clearance of inulin (Fig. 8). Treatment with 5-FdU-ale showed no significant changes after 4 days in  $K_{\text{Fast}}$  ( $p=0.7282$ ), associated with redistribution of the tracer to extracellular fluid (Fig. 8B), or  $K_{\text{Slow}}$  ( $p=0.5113$ ), associated with systemic clearance from the blood (Fig. 8C), relative to controls. To determine the long-term kidney toxicity of repeated 5-FdU-ale injections, kidneys were collected from mice treated weekly with 191 mg/kg 5-FdU-ale after 5 weeks. Histological assessment revealed no signs of toxicity (Fig. 9).

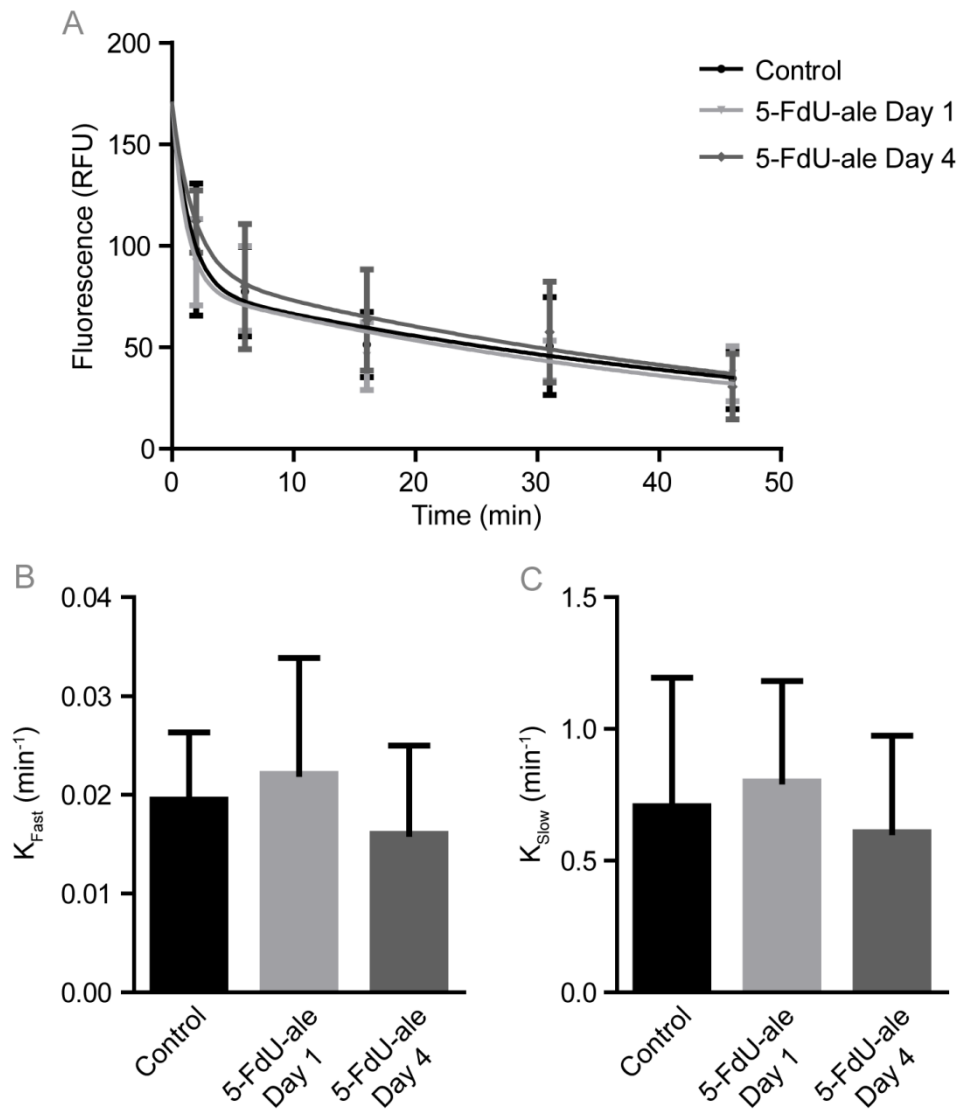


Figure 8 **Treatment with 5-FdU-ale shows no impaired renal function.** Mice were injected with a single dose of 5-FdU-ale and monitored for impaired inulin clearance 1 day and 4 days after drug treatment (A). Mice showed no significant changes in  $K_{Fast}$  (B) or  $K_{Slow}$  (C) compared to untreated control mice.

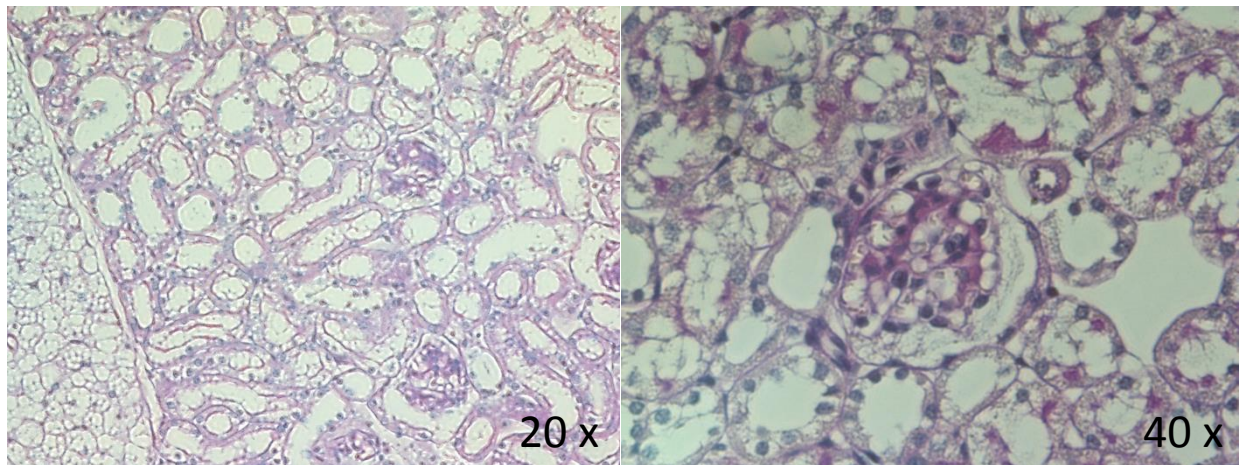


Figure 9 **Nephrotoxicity.** Histological section of PAS stained mice kidneys after treatment with 191 mg/kg 5-FdU-ale weekly over 5 weeks. Magnification 20 x and 40 x

## Discussion

The various recently designed conjugates, linking bisphosphonates (BPs) with antimetabolites<sup>34, 104</sup> can be considered as a successful proof of concept, that a BP-antimetabolite-conjugate achieves a targeting of antimetabolites to the pathogenic sites in the bone. The conjugation of etidronate with cytotoxic 5'-nucleotide analogue via a phosphoanhydrid linkage resulted in nucleoside-5'-triphosphate analogues, in which the  $\beta$ - and  $\gamma$ -phosphorous atoms are connected via a carbon instead of an oxygen atom<sup>104</sup>. The antimetabolite-conjugates evaluated in mouse models showed decreased tumour burden, maintained bone structure and may increase overall survival. Yet, the coupling of the more active amino-BPs such as ale or zoledronate remained impossible according to the described synthesis route using a phosphoanhydrid linkage. A described alternative coupling of methylene-BP with gemcitabine via an unnatural urethane linkage is also no opportunity for amino-BPs conjugation<sup>34</sup>. However, the chemical linkage between BP and the antimetabolite is the key structure element for the therapeutic efficiency of such bone-seeking drug. The linkage should not only be stable during circulation, allowing time to target to the bone after its oral or intravenous application, but also exerting its effect after uptake into the bone.

The new duplex drug 5-FdU-ale couples for the first time an amino-BP as the bone seeking residue with the standard antimetabolite 5-FdU via a N-alkyl-linkage. This linkage between ale and 5-FdU should prevent the *in vivo* metabolism after its systemic administration. The stability of its unnatural linkage suggests that 5-FdU-ale can be orally applied without being markedly metabolised during its circulation. The bone-targeting delivery should result in a local enrichment of the duplex drug in the skeleton caused by the high affinity of the BP residue to the hydroxyapatite of bone. On the one hand, the duplex drug 5-FdU-ale can act as a new amino-BP whose aminoalkyl chain is terminated with 5-FdU via its nucleobase. If the N-glycosidic bond between the deoxyribose and nucleobase is enzymatically cleaved, a new amino-BP results terminating its alkyl chain with a 5-fluoropyrimidinone. Both gained amino-BPs are bone specific agents that can inhibit the activity of osteoclasts differently. It is well known that the P-C-P function of BPs is the prerequisite for the bone targeting activity, whereby the intensity of the anti-osteoclastic activity and the cytotoxic potential



being exclusively dependent upon side chain<sup>40</sup>. On the other hand, 5-FdU-ale represents a new bone seeking prodrug of the highly cytotoxic 5-FdU as well as 5-FU. In contrast to the expected cytotoxic metabolites, the intact 5-FdU-ale itself as an N<sub>4</sub>-alkylated 5-fluoro-2'-deoxyctidine derivate, possesses only moderate cytotoxicity. The cleavage of various, differently stable linkages within 5-FdU-ale could result in a successive metabolism of the duplex. The resulting mixture of different therapeutic high active metabolites can act like a locally applied polychemotherapy initiating additive or synergistic effects, preventing or even overcoming drug resistance.

The dose-dependent growth inhibition in melanoma cell lines *in vitro*, in respect to an equimolare dose of 5-FdU, indicate that 5-FdU-ale itself has a low cytotoxicity. This may be due to the increased size, and subsequently its permeability, or that 5-FdU-ale is only partially metabolised to 5-FdU under *in vitro* cell assay conditions. These results correspond to previously described *in vitro* effects. A preliminary ATP-tumor-chemosensitivity assay demonstrated different chemosensitivities of breast and ovarian cancer cell lines to 5-FdU-ale<sup>126</sup>. Gastric adenocarcinoma cell lines show a slightly higher sensitivity to 5-FdU-ale in comparison to intestinal non-malignant and fibroblast cell lines<sup>150</sup>. The lower chemosensitivity on tested stromal cell lines against 5-FdU-ale in respect to the parental compounds ale and 5-FdU indicated also a slower metabolism and reduced cytotoxicity of the intact duplex drug. The higher growth inhibition of 5-FdU-ale towards myeloma in comparison to stromal cells and osteoblasts proved tumor cell-specific cytotoxicity of 5-FdU-ale.

A low toxicity of 5-FdU-ale was also observed *in vivo* with the embryotoxicity assay as well as in mouse models. Application of up to 200 mg/kg of 5-FdU-ale in mice did not cause weight loss or show any signs of systemic or kidney toxicity. The high *in vivo* tolerance of 5-FdU-ale in respect to clinical used BPs for example pamidronate or zolendronic acid is an important advantage. Zolendronate-related renal tubular lesions were observed in rats after one dose at 6 mg/kg. Application of 50 mg/kg in mice caused mortality and clinical signs. Mice exposed to > 10 mg/kg of pamidronate may exhibit histopathologic changes of kidney injury including focal cellular necrosis, increased cellular vesicles and loss of tubular cell brush border<sup>98</sup>. The therapeutic administration of an even higher dose of the 5-FdU-ale in respect to the clinical used standard BP suggest that a locally high

efficient drug concentration of BP, together with the cytotoxic activity of 5-FdU in the bone microenvironment, could be achieved. 5-FdU-ale could contribute to more efficient polychemotherapy against bone metastases and merits further evaluation.

Chapter 2.2

Modified from:

Schem C\*, Tower RJ\*, Kneissle P, Rambow AC, Campbell GM, Heilmann T, Trauzold A, Jonat W, Glüer CC, Schott S and Tiwari S. (2014). Inhibition of osteolytic tumor growth by 5-FdU-Alendronate, a bisphosphonate conjugate that maintains bone formation: implications for treatment of bone metastases.

**Title Page**

Inhibition of osteolytic tumor growth by 5-FdU-Alendronate, a bisphosphonate conjugate that maintains bone formation: implications for treatment of bone metastases

Schem C.<sup>1\*</sup>, Tower R. J.<sup>2\*</sup>, Kneissl P.<sup>1</sup>, Rambow A. C.<sup>1</sup>, Campbell G. M.<sup>2</sup>, Heilmann T.<sup>1,3</sup>, Trauzold A.<sup>3</sup>, Jonat W.<sup>1</sup>, Glüer C. C.<sup>2</sup>, Schott S.<sup>4</sup>, Tiwari S.<sup>2</sup>

\*These authors contributed equally

<sup>1</sup>Department of Gynecology, University Hospital Schleswig-Holstein, Campus Kiel, Germany

<sup>2</sup>Section Biomedical Imaging, Department of Diagnostic Radiology, University Hospital Schleswig-Holstein, Campus Kiel, Germany

<sup>3</sup>Division of Molecular Oncology, Institute for Experimental Cancer Research, University of Kiel, Germany

<sup>4</sup>Department of Obstetrics and Gynecology, University Hospital Heidelberg, Heidelberg, Germany

Address correspondence to: Christian Schem, MD, PhD, MaHM [schemc@email.uni-kiel.de](mailto:schemc@email.uni-kiel.de)

+49 431 597 2100

Keywords: Bone metastases, bisphosphonates, chemotherapy

**Abstract**

Patients diagnosed with breast cancer in advanced tumor stages show a high frequency of skeletal metastases. These bone lesions uncouple the balance between bone formation and resorption leading to severe osteolysis. This causes increased fracture risk, compression of the spine and hypercalcemia, decreasing the quality of life for the patient. Therefore, anti-cancer chemotherapeutics are often combined with bisphosphonates, a class of drugs with high affinity for bone mineral which inhibit bone-resorbing osteoclasts. Recently, conjugated drugs have been developed which combine the anti-tumor effects of chemotherapeutic agents with the bone-targeting abilities of bisphosphonates. Here we present the novel drug 5-FdU-ale, a conjugate between the anti-metabolite 5-FdU and the bisphosphonate alendronate. Treatment of breast cancer cell lines with 5-FdU-ale *in vitro* shows cell cycle arrest similar to treatment with unconjugated 5-FdU, but no inhibition of protein prenylation observed in alendronate-treated cells. *In vivo*, mice with breast cancer bone lesions treated with 5-FdU-ale showed reductions in both the number of metastases per mouse, as well as in tumor size. In addition, 5-FdU-ale treatment was also found to significantly reduce osteoclast number and activity without impairing osteoblast function. This finding is supported by micro-CT analyses which showed significant improvements in bone parameters, resulting in improved bone health. We also demonstrate that 5-FdU-ale is stable on the bone in mice for 2 weeks and present at significantly greater concentrations within the bone environment in as little as 1 day after injection compared to 5-FdU alone. Overall, 5-FdU-ale represents a novel cytostatic drug with high specificity for the bone and the potential to reduce tumor progression and improve bone health.

## Introduction

Breast cancer occurrence is on the rise, with an estimated 1 in 8 women developing breast cancer in their lives. Once detached from the primary tumor, breast cancer cells metastasize to the skeleton at a high frequency, uncoupling the bone remodeling process resulting in significant osteolysis. Bone metastases can cause severe morbidity as a result of intractable pain, increased risk of fractures, compression of the spine and hypercalcemia, reducing the quality of life for the patient. Treatments of breast cancer include both systemic (e.g. chemotherapy, bisphosphonates) and localized therapies (e.g. radiation, surgery).

Anti-metabolites, such as 5-fluoro-2'-deoxyuridine (5-FdU), function by inhibiting the synthesis of thymidine within the cell, thereby arresting the cell cycle and inducing apoptosis<sup>81</sup>. Additionally, small amounts of 5-FdU may also be incorporated into the DNA in place of thymidine, halting DNA elongation<sup>26</sup>. Bisphosphonates are a class of drugs with high affinity for bone mineral that act to inhibit bone-resorbing osteoclasts, thereby preventing bone loss. They are now established as the main treatment for patients with skeletal metastases<sup>49, 148</sup> and widely prescribed in the treatment of low bone mass diseases such as osteoporosis. While treatment with bisphosphonates significantly reduces bone resorption, increasing evidence also suggests that bisphosphonate treatments may also impair osteoblast function<sup>39, 78, 121</sup>. It remains unclear whether this effect is directly acting on the osteoblasts or whether it is the result of a disruption in the coupled activities of osteoblasts and osteoclasts.

Novel therapeutics are currently under development to combine the anti-tumor effects of chemotherapy agents with the high bone mineral affinity of bisphosphonates<sup>124</sup>. Because of the high longevity on the bone, these novel conjugate therapies have the potential to both increase the concentration of anti-metabolites on the bone surface, as well as minimize off-target toxic effects. Conjugation of the anti-cancer drug Gemcitabine to a bisphosphonate was recently shown to have high bone uptake and a reduction in frequency and severity of osteolytic lesions in a mouse model of bone metastases<sup>34</sup>. Recently, the anti-metabolite-bisphosphonate conjugate 5-FdU-ale was described in which 5-FdU was covalently conjugated to the bisphosphonate alendronate<sup>124</sup>. To determine its utility

as an anti-cancer agent for skeletal metastases, effects of 5-FdU, alendronate or 5-FdU-ale treatment were assessed *in vitro* and *in vivo* using a bone-homing variant of the breast cancer cell line MDA-MB-231.

## Materials and Methods

### *In Vitro Drug Toxicity Assays*

MDA-MB-231-Luc2 bone homing breast cancer cells<sup>151</sup> were left untreated or treated with 5-FdU, alendronate or 5-FdU-ale for 24 h. For protein and cell cycle analyses, cells were treated with 100  $\mu$ M of each drug and either used to prepare whole cell lysates analyzed by western blot, or fixed and sorted by cell cycle phase using FACS. For drug sensitivity studies, an MTT test was conducted on cells treated for 24 h with a drug dilution series with concentrations from 1-1000  $\mu$ M dissolved in PBS.

### *Animals*

5-6 week old female, Balb/c nude mice were purchased from Charles River (Wilmington, MA, USA). All animals were kept in a temperature and humidity-controlled environment, with a 12 h light/dark cycle, with access to food and water *ad libitum*. Animal experiments and care were in accordance with the guidelines of institutional authorities and approved by the Ethics Committee for Animal Experiments at Christian-Albrechts-Universität-zu-Kiel (V312-72241.121-10). Mice were anesthetized with intraperitoneal (ip) injection of 80 mg/kg ketamine (Aveco Pharmaceutical, IA) and 0.5 mg/kg dorbene (Pfizer, Berlin, Germany).  $1.4 \times 10^5$  MDA-MB-231 bone homing cells stably transfected with the Luc2 reporter gene were suspended in 100  $\mu$ l 1x PBS and injected into the left ventricle in 12-16 mice per treatment group. Alendronate (100  $\mu$ g/kg) and 5-FdU-ale (191 mg/kg) were injected ip while 5-FdU (100 mg/kg) was injected subcutaneously in  $\sim 100$   $\mu$ l PBS, and administered weekly starting 1 week after tumor cell injection at the described dose.

### *In vivo Bioluminescence Imaging*

Anesthetized mice received 150 mg/kg D-luciferin substrate (Sigma-Aldrich, Munich, Germany) injected into the intra-peritoneal space. Dorsal and ventral views were imaged for all mice using the NightOwl planar imaging system (Berthold Technologies, Bad Wildbad, Germany). Tumor bioluminescence was quantified using the Indigo software (Berthold Technologies, Bad Wildbad, Germany)



### *Histological Analysis*

Limbs containing metastases detectable by bioluminescence were collected and fixed in 4% buffered formalin for 1 week. Limbs were embedded in paraffin and 5  $\mu\text{m}$  sections were prepared. Serial sections were inspected for the tibial region with the greatest cross-sectional tumor area, assessed by H and E staining. Sections were stained with Goldner's trichrome, imaged and tumor area quantified. A statistical outlier in the 5-FdU-ale group with a  $p < 0.01$  was excluded from calculations. Parallel sections were stained for tartrate-resistant acid phosphatase (TRAP) activity<sup>123</sup>. 150x300 pixel window was selected around the cortical bone-tumor interface with the greatest TRAP activity. Number of osteoclasts, as well as the bone-tumor interface length, was quantified using ImageJ (version 1.48a).

### *Lab Analysis*

Blood was collected from the tail vein prior to injection. Levels of skeletal osteoblast and osteoclast activity were assessed using an osteocalcin (DRG Diagnostics, Germany) and TRAP ELISA assays (Immunodiagnostic Systems, Frankfurt, Germany) on blood serum.

### *Micro-CT Analysis*

Changes in bone mineralization resulting from tumor formation were quantified by *in vivo* micro-CT. Anesthetized mice were placed in full-body holders and the tibiae aligned by visual inspection. Scans were made using a vivaCT 40 micro-CT (ScancoMedical, Brüttisellen, Switzerland) at an isotropic voxel size of 19  $\mu\text{m}$  (70 kVp, 114  $\mu\text{A}$ , 250 ms integration time, 1000 projections on 180° 2048 CCD detector array, cone-beam reconstruction). A 140-slice (2.45 mm) volume of interest (VOI), beginning at the most proximal slice of the epiphysis and extending into the metaphyseal region was defined in the baseline scan of each animal using an automated contouring method<sup>12</sup>. Baseline VOIs were transferred to the follow-up scans using an image registration approach to insure analysis of consistent VOIs at each time point<sup>15</sup>. Bone mineral density (BMD) was calculated from the greyscale micro-CT images (Image Processing Language v5.15, ScancoMedical, Brüttisellen, Switzerland). Z-slab subtraction images were generated from week 1 and 5 scan overlays using 20 slices within the transition zone between the diaphysis and metaphysis.

### *Drug Binding Assay*

4 Mice for each time period and each drug were injected with 5-FdU or 5-FdU-ale at the dose described above and sacrificed 1 day, 1 week or 2 weeks after injection. Excised long bones (tibia and femur) with removed muscle and flushed bone marrow were placed in 20  $\mu$ l decalcifying solution per mg bone. Absorbance of decalcifying fluid at 210 nm and 260 nm was determined 48 h after incubation with excised limbs and adjusted for control, non-drug-injected limbs. Absorbance readings at 210 and 260 nm were compared to standard curve generated for both 5-FdU and 5-FdU-ale to determine bone drug concentrations.

### *Statistical Analysis*

MTT assay results were fitted with three parameter dose-response inhibition curves. Comparison between groups was made using two-sample *t*-tests using the Welch-Satterthwaite method to avoid the assumption of equal variances. Outliers were assessed using the Grubbs' test with a significance level of 0.01. Micro-CT BMD (Table S1) and BV/TV (Table S2) results were analyzed using one-way ANOVAs and Bonferroni's multiple comparison tests. P-values <0.05 were considered to be statistically significant. All graphical and statistical analyses were generated using Prism (version 5, GraphPad Software, CA).

## Results

### *5-FdU-ale inhibits cell cycle progression in vitro*

To determine the relative toxicity of 5-FdU-ale on breast cancer, tumor cells were incubated with varying concentrations of 5-FdU, alendronate or 5-FdU-ale for 24 h and assessed for cell survival (Figure 10A). Treatment with 5-FdU-ale shows an intermediate trend of toxicity between alendronate and 5-FdU, with comparable log IC<sub>50</sub> values for 5-FdU and 5-FdU-ale and significantly lower values than for cells treated with alendronate alone (Figure 10B). Induced cell death was confirmed by western blot which showed cleavage of the caspase-3 substrate poly(ADP-ribose) polymerase (PARP) 24 and 48 h after treatment with 5-FdU, intermediate levels of PARP cleavage in 5-FdU-ale-treated cells and no notable PARP cleavage in cells treated with alendronate compared to untreated controls (Figure 10C). In addition, treatment with 5-FdU-ale showed a dose-dependent increase in levels of Cyclin E and decreased levels of p21, consistent with cells treated with 5-FdU, but failed to show an accumulation of unprenylated proteins associated with bisphosphonate treatment, as seen in alendronate-treated cells (Figure 10D). To study the effects of 5-FdU-ale on cell cycle progression, FACS analysis was performed on adherent cells (Figure 10E). Treatment with 5-FdU-ale resulted in a trend towards increased percentage of dead cells ( $P=0.0717$ ), significantly decreased numbers of cells in G1 phase and a trend towards increased cells in S phase ( $p=0.0634$ ) (Figure 10F). Treatment with 5-FdU similarly resulted in a trend of an increased percentage of dead cells ( $p=0.0880$ ) and a trend towards a significant increase in the number of cells in S phase, but showed a significant decrease in the percentage of cells in G2/M phase. Treatment with alendronate showed no significant changes in cell cycle progression.

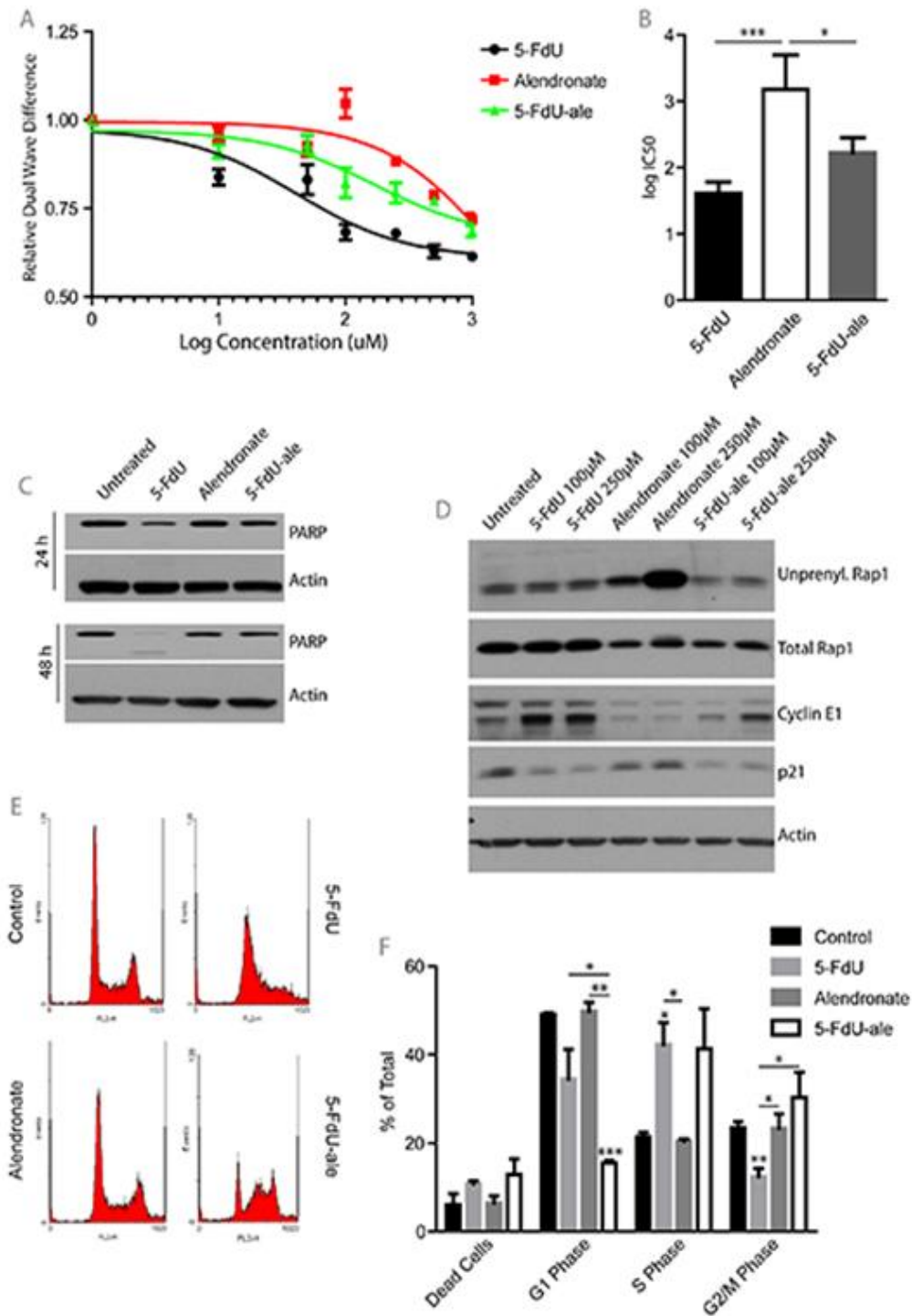


**Figure 10 5-FdU-ale toxicity in breast cancer is mediated by cell cycle arrest *in vitro*.** Cells were treated with varying concentrations of 5-FdU, alendronate or 5-FdU-ale for 24 h and assessed for cell death (A). Treatment with 5-FdU or 5-FdU-ale show comparable log IC<sub>50</sub> values significantly lower than cells treated with alendronate (B). Analyses of PARP 24 and 48 h after treatment revealed increased cleavage in cells treated with either 5-FdU or 5-FdU-ale (C). Analysis of 24 h-treated whole cell lysates show a dose-dependent accumulation of Cyclin E and reduced levels of p21 in 5-FdU-ale-treated cells, consistent with 5-FdU treatment, while treatment with alendronate results in increased accumulation of unprenylated Rap1 (D). FACS analyses were performed to assess cell cycle progression of treated cells (E). Untreated and alendronate-treated cells were found primarily in G1 phase while treatment with 5-FdU and 5-FdU-ale show an accumulation of dead cells and cells in S phase (F). (\*p<0.05, \*\*p<0.01, \*\*\*p<0.001)

*Treatment with 5-FdU-ale significantly reduces the number and size of bone metastases in vivo*

Mice were injected intracardially with tumor cells and the formation of bone metastases was monitored weekly by bioluminescent imaging (Figure 11A). Treatment with 5-FdU, alendronate or 5-FdU-ale significantly reduced the average number of bioluminescent tumors per mouse (Figure 11B), as well as the bioluminescent tumor size compared to untreated controls (Figure 11C). Additionally, treatment with alendronate showed a further significant reduction in bioluminescent tumor size compared to mice treated with 5-FdU or 5-FdU-ale. Because drug treatments showed altered levels of tumor cell bioluminescence *in vitro* (Figure S1), tumor size was further quantified from histological sections (Figure 12A). Tibial sections containing the greatest cross-sectional tumor area were stained with Goldner's trichrome and tumor area quantified (Figure 12B). Mice treated with 5-FdU showed significant increases in tumor area compared to untreated controls. Mice treated with 5-FdU-ale showed a significant reduction in tumor area compared to untreated mice or mice treated with either 5-FdU or alendronate alone.

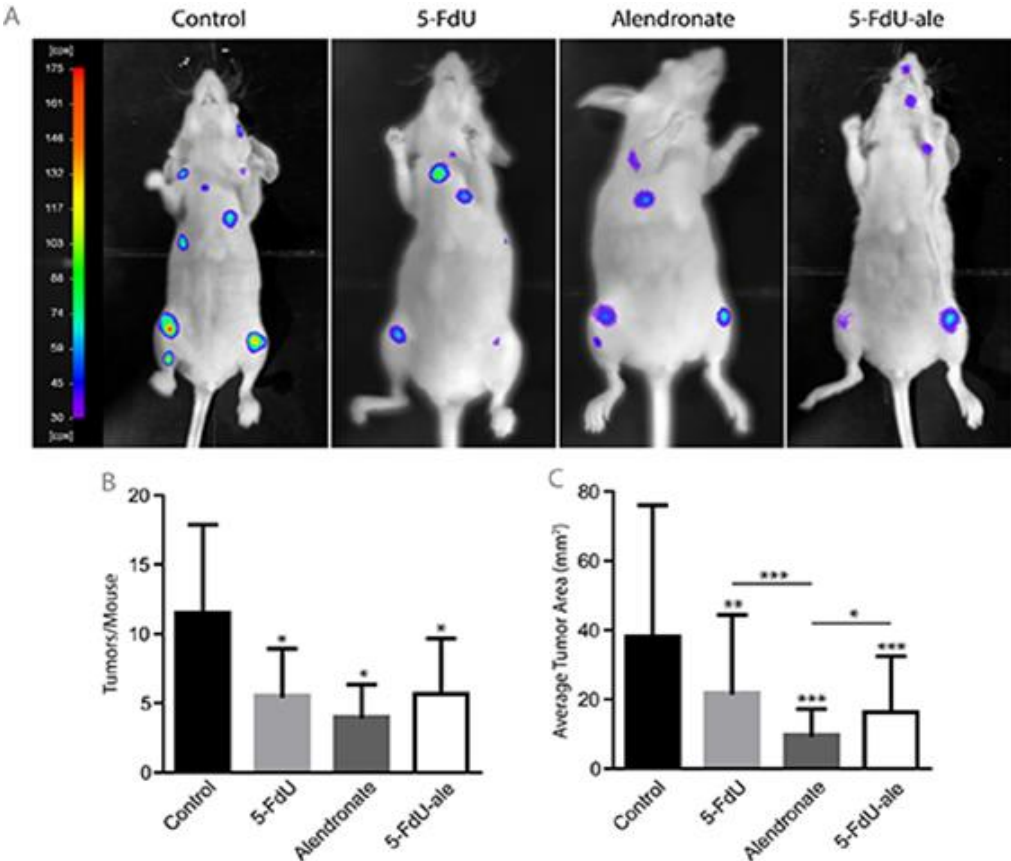


Figure 11 Treatment with 5-FdU-ale reduces the frequency and size of bone metastases *in vivo*. Mice were intracardially-injected with the breast cancer cell line MDA-MB-231 and imaged weekly for 5 weeks by bioluminescence (A). Mice treated with 5-FdU, alendronate or 5-FdU-ale show significant reductions in the number of bioluminescent tumors per mouse (B), as well as the average bioluminescent tumor area (C), relative to untreated control mice. (\*p<0.05, \*\*p<0.01, \*\*\*p<0.001) (n=12)

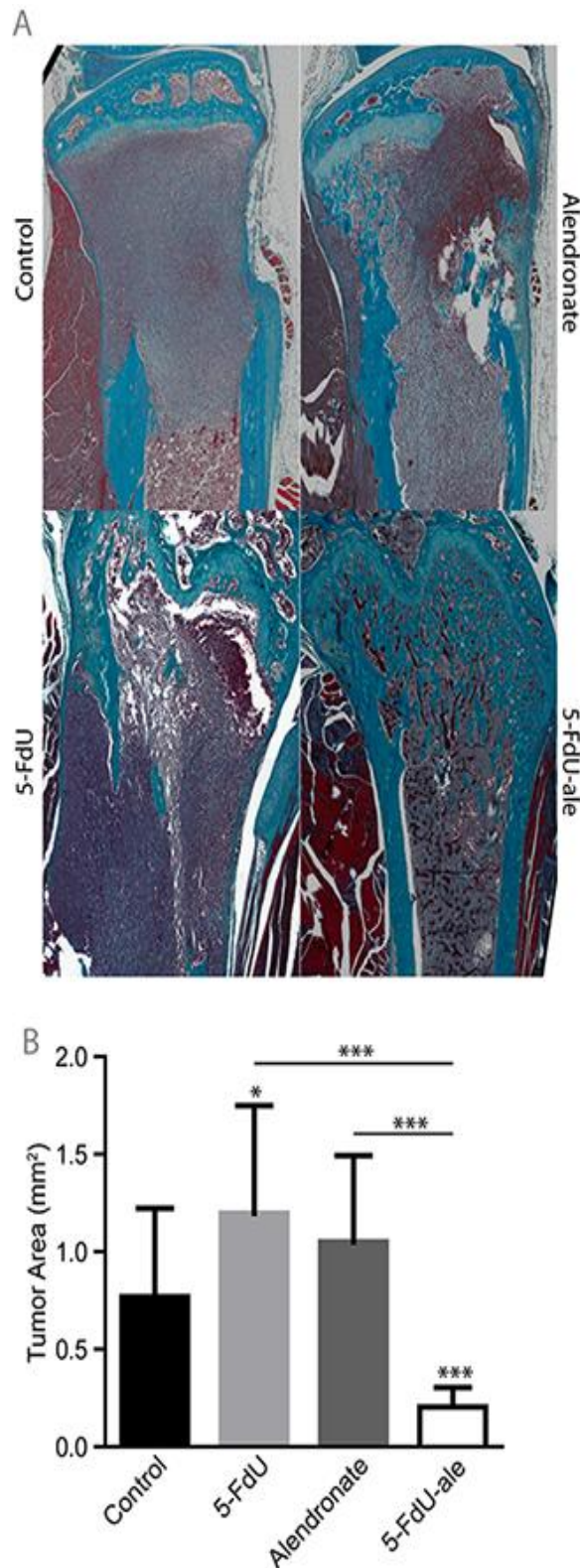


Figure 12 **Mice treated with 5-FdU-ale show significant reductions in tumor burden.** Limbs found to contain bioluminescent tumor signals were further analyzed by histology for tumor area. Sections containing the greatest tumor burden were stained with Goldner's trichrome (A). Mice treated with 5-FdU showed significantly increased tumor areas compared to untreated mice while mice treated with 5-FdU-ale show significantly smaller tumor areas compared to mice treated with either 5-FdU or alendronate (B). (\*p<0.05, \*\*p<0.01) (n=10)

*Treatment with 5-FdU-ale significantly attenuates disruption of normal bone morphology*

To determine the systemic effects of 5-FdU-ale on bone metabolism, serum levels of the osteoblast marker osteocalcin and the osteoclast marker TRAP were quantified (Figure 13). Osteocalcin levels were maintained in mice treated with 5-FdU-ale, comparable with untreated mice. In contrast, treatment with either 5-FdU or alendronate led to significant reductions in osteocalcin levels compared to both untreated and 5-FdU-ale-treated mice (Figure 13A). Serum TRAP levels were significantly reduced in mice treated with alendronate, and a trend towards decreased TRAP activity in mice treated with 5-FdU-ale ( $p=0.0736$ ) was observed relative to mice treated with 5-FdU (Figure 13B). In addition, osteoclast numbers along cortical bone-tumor surface interfaces were determined in histological sections (Figure 14A). Mice treated with 5-FdU-ale showed significantly fewer osteoclasts compared to untreated mice, as well as mice treated with either 5-FdU or alendronate alone (Figure 14B). To assess changes in bone mineralization, tumor-burdened tibia were imaged weekly by *in vivo* micro-CT. Mice treated with alendronate or 5-FdU-ale show significantly increased relative BMD values as compared to either untreated mice or mice treated with 5-FdU (Figure 15A). BV/TV analysis revealed mice treated with 5-FdU-ale exhibit significantly greater values compared to mice treated with alendronate alone, which in turn showed significantly greater BV/TV values from untreated and 5-FdU-treated mice (Figure 15B). Treatment with 5-FdU-ale also significantly reduced loss of BMD values from week 4 to week 5 compared to untreated mice (Figure 15C) while corresponding losses in BV/TV values failed to show any significant differences in any of the treatment groups (Figure 15D). Consistent with bone mineral assessments and serum analyses, mice treated with 5-FdU-ale showed minimal regions of bone resorption along with regions of robust bone formation within the trabeculae (figure 15E), while treatment with alendronate resulted in reduced regions of bone resorption and mice treated with 5-FdU showed increased regions of osteolysis compared to control mice.



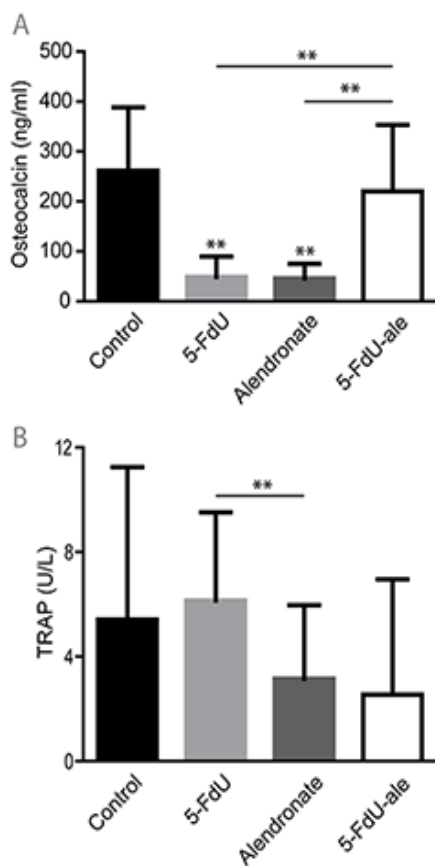


Figure 13 **Mice treated with 5-FdU-ale results in significantly greater osteoblast activity than mice treated with 5-FdU or alendronate.** Systemic effects of drug treatment were assessed in the serum of week 5 mice. Treatment with 5-FdU or alendronate significantly decreased the levels of the osteoblast marker osteocalcin compared to untreated mice while treatment with 5-FdU-ale resulted in significantly elevated levels of osteocalcin compared to other drug-treated groups (A). Analysis of the osteoclast activity marker TRAP shows significantly reduced levels in alendronate-treated mice, as well as a trend towards decreased levels in 5-FdU-ale-treated mice ( $p=0.0736$ ), compared to mice treated with 5-FdU (B). (\*\* $p<0.01$ ) ( $n=12$ )

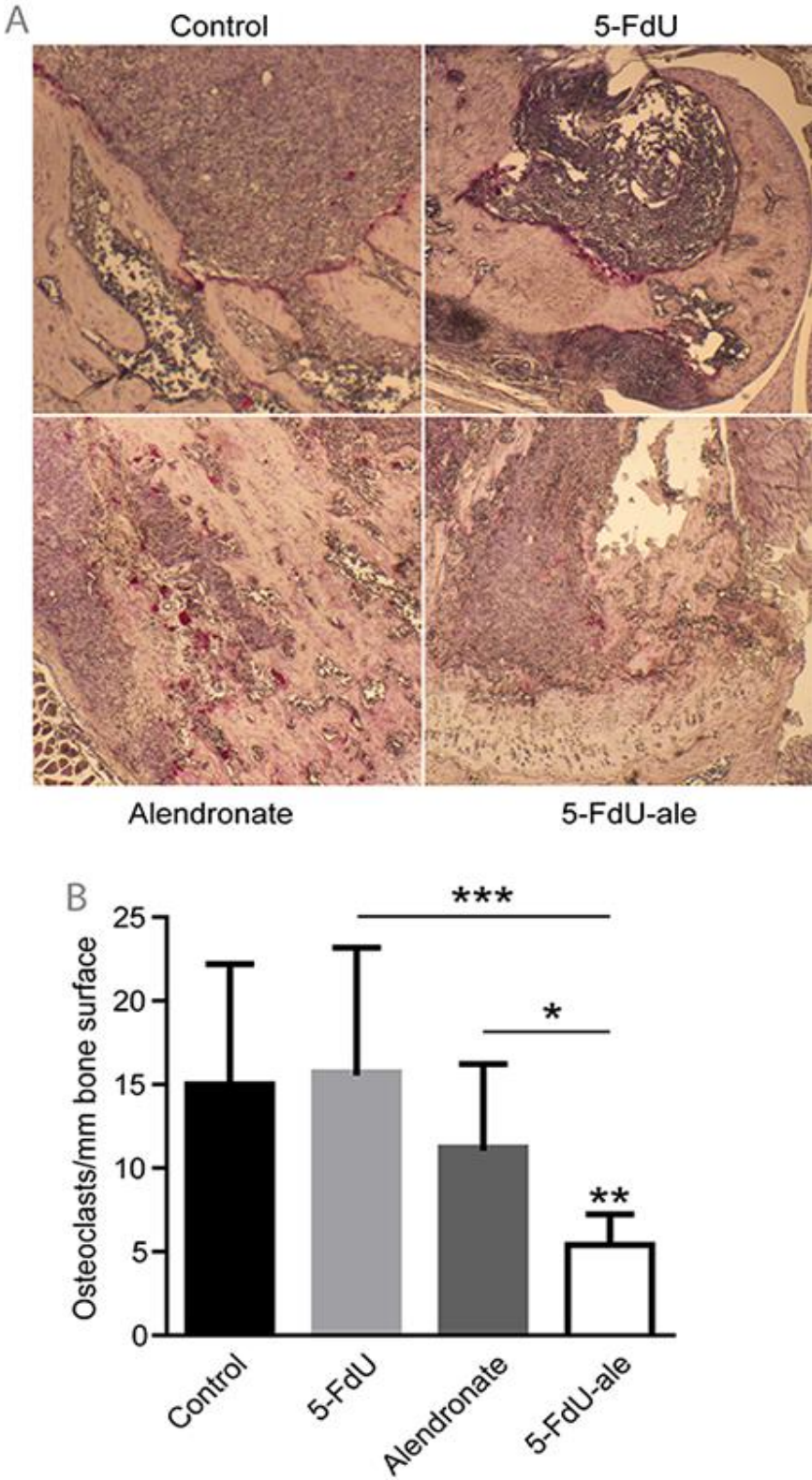
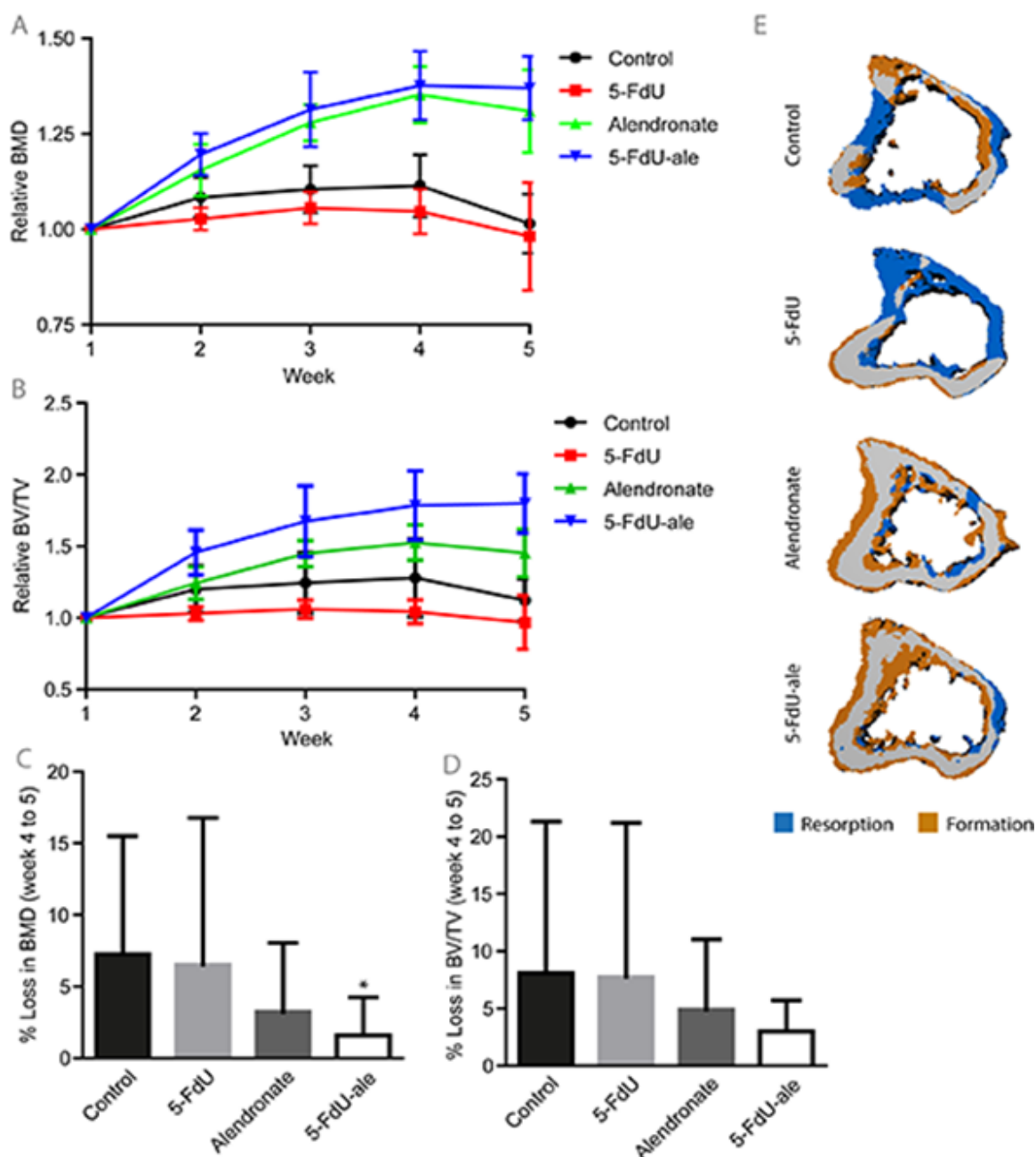


Figure 14 **Treatment with 5-FdU-ale significantly reduces the number of tumor-associated osteoclasts.** Limb sections were stained for TRAP activity and the number of osteoclasts was quantified along tumor-cortical bone surfaces (A). Mice treated with 5-FdU-ale showed significantly fewer osteoclasts than untreated mice or mice treated with 5-FdU or alendronate (B). (\* $p < 0.05$ , \*\* $p < 0.01$ , \*\*\* $p < 0.001$ ) (n=8)



**Figure 15 Mice treated with 5-FdU-ale show increased bone quality.** Changes in bone mineralization was assessed by weekly *in vivo* micro-CT. Mice treated with either alendronate or 5-FdU-ale show significantly increased BMD values compared to untreated mice or mice treated with 5-FdU (A). Treatment with 5-FdU-ale was also found to significantly increase BV/TV values compared to mice treated with alendronate, which in turn showed significantly increased BV/TV values compared to both untreated mice or mice treated with 5-FdU (B). Statistical analyses are found in Table S1 and S2. Measurements of bone loss from week 4 to week 5 found treatment with 5-FdU-ale resulted in significant reductions in BMD values compared to untreated mice (C), while analyses of changes in BV/TV values show no significant differences between any groups (D). Negative subtraction images were generated to assess localized bone turnover visualized in z-slabs of bone in the proximal tibia metaphysis (E). Treatment with alendronate reduces regions of bone resorption while treatment with 5-FdU-ale results in decreased bone resorption as well as increased bone formation. (\* $p < 0.05$ ) (n=10)

*5-FdU-ale shows prolonged retention on the bone*

To assess the stability and affinity of 5-FdU-ale for the bone *in vivo*, mice were given a single standard dose injection of 5-FdU or 5-FdU-ale and assessed for drug retention over time (Figure 16). 5-FdU-ale was detected at significantly greater concentrations than 5-FdU 1 day after injection and continued to be detected at significantly greater values for up to 2 weeks after injection.

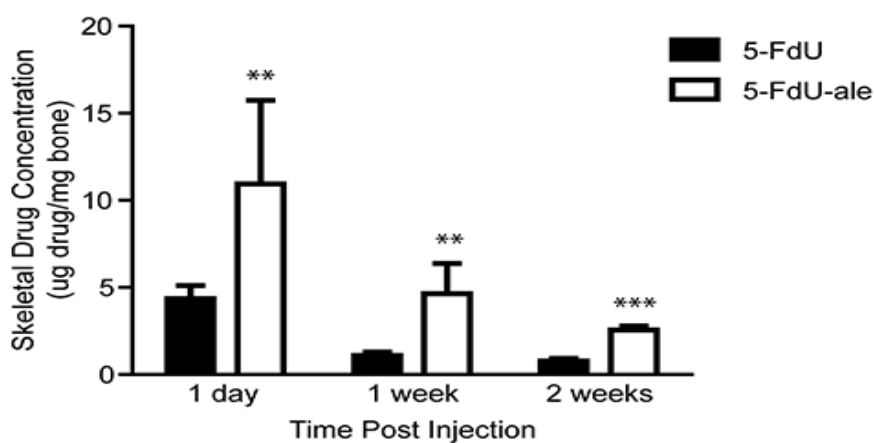


Figure 16 **5-FdU-ale is detectable on the bone several weeks after injection at levels significantly greater than 5-FdU alone.** Tumor-free mice were given a single injection of either 5-FdU or 5-FdU-ale and assessed for bone drug retention of the hind limbs. 5-FdU-ale was detected at significantly greater levels in mice 1 day after injection and persisted at significantly elevated levels, relative to 5-FdU, for up to 2 weeks after injection. (\*\* $p < 0.01$ , \*\*\* $p < 0.001$ ) (n=4)

## Discussion

With thousands of patients diagnosed with breast cancer every year, new treatments are needed to combat, not just the primary tumor, but the secondary metastases which complicate treatment and severely depress the patient's quality of life. Here, we present a novel drug conjugate between the anti-metabolite 5-FdU and the bisphosphonate alendronate for the treatment of breast cancer bone metastases. *In vitro*, 5-FdU-ale functions mechanistically similar to 5-FdU, inhibiting cell cycle progression at similar IC<sub>50</sub> concentrations. Further analyses revealed that 5-FdU-ale does not show bisphosphonate-mediated inhibition through inhibition of protein prenylation. Treatment of mice injected with a bone-homing breast cancer cell line variant with 5-FdU-ale showed significant reductions in both bioluminescent tumor number and area compared to untreated control. Since tumor bioluminescence can be affected by many variables, such as tumor perfusion and levels of skeletal destruction, tumor-burdened tibia were excised and analyzed histologically. Mice treated with 5-FdU-ale showed significant reductions in tumor area compared to mice treated with either 5-FdU or alendronate alone. Mice treated with 5-FdU showed significantly increased tumor areas compared to untreated controls while bioluminescence assessment showed significant reductions in tumor area. Our data, along with previous reports, have shown that treatment with 5-FU or 5-FdU can upregulate expression of the ATP-binding cassette transporter member ABCG2/BCRP<sup>155</sup>. Since D-luciferin has been identified as a substrate of ABCG2, transport activity could reduce the cytoplasmic levels of the bioluminescent substrate, reducing bioluminescent signal<sup>160</sup> and possibly explaining the differential results obtained between histology and bioluminescence. Alendronate has also been previously shown to have anti-angiogenic activity<sup>57</sup> which could also result in reduced delivery of the luciferin throughout the tumor, diminishing bioluminescent signal. These aspects highlight the need for caution when using bioluminescent imaging in the context of therapeutic interventions and the need for confirmatory histology.

Analyses of serum biomarkers revealed that, while treatment with 5-FdU or alendronate significantly reduced the levels of the osteoblast marker osteocalcin, mice treated with 5-FdU-ale showed no impairment of osteoblast function, with serum osteocalcin levels comparable to untreated

mice. Analysis of the osteoclast activity marker TRAP showed significant reductions in mice treated with alendronate and a trend towards decreased TRAP activity ( $p=0.0736$ ) in mice treated with 5-FdU-ale. This highlights a significant draw back in current bisphosphonate treatments in that, while they preferentially target and inhibit bone resorption, bone formation is often inhibited as well<sup>3</sup>. Serum analyses suggest 5-FdU-ale inhibits bone-resorbing osteoclast without negatively impacting bone-forming osteoblasts. As a result, treatment with 5-FdU-ale has the potential to reduce the fracture risk of patients even further, compared to classical bisphosphonate treatment<sup>145</sup>. With inhibition of osteoclast activity, a disruption of the vicious cycle between the bone microenvironment and tumor cells is expected to occur which may also be a contributing factor in the observed reduction in tumor size. Without the osteolytic activity of osteoclasts, tumor cells are no longer stimulated by growth factors released from the resorbed bone matrix and, with unperturbed osteoblast activity, may even be physically constrained by the bone, limiting size and possibly preventing secondary metastases by hindering the “seed and soil” mechanism of tumor spread<sup>79, 115, 116</sup>.

Analyses of histological sections showed a significant reduction in the number of osteoclasts present along the bone-tumor interface in mice treated with 5-FdU-ale compared to untreated mice as well as mice treated with either 5-FdU or alendronate. Consistent with previous findings, treatment with alendronate alone failed to show a significant reduction in osteoclast numbers associated with bone lesions<sup>64</sup>. *In vivo* longitudinal micro-CT demonstrated that mice treated with 5-FdU-ale or alendronate resulted in significantly greater BMD values compared to 5-FdU or untreated controls as well as a significant reduction in loss of BMD values from week 4 to 5. Bone volume analyses also revealed significantly greater BV/TV values in 5-FdU-ale-treated mice compared to alendronate, 5-FdU or untreated mice. Preferential increases in BV/TV relative to BMD values in mice treated with 5-FdU-ale, as compared to mice treated with alendronate, suggest that even in the presence of a lytic bone tumor, new, lowly mineralized bone is present within the tibia, consistent with serum results which suggest 5-FdU-ale inhibits osteoclast activity without inhibiting osteoblasts. This conclusion is supported by negative subtraction images which show new bone formation in the trabeculae within tumor-burdened limbs.

To determine stability and longevity *in vivo*, we next assayed the retention characteristics of 5-FdU and 5-FdU-ale. 5-FdU-ale is present in the bone in greater concentrations than 5-FdU 1 day after injection and remains on the bone at significantly greater concentrations for as long as 2 weeks after a single injection. This highlights an important advantage of targeted drug therapy. 5-FdU has a relatively short half-life in the blood stream and can be taken up by a variety of different cell types causing off-target effects. Because of its conjugation with alendronate, 5-FdU-ale is specifically targeted to the bone and remains there for extended periods of time. This substantially increases both its concentration in the bone and the window of its activity compared to 5-FdU. The use of radioactively-labeled 5-FdU-ale should provide a more sensitive, quantitative assessment of long-term binding within the bone environment. Our results also demonstrate the high stability of 5-FdU-ale, as the conjugated drug remains linked within the bone environment for several weeks. This longevity, stability and high specificity towards bone greatly contributes to 5-FdU-ale's ability to function as an anti-tumor drug within the bone environment.

In summary, 5-FdU-ale is a novel bone-targeted drug conjugate which combines the anti-tumor effects of 5-FdU with the bone-homing qualities of alendronate. Mice treated with 5-FdU-ale showed significant reductions in tumor size and significant increases in bone health measures. Because treatment with 5-FdU or alendronate alone failed to show any significant reductions in tumor size by histological analyses, it is likely that both anti-tumor and pro-bone forming effects are responsible for the observed reduction in tumor burden. Further work is required to reveal optimal treatment regimens i.e. dosing and injections frequencies. With preferential targeting of osteoclasts, without inhibiting osteoblast function, it remains to be seen whether 5-FdU-ale has the potential to serve in the therapeutic application for other cancers and diseases associated with excessive bone turnover/loss. It also remains to be determined whether possible depot effects and interactions with the microenvironment of the metastatic niche could be used as a preventative treatment against the initial formation of bone metastases. Overall, 5-FdU-ale has great potential as a novel therapeutic in the treatment of breast cancer bone metastases and other bone-related illnesses.



## **Acknowledgements**

The authors are grateful to Gabriele Trompke from the MOIN CC for her assistance preparing histological bone sections and the support of Professor Acil from the UKSH MKG for the use of the microscope. We would also like to thank Frank Rösel and Sigrid Hamann from the department of gynecology for assistance with the MTT assay and analyses of the histological sections. Financial support was provided by the Deutsche Forschungsgemeinschaft (DFG) through the forscherguppe 1586 SKELMET and by the research grant from the state of Schleswig-Holstein and the European Union ERDF-European Regional Development Fund (MOIN CC, Zukunftsprogramm Wirtschaft).

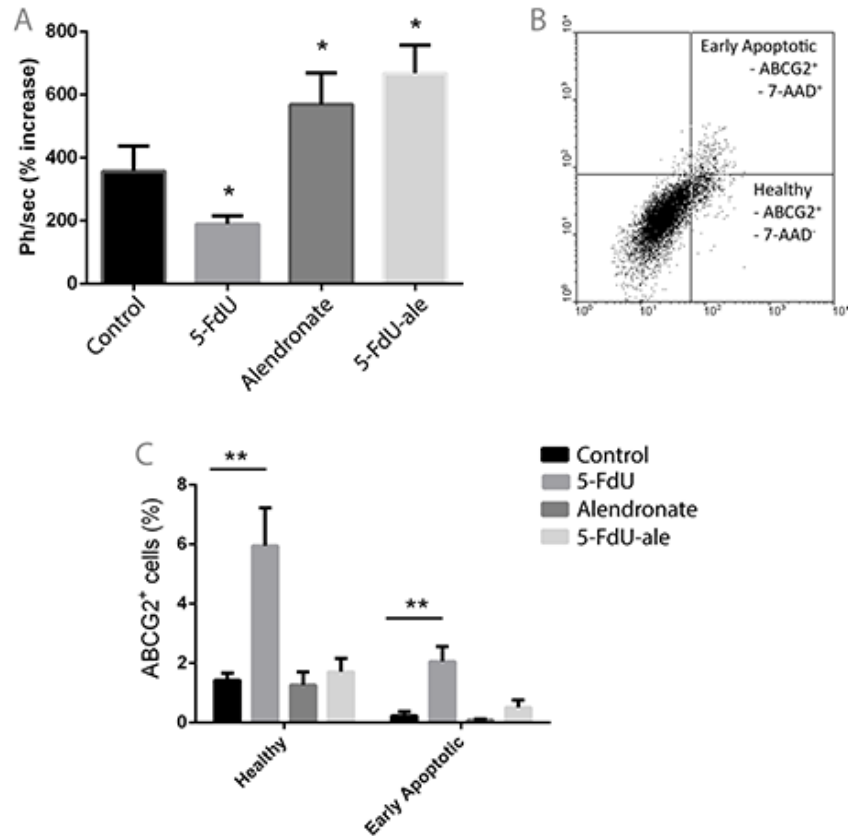


Figure S1 **Treatment with 5-FdU, alendronate or 5-FdU-ale results in altered bioluminescence *in vitro*.** Bioluminescent signal of plated cells was measured prior to drug administration and following treatment for 36 hours with 100 $\mu$ M of the respective drug (A). FACS analyses of ABCG2 expression in living cells was performed by gating on the live population of cells according to the forward scatter and side scatter profile and placing quadrant gates for determining populations of cells expressing 7-AAD and ABCG2 (B). Cells positive for 7-AAD expression were deemed to be early apoptotic cells. Expression of ABCG2 in healthy and early apoptotic cells 36 hours following drug treatment (C). Treatment with 5-FdU significantly increases the number of ABCG2-expressing cells.

Table S1 **Treatment with alendronate of 5-FdU-ale results in significantly greater BMD values than untreated mice or mice treated with 5-FdU.** Statistical analyses of BMD values from untreated mice and mice treated with 5-FdU, alendronate or 5-FdU-alendronate.

One-way analysis of variance						
P value	P<0.0001					
P value summary	***					
Are means signif. different? (P < 0.05)	Yes					
Number of groups	4					
F	36.97					
R squared	0,7601					
Bartlett's test for equal variances						
Bartlett's statistic (corrected)	3,045					
P value	0,3847					
P value summary	ns					
Do the variances differ signif. (P < 0.05)	No					
ANOVA Table						
	SS	df	MS			
Treatment (between columns)	1,286	3	0,4286			
Residual (within columns)	0,4057	35	0,01159			
Total	1,691	38				
Bonferroni's Multiple Comparison Test						
	Mean Diff.	t	Significant? P < 0.05?	Summary	95% CI of diff	
Control vs 5-FdU-ale	-0,3623	6,925	Yes	***	-0.5086 to -0.2160	
Control vs Alendronate	-0,2947	5,632	Yes	***	-0.4410 to -0.1484	
Control vs 5-FdU	0,05806	1,262	No	ns	-0.07058 to 0.1867	
5-FdU-ale vs Alendronate	0,06763	1,256	No	ns	-0.08292 to 0.2182	
5-FdU-ale vs 5-FdU	0,4204	8,809	Yes	***	0.2869 to 0.5538	
Alendronate vs 5-FdU	0,3527	7,392	Yes	***	0.2193 to 0.4862	

Table S2 **Treatment with 5-FdU-ale results in significantly greater BV/TV values than untreated mice or mice treated with 5-FdU or alendronate.** Statistical analyses of BV/TV values from untreated mice and mice treated with 5-FdU, alendronate or 5-FdU-alendronate.

One-way analysis of variance						
P value	P<0.0001					
P value summary	***					
Are means signif. different? (P < 0.05)	Yes					
Number of groups	4					
F	49,72					
R squared	0,8100					
Bartlett's test for equal variances						
Bartlett's statistic (corrected)	0,8788					
P value	0,8305					
P value summary	ns					
Do the variances differ signif. (P < 0.05)	No					
ANOVA Table						
	SS	df	MS			
Treatment (between columns)	4,491	3	1,497			
Residual (within columns)	1,054	35	0,03011			
Total	5,545	38				
Bonferroni's Multiple Comparison Test						
	Mean Diff.	t	Significant? P < 0.05?	Summary	95% CI of diff	
Control vs 5-FdU-ale	-0,6991	8,292	Yes	***	-0.9349 to -0.4633	
Control vs Alendronate	-0,3289	3,901	Yes	**	-0.5647 to -0.09312	
Control vs 5-FdU	0,1904	2,569	No	ns	-0.01689 to 0.3978	
5-FdU-ale vs Alendronate	0,3702	4,267	Yes	***	0.1276 to 0.6128	
5-FdU-ale vs 5-FdU	0,8895	11,57	Yes	***	0.6745 to 1.105	
Alendronate vs 5-FdU	0,5193	6,753	Yes	***	0.3043 to 0.7344	

Chapter 2.3

Modified from:

Tower RJ, Campbell GM, Müller M, Will O, Glüer CC and Tiwari S. (2014) Binding kinetics of a fluorescently-labeled bisphosphonate as a tool for dynamic monitoring of bone mineral deposition *in vivo*. *J Bone Miner Res*, 29(9):1993-2003

**Title Page**

Binding kinetics of a fluorescently-labeled bisphosphonate as a tool for dynamic monitoring of bone mineral deposition *in vivo*

Tower R. J., Campbell G. M., Müller M., Will O., Glüer C. C., Tiwari S.

Section Biomedical Imaging, Department of Diagnostic Radiology, University Hospital Schleswig-Holstein, Campus Kiel, Germany

Address correspondence to: Sanjay Tiwari, PhD [stiwari@email.uni-kiel.de](mailto:stiwari@email.uni-kiel.de) +494318805836

No supplemental data has been included in the submission

Disclosures:

Research support was provided by Perkin Elmer in the form of discounted reagents.

## **Abstract**

Bone mineral deposition during the modeling of new bone and remodeling of old bone can be perturbed by several pathological conditions, including osteoporosis and skeletal metastases. A site-specific marker depicting the dynamics of bone mineral deposition would provide insight into skeletal disease location and severity, and prove useful in evaluating the efficacy of pharmacological interventions. Fluorescent labels may combine advantages of both radioisotope imaging and detailed microscopic analyses. The purpose of this study was to determine if the fluorescent bisphosphonate Osteosense could detect localized changes in bone mineral deposition in established mouse models of accelerated bone-loss (ovariectomy) (OVX) and anabolic bone-gain resulting from parathyroid hormone (PTH) treatment. We hypothesized that the early rate of binding, as well as the total amount of bisphosphonate which binds over long periods of time, could be useful in evaluating changes in bone metabolism. Evaluation of the kinetic uptake of bisphosphonates revealed a significant reduction in both the rate constant and plateau binding after OVX, while treatment with PTH resulted in a 36-fold increase in the bisphosphonate binding rate constant compared to untreated OVX controls. Localization of bisphosphonate binding revealed initial binding at sites of ossification adjacent to the growth plate and, to a lesser extent, along more distal trabecular and cortical elements. Micro-CT was used to confirm that initial bisphosphonate binding is localized to sites of low tissue mineral density, associated with new bone mineral deposition. Our results suggest monitoring binding kinetics based on fluorescently-labeled bisphosphonates represent a highly sensitive, site-specific method for monitoring changes in bone mineral deposition with the potential for translation into human applications in osteoporosis and bone metastatic processes and their treatment.

**Keywords:** Bisphosphonates, Molecular Imaging, Bone Turnover, Bone Mineralization, Osteoporosis

## Introduction

Bone is in a continual state of remodeling, which facilitates mineral transport and provides structural integrity. This tightly regulated process is mediated through bone-resorbing osteoclasts and bone-forming osteoblasts. Maintaining the balance of these two dynamic processes is essential to ensure skeletal homeostasis. Many diseases upset this balance and result in either general or localized bone loss or gain. Therefore, the measurement of the rates of bone formation and resorption can be indicative of disease severity. Bone formation and resorption can be measured using immunoassays that measure the serum concentration or urinary excretion of bone turnover biomarkers<sup>31</sup>. However, these markers provide an assessment only of the overall skeletal dynamics and fail to localize aberrant cellular function to a specific location. Current standard radiological modalities such as radiographs, bone densitometry and computed tomography (CT) provide a static assessment of bone mineral and structure<sup>89</sup>, but do not describe the cellular dynamics of osteoblasts and osteoclasts<sup>144</sup>. Radioisotope labeling provides insights into bone turnover using scintigraphy (bone scan), or tomographic methods like Single Photon Emission Computed Tomography (SPECT) or Positron Emission Tomography (PET)<sup>7, 132</sup>. Optical molecular imaging, where photons are detected from enzymatic reactions (bioluminescence) or fluorescent proteins or dyes (fluorescence), offers the possibility to assess the complex and highly regulated site-specific processes associated with bone remodeling<sup>134</sup> longitudinally, thus circumventing the limitations associated with static assessment of bone mineral and structure.

Because of their high affinity for bone and their ability to inactivate osteoclast activity, bisphosphonates have become a widely utilized treatment option for diseases with high bone turnover, such as osteoporosis, Paget's disease and cancer-associated bone diseases<sup>110</sup>. Nitrogen-containing bisphosphonates function by inhibiting the intracellular enzyme farnesyl pyrophosphate synthase, depleting isoprenoid lipids used in the prenylation of protein<sup>38, 70</sup>. This results in the accumulation of unprenylated proteins with aberrant functions within the cell<sup>31</sup>. With the conjugation of infrared and near-infrared fluorescent dyes, bisphosphonates are now being assessed for their utility as a tool for monitoring bone dynamics in preclinical models. Recent works have demonstrated the complexity of



bisphosphonate binding, showing not only binding to newly mineralized bone surfaces, but uptake by osteoclasts, bone marrow monocytes and osteocyte lacunae<sup>111</sup>. It has also been shown that while the potency of inhibition of farnesyl pyrophosphate synthase strongly correlates with anti-resorptive potency *in vivo*, bisphosphonate affinity also plays a critical role in skeletal uptake, distribution and retention<sup>113</sup>.

Along with determining their skeletal distribution, researchers have attempted to use fluorescently-conjugated bisphosphonates as a tool for monitoring changes in skeletal metabolism. With the use of molecular imaging, fluorescent bisphosphonates are now being assayed for their ability to label skeletal regions associated with increased bone formation, such as bone fracture healing and skeletal metastases<sup>71, 72</sup>. These studies demonstrate bisphosphonate binding to bone occurs not only to regions of robust osteoblast activity, but also to quiescent bone surfaces. Longitudinal studies have also used fluorescent bisphosphonates as a tool to monitor changes in bone metabolism resulting from mechanical loading using fluorescent molecular tomography (FMT)<sup>76</sup>. FMT sequentially obtains excitation and fluorescent emission measurements to allow the quantitative, 3-dimensional determinations of fluorescence probes *in vivo*<sup>50, 85, 94</sup>. Lambers *et al.* recently showed acceptable reproducibility of FMT imaging and reasonable correlations between loss of fluorescent intensity of Osteosense and the bone resorption rate determined from micro-computed tomography (micro-CT) ( $R^2=0.81$ ,  $p<0.01$ ). However, no significant difference in fluorescent intensity loss was observed between treatment groups. Similarly, while significant increases in Osteosense binding were observed after loading compared to control mice ( $p<0.05$ ), large intra-group variation resulted in a lack of significant correlation with dynamic bone formation determined by micro-CT.

These previous studies<sup>72, 76</sup> focused on bisphosphonate localization 24 h after injection and assayed for binding capacity assuming a correlation to bone formation. Their data document both the strengths and limitations of fluorescent measurements based on assessments of binding plateaus reached 24 h after injection. While they were able to detect changes in bisphosphonate uptake, these studies were not able to account for the dynamics of bisphosphonate binding at earlier time points affected by the affinity of the bisphosphonate used in relation to changes in the pattern of mineral

deposition and resorption. With the injection of sub-saturation concentrations of bisphosphonates in which not all potential binding sites will be occupied, the analysis of bisphosphonate binding levels 24 h after injection does not necessarily reflect binding capacity. The specific measurement of both the rate of bisphosphonate uptake as well as the binding plateau may better reflect interaction of these compounds within the bone matrix. The aim of this study was to determine whether binding kinetics of bisphosphonates, assessed by repeated FMT measurements during the early phase of bisphosphonate binding, could temporally resolve localized changes in bisphosphonate uptake in bone-loss and bone-gain mouse models *in vivo*.

## Materials and Methods

### *Animals*

12 week old female, CD-1 nude mice were purchased from Charles River (Wilmington, MA). All animals were kept in a temperature and humidity-controlled environment, with a 12 h light/dark cycle, with access to food and water *ad libitum*. Animal experiments and care were in accordance with the guidelines of institutional authorities and approved by the Ethics Committee for Animal Experiments at Christian-Albrechts-Universität-zu-Kiel [V 312-72241.121-33]. Mice were anesthetized with intraperitoneal injections of 80 mg/kg ketamine (Aveco Pharmaceutical, IA) and 10 mg/kg xylazine (Rugby Laboratories, GA). For long term anesthetization, additional half-dose administrations of ketamine and xylazine was given upon initial signs of waking. Animals were separated into 3 groups. 9 non-operated control animals, 9 ovariectomized (OVX) animals, imaged 3 days (short-term) and 14 days (long-term) after OVX, and 9 PTH treated mice which were OVX for 11 days, then received daily PTH injections for 3 days for a total of 14 days OVX and 3 days PTH treatment (Figure 17). PTH-treated and long-term OVX mice were further divided into two groups with 7 mice being subjected to kinetics analysis and 2 mice used for non-decalcified sectioning as described later. Animals were ovariectomized via their dorsal side. Human parathyroid hormone fragment 1-34 (Sigma-Aldrich, MO) was given subcutaneously at a dose of 100 µg/kg daily.

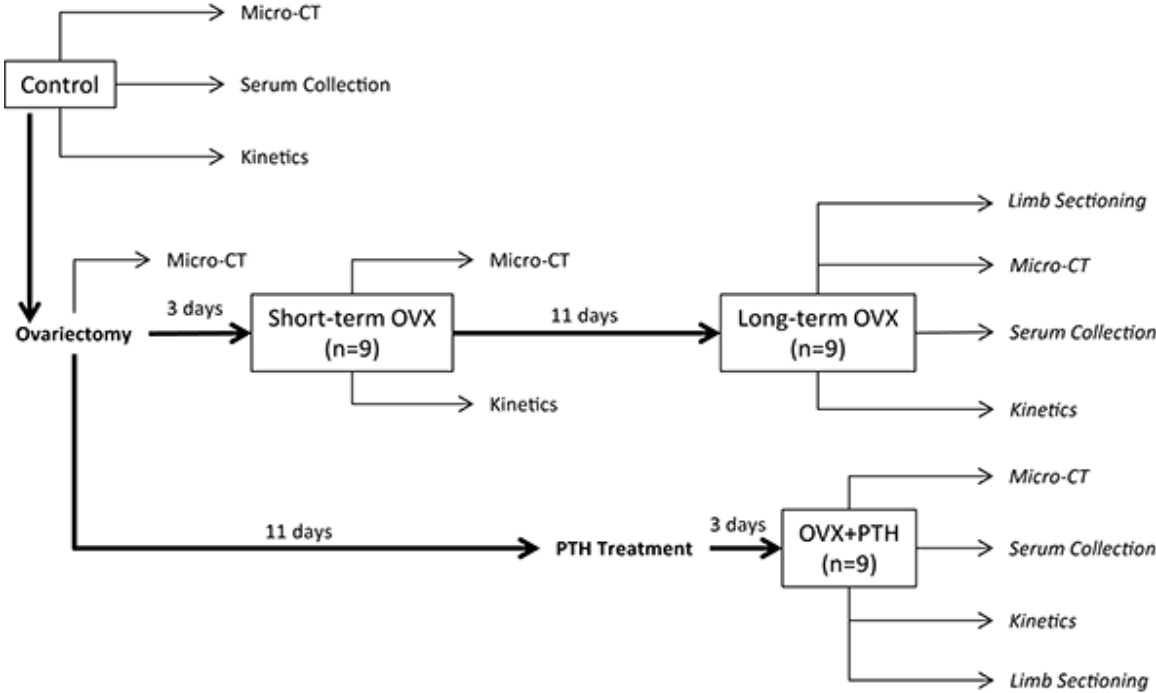


Figure 17 **Study design overview.** Sample groups are boxed, treatments are bolded and experimental measurements are italicized.

### *In Vivo Micro-CT Analysis*

Confirmation of expected bone loss or gain resulting from ovariectomy or PTH treatment was obtained from micro-CT assessment of skeletal changes *in vivo*. Anesthetized mice were placed in full-body holders and the tibiae aligned by visual inspection. Scans were made using a vivaCT 40 micro-CT (ScancoMedical, Brüttisellen, Switzerland) at an isotropic voxel size of 19  $\mu\text{m}$  (70 kVp, 114  $\mu\text{A}$ , 250 ms integration time, 1000 projections on 180° 2048 CCD detector array, cone-beam reconstruction). A 60-slice (1.05 mm) volume of interest (VOI), beginning at the most proximal point of the epiphyseal trabecular bone and extending into the metaphyseal region, and drawn along the periosteal surface, was defined in the baseline scan of each animal using an automated contouring method<sup>12</sup>. Baseline VOIs were transferred to the follow-up scans using an image registration approach to insure analysis of consistent VOIs at each time point<sup>15</sup>. Bone mineral density (BMD) was calculated from the greyscale micro-CT images as the mineral content divided by the total volume, encompassing both bone tissue and marrow (Image Processing Language v5.15, ScancoMedical, Brüttisellen, Switzerland).

### *Bisphosphonate Binding Kinetics*

Anesthetized mice were injected intravenously with 100  $\mu\text{l}$  PBS containing 2 nmol of dissolved Osteosense750EX (Perkin Elmer, MA), a fluorescently-conjugated pamidronate derivative<sup>157</sup>, and imaged 2, 4, 6, 8, 10, 15, 20 and 30 min after injection using the NightOwl planar imaging system (Berthold Technologies, Bad Wildbad, Germany) to qualitatively determine kinetic distribution. A phantom was placed over the mouse bladder to help position the limbs and prevent obscuring of the limb signal from the urinary pool of bisphosphonate. For all *in vivo*, quantitative assessments of bisphosphonate binding, anesthetized mice were imaged immediately following injection and every subsequent ~15 min interval for 210 min using the FMT 2500LX from Visen Medical (Perkin Elmer, MA). Images were reconstructed and VOIs around the proximal tibia region, as determined from the photographic image, were quantified using the TrueQuant software as previously described<sup>72</sup>. Kinetics curves were generated using the average fluorescent intensity of both proximal tibia regions over time using one-phase association curves, with  $Y_0$  values constrained to zero, generated from Prism (version

5, GraphPad Software, CA). Graphs show only the first 100 min of imaging to more clearly show changes in initial binding kinetics. Due to the low resolution of FMT, proximal tibia VOIs may also contain partial fluorescence of the distal femur.

#### *Lab Analysis*

Blood was collected from the tail vein of control, long-term OVX and PTH-treated mice prior to bisphosphonate injection. Levels of skeletal osteoblast and osteoclast activity were assessed using an osteocalcin (DRG Diagnostics, Germany) and tartrate-resistant acid phosphatase (TRAP) ELISA assays (Immunodiagnostic Systems, Frankfurt, Germany) on blood serum.

#### *Fluorescent and micro-CT imaging of bone sections*

PTH-treated and untreated OVX control mice were injected with Osteosense750 intravenously then killed 15 min or 100 min after injection. Non-decalcified femurs and tibia were fixed in 10% buffered formalin, embedded in methacrylate, then cut in ~50  $\mu\text{m}$  sections. Bone sections were scanned on the LI-COR Odyssey infrared imaging system with a resolution of 21  $\mu\text{m}$  and an offset of 1 mm, excited at 785 nm and collected at wavelengths greater than 810 nm. Several regions of interest of equal size were placed randomly over growth plate, trabecular and cortical bone regions of Odyssey bone section scans and subsequent fluorescence signal intensity was quantified using ImageJ. A Leica DM2500 fluorescent microscope equipped with a DFC 360FX camera and Y7 filter cube (Leica Microsystems, Wetzlar, Germany) was used to visualize bisphosphonate binding at the growth plate and along trabecular and cortical bone surfaces. Lacunae and osteocyte labeling was visualized using a fluorescent microscope equipped with an Imager Intense CCD camera from LaVision (Bielefeld, Germany), epilumination source with LP590 filter and a LP640 emission filter. Micro-CT scans of the slides using the same settings as described above but with a voxel size of 10 $\mu\text{m}$  were made with the slide surface aligned with the axial scan direction. Following reconstruction, the images were re-aligned such that the slide surface was perpendicular to the axial scan direction to allow viewing in 2D. The central slice containing bone was used for analysis. Images from the Odyssey fluorescent scanner and micro-CT scans were overlaid using an affine registration with a normalized mutual information metric (Amira 5.4.3, Visualization Sciences Group, Berlin, Germany). The images were then processed in Matlab (R2010b; Mathworks, Natick, MA, USA), where a threshold (CT value 100,

fluorescence value 50) was applied to create binarized masks, which were combined to determine the pixels containing both micro-CT values within the bone tissue region and fluorescence signal. Histograms of the percentage of total fluorescence vs. CT value (i.e. tissue mineral density, or TMD) were created and fitted to Gaussian distributions.

#### *Statistical Analysis*

Fluorescent rate constants (K) and plateau values were calculated for curves from the line of best fit for each subject using the formula:  $Y=Y_0+(Plateau-Y_0)(1-\exp^{-Kx})$ . Plateau and rate constant were multiplied to generate a plateau-weighted rate constant for each mouse representing overall curve characteristics. Comparison between groups was made using two-sample *t*-tests using the Welch-Satterthwaite method to avoid the assumption of equal variances. For micro-CT versus fluorescence comparison in co-registered images, Gaussian distributions were fitted to binned data and difference in mean CT values 15 min and 100 min after injection was assessed. P values of <0.05 were considered to be statistically significant. T-values and effect measures, *i.e.* a z-transform calculated as the difference in mean between groups divided by pooled standard deviations, were determined from 2 sample *t*-tests in order to assess the ability of the plateau, rate constant and plateau-weighted rate constant to detect differences between control, short and long-term OVX mice.

## **Results**

### *Fluorescently-labeled bisphosphonate localize to the bone within minutes of injection*

To understand the kinetics and distribution of fluorescent bisphosphonates, control mice were subjected to NightOwl planar imaging following injection (Figure 18). Bisphosphonate fluorescence initially appears diffuse throughout the mouse following injection, but is lost in the soft tissue as it accumulates on the bones over 30 min.



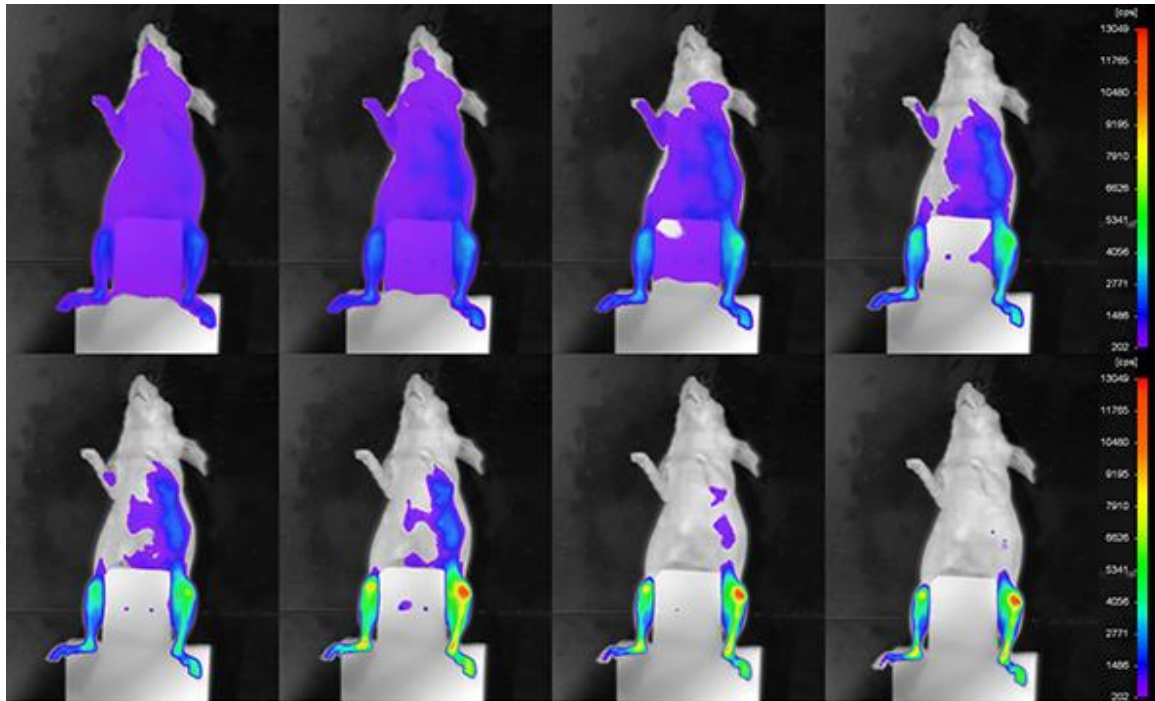
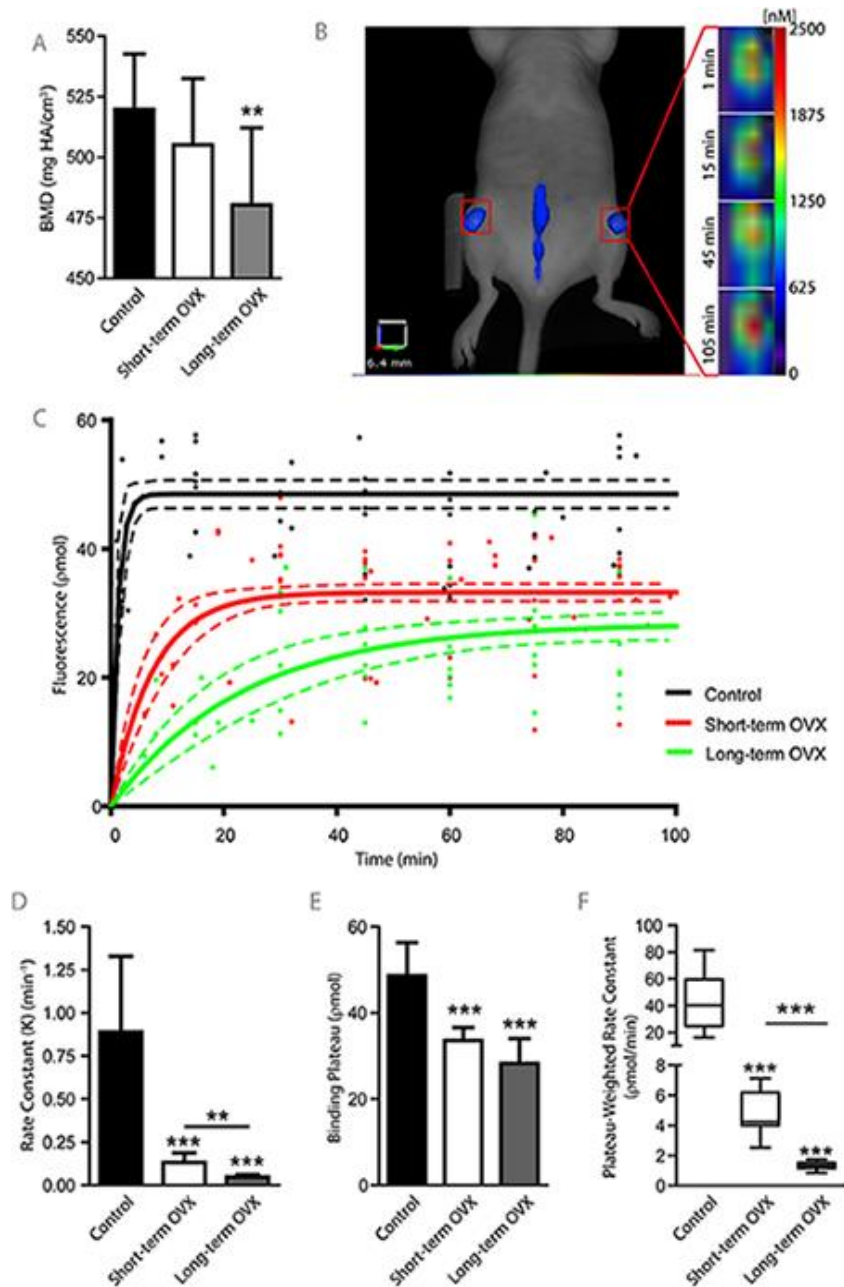


Figure 18 **Kinetic distribution of fluorescent bisphosphonate.** Fluorescently-conjugated bisphosphonate was injected and imaged 2, 4, 6, 8, 10, 15, 20 and 30 min after injection using the NightOwl fluorescent planar imaging system documenting accumulation in the knee region and clearance from soft tissue. A non-transparent part of the animal holder was used to position the limbs and prevent the obscuring of limb fluorescence the urinary bisphosphonate pool. Signals on this 2D image are affected by attenuation of overlying soft tissue, precluding, e.g. visualization of the spine, in this ventral exposure.

*Ovariectomized mice show decreased rate constant and binding plateau values compared to control mice*

Following ovariectomy, serum biomarker analysis of the osteoblast marker osteocalcin showed a significant reduction in osteoblast activity ( $p=0.047$ ) in ovariectomized mice ( $1.70\pm 0.51$  ng/ml) as compared to control mice ( $4.18\pm 0.85$  ng/ml), while the osteoclast activity marker TRAP showed no significant changes ( $p=0.711$ ). *In vivo* micro-CT analysis showed significant losses in bone mineral density after 14 days (long-term) ovariectomy (Figure 19A). Fluorescent bisphosphonate-injected mice were imaged and the fluorescent intensity of the proximal tibia regions (Figure 19B) quantified and subjected to nonlinear regression analysis (Figure 19C). Mice ovariectomized for 3 days (short-term OVX) showed significantly reduced rate constants and binding plateaus compared to control mice (Figure 19D and E). Long-term ovariectomized mice showed a further significant reduction in rate constant values from short-term ovariectomized mice but no significant change in binding plateau values. To quantify overall changes in bone mineral deposition in a single parameter, plateau-weighted rate constants were calculated for each individual mouse (Figure 19F). Long-term ovariectomized mice showed significantly lower plateau-weighted rate constants compared to short-term ovariectomized mice, which in turn showed significantly lower values than control mice.



**Figure 19 Ovariectomy results in decreased rate constant and binding plateau values of fluorescently-labeled bisphosphonate.** Control, short-term (day 3) and long-term (day 14) OVX mice were imaged by micro-CT to confirm loss of bone mineral density (BMD) (A). Mice were injected with fluorescently-conjugated bisphosphonate and imaged by FMT. (B) Isosurface rendering of 3D FMT reconstruction. Expanded windows show representative, control tibia region fluorescence over time after injection. Tibiae regions were quantified and subjected to nonlinear regression analysis. (C) Overall best-fit nonlinear regression curves are shown for each group. Rate constants and plateau values were then calculated for each individual mouse. Ovariectomized mice showed significantly reduced rate constants (D) and binding plateau values (E) compared to control mice. Plateau values and rate constants were multiplied to generate a single numerical parameter for each mouse (F). Long-term OVX mice show a significant reduction in plateau-weighted rate constants from short-term OVX mice, which in turn show a significant decrease from control mice, with no overlap between groups. Dotted lines represent 95% confidence interval of fitted curve. Graphs represent mean values  $\pm$  SD. Whiskers represent extreme maximum and minimum values. (\* $p < 0.05$ , \*\* $p < 0.01$ , \*\*\* $p < 0.001$ ) ( $n = 9$ )

*Bisphosphonate binding kinetics as a tool to monitor pharmacological intervention*

In our assessment whether bisphosphonate binding kinetics could be used as a tool to monitor increases in new bone formation resulting from pharmacological intervention, binding curves were created for ovariectomized mice with or without PTH treatment (Figure 20A). Mice treated with PTH showed a significantly increased rate constant (Figure 20B) and plateau-weighted rate constant values (Figure 20D), as well as significantly increased osteocalcin ( $6.44 \pm 1.49$  ng/ml) ( $p=0.017$ ) and TRAP levels ( $6.58 \pm 0.28$  U/L) ( $p=0.044$ ) compared to untreated controls ( $1.70 \pm 0.51$  ng/ml and  $4.69 \pm 0.69$  U/L respectively). No significant changes in binding plateau values were observed (Figure 20C). BMD, assessed by micro-CT, showed no significant increase 3 days after PTH treatment ( $p=0.233$ ) (Figure 20E), however, to confirm the expected bone anabolic effect, additional micro-CT assessment was carried out after 14 days of PTH treatment which showed a significant BMD increase of  $32.7$  mg HA/cm<sup>3</sup> compared to untreated controls ( $p=0.007$ ).

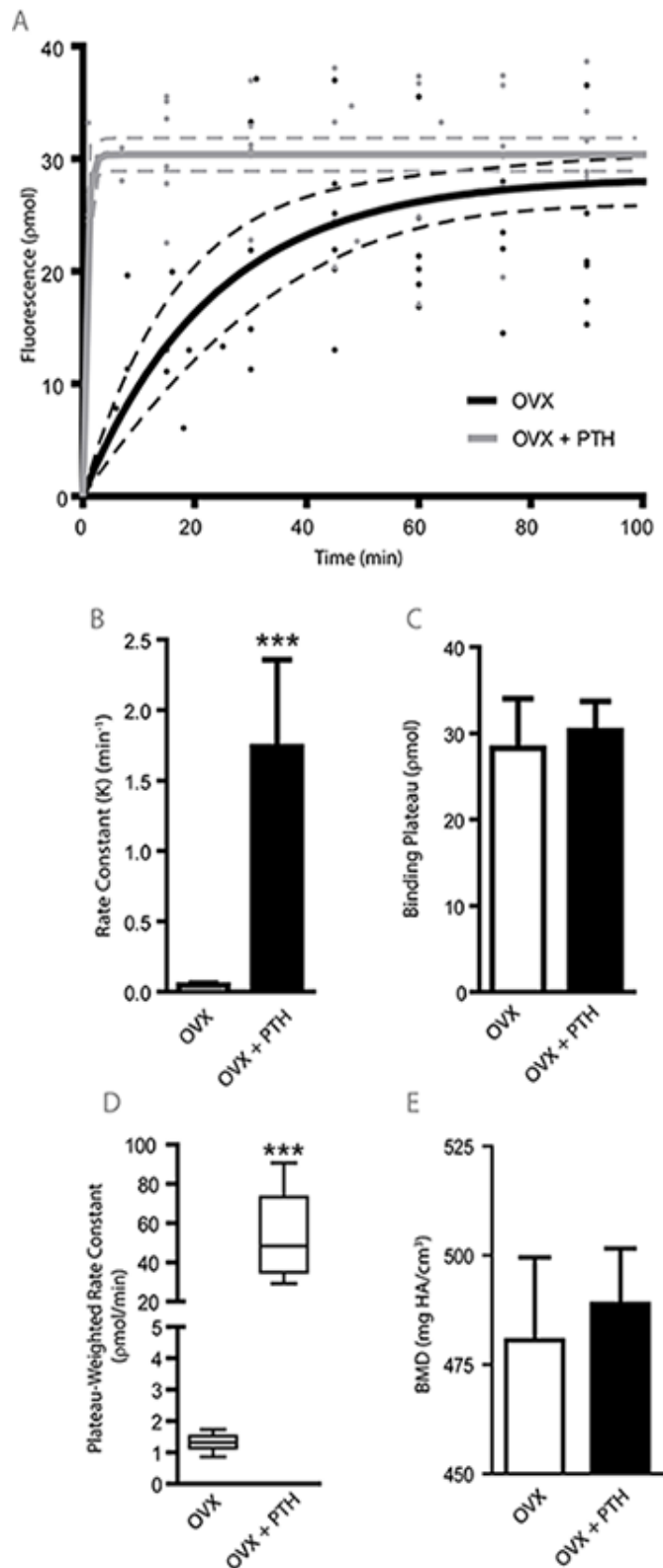


Figure 20 **Ovariectomized mice treated with PTH showed increased rate constants and plateau-weighted rate constants.** OVX mice were treated with PTH for 3 days, then assayed for bisphosphonate binding kinetics using FMT (A). Bisphosphonate binding curves were used to calculate rate constants (B), binding plateaus (C) and plateau-weighted rate constants (D) for each group. (E) Micro-CT showed a nonsignificant 2% increase in BMD ( $p=0.233$ ). Dotted lines represent 95% confidence interval. Graphs represent mean values  $\pm$  SD. Whiskers represent extreme maximum and minimum values. (\*\*\*) $p<0.001$  ( $n=9$ )

*Bisphosphonates bind preferentially to low TMD regions associated with bone ossification and modeling*

To determine the spatial distribution of bisphosphonate binding at early and late time-points, non-decalcified limb sections of OVX and PTH-treated mice were imaged *ex vivo* 15 and 100 min after bisphosphonate injection using a near infrared imaging scanner (Figure 21A). Relative fluorescent intensity in the growth plate, trabecular and cortical bone regions were quantified (Figure 21B). Mice treated with PTH showed significantly increased bisphosphonate binding near the growth plate, as well as a trend towards increased binding in the trabecular region 15 min after injection ( $p=0.053$ ), as compared to untreated controls. Bisphosphonate localization in OVX and PTH-treated mice was confirmed by fluorescent microscopy (Figure 21C). Analysis of these images shows bisphosphonates highly localize to regions adjacent to, but not within, the growth plate 15 min after injection, and to a lesser extent, along cortical and trabecular bone surfaces in OVX mice 100 min after injection. Treatment with PTH resulted in increased labeling of all bone surfaces, including osteocyte lacunae near the cortical bone surfaces 15 min after injection.

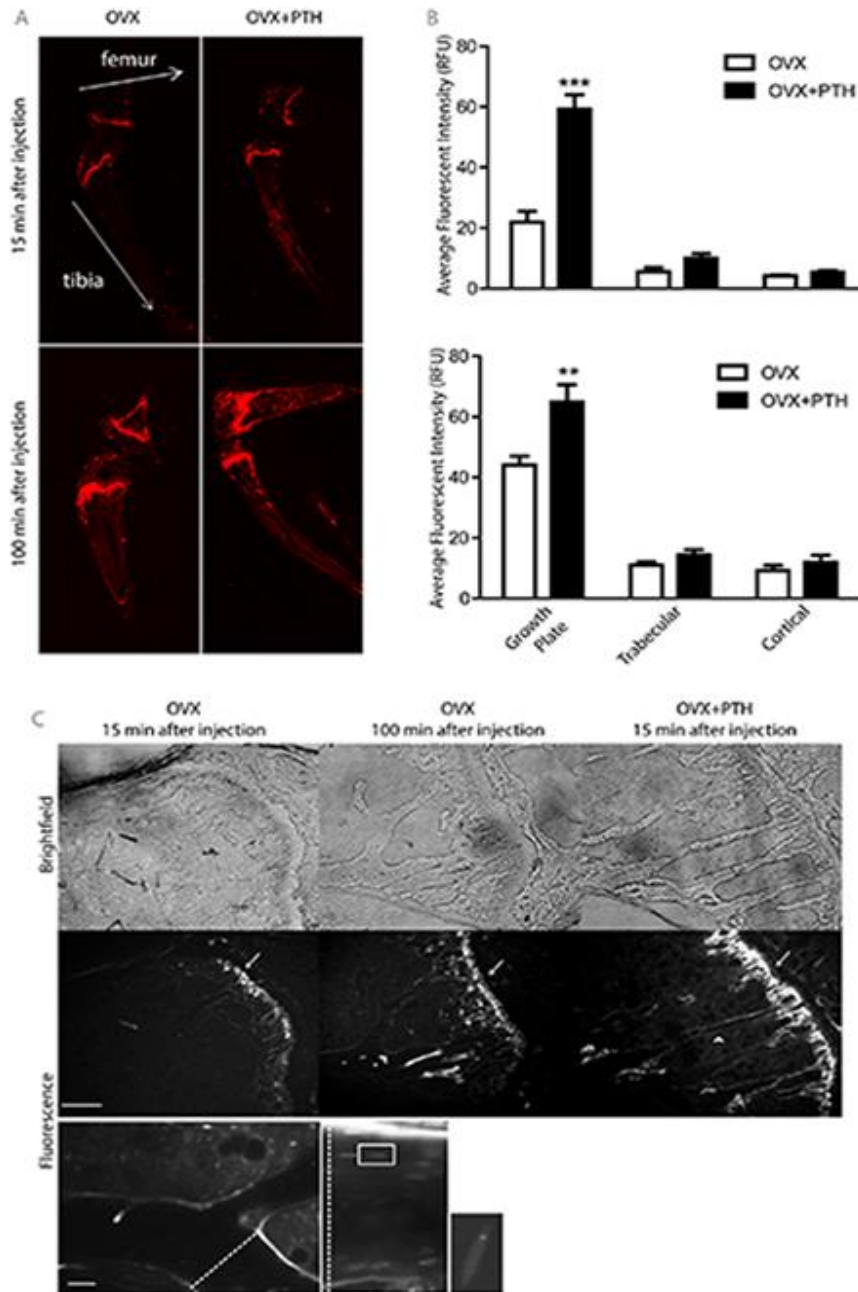


Figure 21 **Bisphosphonates preferentially bind to bone regions associated with new bone formation.** Ovariectomized, untreated mice and OVX mice treated with PTH were injected with fluorescent bisphosphonate and sacrificed 15 or 100 min after injection. Non-decalcified sections of the tibia and femur were prepared and imaged using the Odyssey near infrared fluorescent scanner (A). Regions of interest encompassing the growth plate, trabecular bone or cortical bone were quantified in relative fluorescent units (RFU) (B). Fluorescence localization was confirmed by fluorescent microscopy (C). Top panels show brightfield images to depict microstructures of bone sections and middle panels show overall fluorescent localization of bisphosphonates. Labeling initially occurs adjacent to the growth plate (OVX 15 min) and later along trabecular and cortical surfaces (OVX 100min). Treatment with PTH results in increased labeling of all bone surfaces 15 min after injection. Arrows indicate the growth plate region, arrow heads, the labelled trabecular bone surfaces. Bar 200  $\mu\text{m}$ . Lower panels show high magnification fluorescent images of the cortical bone, showing labeling of bone surfaces, as well as osteocyte lacunae. Bar 50  $\mu\text{m}$ . Graphs represent mean values  $\pm$  SD. (\* $p < 0.05$ , \*\* $p < 0.01$ , \*\*\* $p < 0.001$ )

In order to spatially correlate bisphosphonate binding and local TMD, micro-CT and fluorescent Odyssey scans from PTH-treated mouse sections were co-registered and pixels containing both bone mineral and fluorescence was compared (Figure 22A). Analysis shows binding of fluorescent bisphosphonates occurs preferentially at regions of low TMD 15 min after injection, and later, to regions of significantly greater TMD ( $p=0.0175$ ) 100 min after injection.



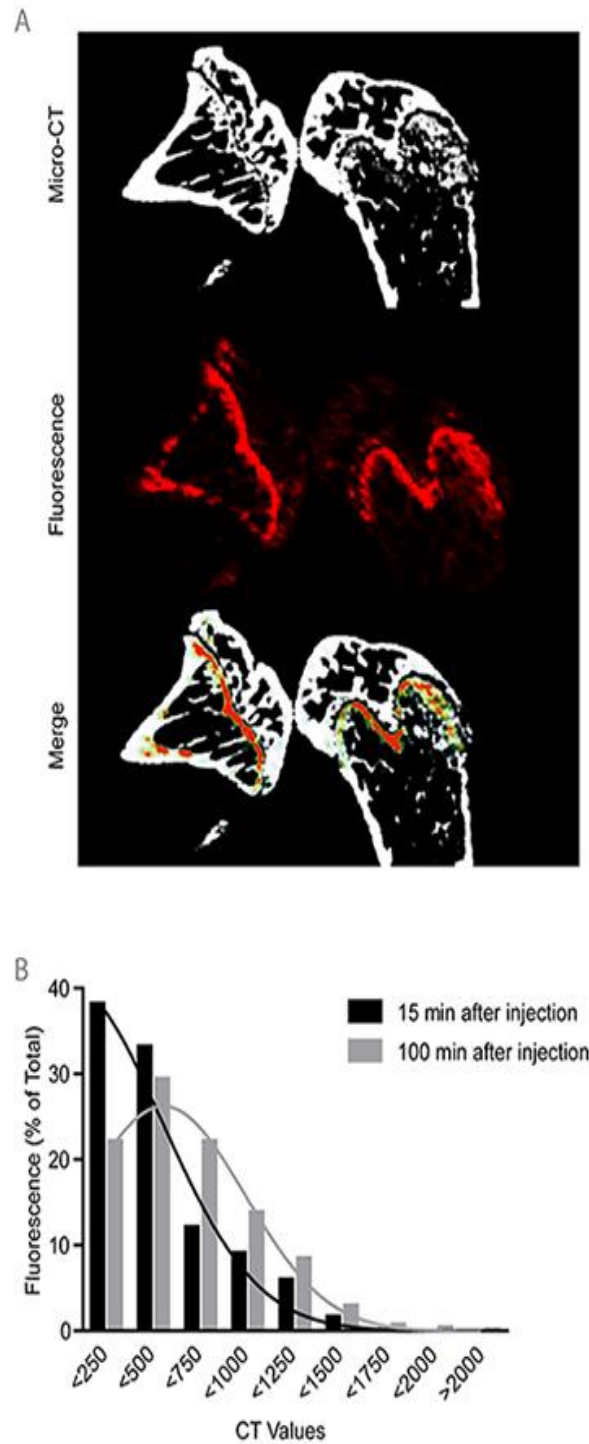


Figure 22 **Bisphosphonates preferentially bind to regions of low bone density.** Non-decalcified sections from PTH-treated mice sacrificed 15 and 100 min after bisphosphonate injection were imaged using the Odyssey near infrared fluorescent scanner as well as by micro-CT (A). Micro-CT image was binarized and bone tissue segmented from bone marrow signal. Images were registered and subjected to pixel-by-pixel analysis within the bone tissue compartment using grey scale micro-CT images. (B) Gaussian distributions show bisphosphonates bind preferentially to significantly lower tissue mineral density regions 15 min after injection as compared to 100 min ( $P=0.0175$ ).

## Discussion

In this study we demonstrate fluorescently-labeled bisphosphonates to be a valuable tool for quantifying localized changes in bone metabolism *in vivo*. While previous longitudinal studies have focused on plateau values of fluorescence days after injection, our results suggest expanded utility may be obtained by monitoring bisphosphonate binding immediately following injection. By analyzing the early binding kinetics of bisphosphonates, we were able to monitor dynamic properties of the bone environment. Furthermore, the ease and simplicity of this approach allows for expanded application in the field of preclinical drug testing and a greater understanding of the complex processes associated with bone remodeling.

Mice ovariectomized for 3 days showed significant reductions in binding rate constants and plateau binding values with further reductions in both parameters after 14 days of ovariectomy. These results are consistent with serum data, which shows a significant reduction in osteoblast activity leading to a reduction in new mineral deposition. Although no significant changes in serum TRAP levels were observed in our model, we cannot discount the important role of osteoclasts, and resorbing bone surfaces, on bisphosphonate binding. Previous works have suggested extensive bisphosphonate binding in resorption pits, especially in the case of lower affinity bisphosphonates<sup>113</sup>. A lack of detectable change in osteoclast activity may be due in part to the absence of T-cells in nude mice, which have previously been implicated in stimulating osteoclastogenesis and shown to play a role in estrogen-deficient bone loss<sup>17, 96, 153, 154</sup>. However, the lack of significant serum TRAP changes suggests that the changes in binding kinetics observed in this study are primarily reflecting changes in osteoblast activity. With no detectable difference in serum osteoclast activity, and a significant decrease in osteoblast activity, a reduction in total bone can be expected, consistent with micro-CT data showing a significant reduction in bone mineral density as the result of ovariectomy. By combining the rate constant with the plateau binding values, we have generated a single numerical parameter for each subject<sup>156</sup>. This plateau-weighted rate constant summarizes changes in the rate constant and plateau values, thereby facilitating interpretation of the kinetic data. Furthermore, plateau-weighted rate constants showed greater average t-values and effect measures ( $t=5.0786$ ,  $z-$

transform=2.625) compared to either plateau ( $t=4.385$ ,  $z$ -transform=2.261) or rate constant values ( $t=4.446$ ,  $z$ -transform=2.293), suggesting plateau-weighted rate constant values show the greatest ability to distinguish control, short-term and long-term OVX sample groups. This may suggest greater utility in using plateau-weighted rate constants, perhaps not only for fluorescent markers in animals but also in a clinical setting using radioactive tracers to easily distinguish healthy patients from those with altered bone metabolism.

Next we sought to investigate whether binding kinetics could be used to assess pharmacological intervention leading to increased bone formation. After 3 days of intermittent PTH treatment, no significant differences were observed by micro-CT or plateau binding values. However, rate constants showed a highly significant increase after PTH treatment compared to the untreated control. Serum analysis showed significantly elevated osteoblast and osteoclast activity suggesting that, while micro-CT showed no significant net bone mineral gained within 3 days of PTH treatment, composition of the bone surface may have been altered. Other researchers have reported that administration of PTH for 3 days in rats failed to show significant changes in the uptake of  $^{99m}\text{Tc}$ -pyrophosphate 2 h or 6 h after radiotracer injection<sup>55</sup>. Using our binding kinetics approach, we were able to detect early changes in bone metabolism in mice after 3 days of PTH treatment, prior to conventional micro-CT or single time point FMT measurements 24 h after injection further supporting increased utility of monitoring binding kinetics. It would be of interest to investigate whether different types of bone-anabolic treatments may show dissimilar patterns of rate constants and plateau values potentially reflecting variable degrees of bone activation.

Localization studies of bisphosphonate binding 15 and 100 min after injection show preferential binding of the bisphosphonate probe Osteosense to the region adjacent to the growth plate, associated with endochondral ossification<sup>83</sup>, and to a lesser extent, along trabecular and cortical regions associated with bone remodeling, or quiescent bone surfaces. Quantification of Odyssey bone scans showed increased bisphosphonate binding near the growth plate in PTH-treated mice 15 min after injection compared to the untreated controls. Further analysis of early binding shows bisphosphonates localize preferentially to low-TMD bone, associated with new bone in a state of

primary mineralization, shortly after injection and to a lesser extent, to highly-mineralized bone associated with fully mineralized, quiescent bone<sup>8</sup>. These data are consistent with increased binding of bisphosphonate at regions associated with high osteoblast activity and newly forming bone.

From these observations, we propose that the dynamics of bisphosphonate binding observed in this study reflects the binding to two bone types, high uptake capacity and low uptake capacity, comprising the bone surface. High uptake capacity bone would be comprised of newly deposited mineral at the site of osteoblast activity and contains a high volume of exposed surface minerals. The amount of high uptake capacity bone reflects both the density of active osteoblasts along the bone surface, as well as the level of bone-forming activity of these osteoblasts<sup>11</sup>. Additionally, newly deposited bone may transition to fully mineralized, low uptake capacity bone when not undergoing bone remodeling. This transition may also affect the form of mineral present within the bone. Calcium phosphate in an amorphous state, present in newly forming bone, has previously been shown to have higher uptake of diphosphonates compared to calcium phosphate in its crystalline form, present in fully mineralized, quiescent bone, *in vitro*<sup>42</sup>. We propose changes in the amount of high and low uptake capacity bone, along with injected dose, would both be reflected in the rate constant and binding plateau of bisphosphonate binding kinetics.

This ability to distinguish sites of high bone turnover from regions of low or no bone activity may also have important implications in tumor site identification and treatment. Osteosclerotic bone lesions, such as in the case of prostate cancer, result in marked increases in bone formation. According to the findings presented here, the expected increase in bone turnover at the tumor site would accumulate bisphosphonate probes more rapidly than in the surrounding tissue, enabling the detection and preferential targeting of the lesions. Binding kinetics may also prove useful for detecting metastases that result in mixed osteolytic/osteosclerotic lesions<sup>1, 62</sup>. These lesions may result in mild or no overall bone loss or gain making them difficult to detect by CT, but the marked increase in bone turnover within the tumor environment could still be detected from the corresponding kinetic uptake parameters.

One aspect that requires consideration in future methodological refinements is the differentiation of localized changes (as induced by bone metastases) versus systemic changes (e.g. due to medications) and the effects of surrounding soft tissue on fluorescent measurements. In this study we present data on the proximal tibia region because of the relatively small soft tissue present to attenuate and scatter fluorescence, as well as its importance as a high frequency site of bone metastases in preclinical models. However, overall changes in skeletal bone uptake outside our region of interest will affect the blood pool levels, and correspondingly, the ability of the tibia to bind free bisphosphonate. In the instance of PTH treatment, mice showed rapid uptake of bisphosphonate at the proximal tibia region but failed to show any significant changes in binding plateau values. This may be due to rapid uptake of available bisphosphonate by other skeletal sites, reducing the blood pool of bisphosphonate available for binding, and thus, preventing further binding at the proximal tibia at later time points<sup>45</sup>. Clinical evaluation of bisphosphonate binding using radioactive labels supplement bone accumulation measurements with blood serum levels, urinary pool or soft tissue retention of unbound bisphosphonates<sup>5, 41, 92, 97</sup>. Body mass of the mouse will also play a role in bisphosphonate uptake, clearance and dosing. And, while body mass was not significantly altered in this study, consideration must be given for situations in which significant weight loss may be observed. A measure of blood pool bisphosphonate may reveal that tibia fluorescence was limited more by the rapid clearance of bisphosphonate from the blood and not by the uptake of bisphosphonate by the tibia itself. FMT is tomographic, but with limited spatial resolution and scan region obtained, we were unable to calculate arterial input functions, renal clearance or blood perfusion within the proximal tibia region for each mouse. As a result, we cannot discount either decreased delivery of bisphosphonate to the bone or increased renal clearance of unbound bisphosphonate in the case of ovariectomy. No significant changes in health or weight, common symptoms of impaired renal function, were detected; however, recent bone perfusion experiments using laser Doppler techniques suggests blood perfusion may be affected in ovariectomized mice depending on their genetic background<sup>109</sup>. These uncontrolled parameters limit the exact quantification of bone kinetic parameters as done in this study, but with improvements in imaging technology, and implementation of more complex imaging protocols, may become feasible in the future.

It is also of interest to note that binding curves in this study were obtained using a pamidronate derivative, reflecting the binding kinetics of a relatively high affinity bisphosphonates. Previous works have shown that different bisphosphonates vary in their affinity for bone surfaces and their level of bone penetration<sup>77, 113</sup>. The use of medium or low affinity bisphosphonates as the targeting molecule may better reflect changes in osteoclast activity because of their relatively greater uptake in regions of bone resorption compared to quiescent surfaces<sup>113</sup>. Additional histological analyses will be needed to more precisely define sub-regions within the bone with more rapid uptake of high versus low affinity bisphosphonates. In particular, methodological refinement should include histological analyses of bone surfaces revealing quiescent, resorbing and bone-forming regions and the corresponding levels of bisphosphonate binding.

The use of fluorescent probes suggests this method has the possibility to be applied to monitoring multiple wavelengths and multiple probes detecting multiple aspects of bone dynamics *in vivo* at macroscopic resolution simultaneously, while also allowing the use of more high resolution modalities such as fluorescent confocal or two-photon microscopy for analysis at the microscopic level. The challenge remains to validate this method in patients using radioactive tracers conjugated to bisphosphonates and translate this simpler approach into wider clinical use. Since <sup>99m</sup>Tc-MDP display relatively slow blood and soft-tissue clearance the measurement of bisphosphonate binding at early time points is confounded by the high percentage of tracer retained in the soft tissue in the moments immediately following injection of tracer. The application of new radioactive bisphosphonates with variable affinities for the bone matrix can have an impact in nuclear medicine in the refined assessment of metabolic bone disorders and warrants clinical investigation.

In conclusion, we have developed and tested a new molecular imaging method for *in vivo* assessment of bone metabolism, specifically bone mineral deposition. Using Osteosense, a fluorescently labeled bisphosphonate, we were able to noninvasively visualize localized changes in bone turnover, including bone loss and bone anabolic treatment models, at very early time points. The analysis of three parameters, the rate constant, the binding plateau, and the plateau-weighted rate constant, provides non-invasive insights into the presence of high and low uptake capacity bone

mineral, important aspects in osteoporosis and for the detection and differentiation of lytic versus osteosclerotic bone metastases. Our method has potential for further refinement with the goal of better quantification and for translation to human application using radionuclide tracers instead of fluorescent markers.

## **Acknowledgements**

The authors are grateful to Gabriele Trompke and Gaby Nessenius from the UKSH clinic of oral and maxillofacial surgery for their assistance preparing non-decalcified bone sections. We would like to thank Dr. Vladimir Ermolayev and Sarah Glasl (Technische Universität München), Dr. twan Lammers (University of Aachen) and Dr. Arndt Rohwedder (UKSH) for assistance with fluorescent microscopy images and Dr. Jürgen Baudewig for his assistance with image registrations using Amira. Financial support was provided by the Deutsche Forschungsgemeinschaft (DFG) through the forscherguppe 1586 SKELMET and by the research grant from the state of Schleswig-Holstein and the European Union ERDF-European Regional Development Fund (MOIN CC, Zukunftsprogramm Wirtschaft). Authors' roles: Study design: RJT, GMC, OW, CCG and ST. Study conduct: RJT, GMC, MM and OW. Data collection: RJT and MM. Data analysis: RJT, GMC and MM. Data interpretation: RJT, GMC and CCG. Drafting manuscript: RJT. Revising manuscript content: GMC, MM and CCG. Approval of final version of manuscript: RJT, GMC and CCG. ST takes responsibility for the integrity of the data analysis.



Chapter 2.4

Modified from:

Tower RJ\*, Campbell GM\*, Müller M, Glüer CC and Tiwari S. (2014). Utilizing time-lapse micro-CT-correlated bisphosphonate binding kinetics and soft tissue-derived input functions to differentiate site-specific changes in bone metabolism *in vivo*. *Bone accepted*

**Title Page**

Utilizing time-lapse micro-CT-correlated bisphosphonate binding kinetics and soft tissue-derived input functions to differentiate site-specific changes in bone metabolism *in vivo*

Tower R. J. \*, Campbell G. M. \*, Müller M., Glüer C. C., Tiwari S

\*These authors contributed equally

Section Biomedical Imaging, Department of Radiology and Neuroradiology, University Hospital Schleswig-Holstein, Campus Kiel, Germany

Address correspondence to: Sanjay Tiwari, PhD  
[stiwari@email.uni-kiel.de](mailto:stiwari@email.uni-kiel.de)  
+494318805836  
Am Botanischen Garten 14  
24118 Kiel, Germany

**Disclosures**

Research support was provided by Perkin Elmer in the form of discounted reagents

**Abstract**

The turnover of bone is a tightly regulated process between bone formation and resorption to ensure skeletal homeostasis. This process differs between bone types, with trabecular bone often associated with higher turnover than cortical bone. Analyses of bone by micro-computed tomography (micro-CT) reveals changes in structure and mineral content, but is limited in the study of metabolic activity at a single time point, while analyses of serum markers can reveal changes in bone metabolism, but cannot delineate the origin of any aberrant findings. To obtain a site-specific assessment of bone metabolic status, bisphosphonate binding kinetics were utilized. Using a fluorescently-labeled bisphosphonate, we show early binding kinetics monitored *in vivo* using fluorescent molecular tomography (FMT) can monitor changes in bone metabolism in response to bone loss, stimulated by ovariectomy (OVX), or bone gain, resulting from treatment with the anabolic bone agent parathyroid hormone (PTH), and is capable of distinguishing different, metabolically distinct skeletal sites. Using time-lapse micro-CT, longitudinal bone turnover was quantified. The spine showed a significantly greater percent resorbing volume and surface in response to OVX, while mice treated with PTH showed significantly greater resorbing volume per bone surface in the spine and significantly greater forming surfaces in the knee. Correlation studies between binding kinetics and micro-CT suggest that forming surfaces, as assessed by time-lapse micro-CT, are preferentially reflected in the rate constant values while forming and resorbing bone volumes primarily affect plateau values. Additionally, we developed a blood pool correction method which now allows for quantitative multi-compartment analyses to be conducted using FMT. These results further expand our understanding of bisphosphonate binding and the use of bisphosphonate binding kinetics as a tool to monitor site-specific changes in bone metabolism *in vivo*.

Keywords: bone turnover, bone metabolism, bisphosphonates, molecular imaging, osteoporosis

## Introduction

Bone turnover is tightly regulated by osteoblasts and osteoclasts, and is essential for maintaining the integrity and adaptation of the skeleton. This process is both spatially and temporally regulated, ensuring equal bone resorption and new bone formation, in order to maintain bone mass<sup>75, 133</sup>. Disruption of this coupled process can lead to abnormal bone loss or gain, both with severe ramifications. Remodeling is also essential for the turnover of aged bone, which removes microfractures and maintains the mechanical competence of the bone tissues throughout the body<sup>99</sup>. Long and vertebral bones differ in their composition of trabecular and cortical bone, and in their levels of metabolic activity. While both cortical and trabecular bone requires constant remodeling to maintain the integrity of the skeleton, trabecular bone resorption additionally contributes, to a greater extent, to blood calcium homeostasis, resulting in a higher level of metabolic activity<sup>20, 105</sup>.

While longitudinal analyses of bone by micro-computed tomography (micro-CT) provides detailed insights into structural adaptations, as well as changes in bone mineral content over time, such studies require weeks or months in mice before changes are observed and the assessment of the short-term changes in metabolic status of these bones remains difficult. Recent method developments have allowed the assessment of bone formation and resorption rates *in vivo*<sup>82, 127</sup>, but fail to show the instantaneous state of bone metabolism. In contrast, analyses of serum markers can provide insight into the current metabolic status of the skeleton, but fail to differentiate the individual metabolic statuses of different skeletal regions<sup>28</sup>. In humans, (18) F-fluoride positron emission tomography (PET) has proven to be a feasible tool for metabolic monitoring<sup>101</sup>. However, in mice, only cases of extreme changes in bone activity (complete fracture or cancer-induced severe osteolysis) have been successfully documented<sup>4</sup> and require the repeated injection of radioactive material. To this end, new methods are required for the site-specific monitoring of bone metabolic status.

Because of their anti-resorptive properties, bisphosphonates are in widespread clinical use in patients with excessive bone loss (i.e. osteoporosis, tumor osteolysis)<sup>87</sup>. Recent research has also exploited the bisphosphonates' ability to bind bone mineral with high affinity as a bone metabolic marker rather than as a therapeutic agent. Conjugation of bisphosphonates with fluorescent dyes is

currently under great scrutiny to help characterize bisphosphonate binding<sup>72, 113</sup>, as well as in the use as a bone-specific turnover marker<sup>72, 76</sup>. While early works focused on bisphosphonate binding days after injection, new data suggests monitoring the kinetics of early binding (as little as 5 minutes after injection) may provide additional information about the metabolic status of the bone<sup>142</sup>. One limitation in previous *in vivo* kinetic assessments has been the lack of indicators of blood pool bisphosphonates available for bone binding, which are used in more refined, quantitative, multi-compartment analyses commonly seen in the context of radiolabeled bisphosphonates<sup>92</sup>. Recent radionuclide studies in humans have also suggested that significant overall changes in skeletal activity, such as those seen in the case of treatment with parathyroid hormone (PTH), may alter the plasma time-activity curve<sup>6</sup>. This effect would alter both the rate and total binding values of a fluorescently-labeled bisphosphonate as discussed previously<sup>142</sup>.

The purpose of this study was to assess whether the binding kinetic characteristics previously observed in the proximal tibia could be distinguished from other, metabolically distinct skeletal sites and to compare the relationship between observed binding kinetic parameters and longitudinal changes in bone structure, as assessed by time-lapse micro-CT<sup>82</sup>. Additionally, we have generated a blood pool correction factor allowing multi-compartment, quantitative kinetic analyses to be conducted using a modified Patlak's method<sup>92</sup>, accounting for changes in the quantity of bisphosphonate probe available for binding.

## Materials and Methods

### *Animals*

12 week old female, CD-1 nude mice were purchased from Charles River (Wilmington, MA). All animals were kept in a temperature and humidity-controlled environment, with a 12 h light/dark cycle, and access to food and water *ad libitum*. Animal experiments and care were in accordance with the guidelines of institutional authorities and approved by the Ethics Committee for Animal Experiments at the Christian-Albrechts-Universität-zu-Kiel [V 312-72241.121-33]. Mice were anesthetized with intraperitoneal injections of 80 mg/kg ketamine (Aveco Pharmaceutical, IA) and 10 mg/kg xylazine (Rugby Laboratories, GA). For long-term anesthetization, additional administration of ketamine and xylazine at half dose was administered upon initial signs of mouse waking. Animals were separated into 3 groups (n=9/group): i) non-operated, control animals, ii) ovariectomized (OVX) animals, imaged 3 days (short-term) and 14 days (long-term) after OVX, and iii) PTH-treated mice, which were subjected to OVX, then received daily PTH injections for 3 days beginning 11 days post-surgery (total of 14 days OVX and 3 days PTH treatment) as previously described<sup>142</sup>. Animals were ovariectomized via their dorsal side. Human parathyroid hormone fragment 1-34 (Sigma-Aldrich, MO) was given subcutaneously at a dose of 100 µg/kg daily.

### *Bisphosphonate Binding Kinetics*

Anesthetized mice were injected intravenously with 100 µl PBS containing 2 nmol of dissolved OsteoSense750, a fluorescently-conjugated pamidronate derivative<sup>157</sup>. For all *in vivo*, quantitative assessments of bisphosphonate binding, anesthetized mice were imaged immediately following injection and every subsequent ~15 min interval for 210 min by FMT using the 750 nm channel of the FMT2500LX (Perkin Elmer, MA, USA). Images were reconstructed and VOIs of equal dimensions were positioned using the photographic image around the proximal tibia region, as well as the L1 and L2 vertebrae, and quantified using the TrueQuant software. Kinetics curves were generated using the average fluorescent intensity of either the proximal tibiae or vertebral regions over time using one-phase association curves, with  $Y_0$  values constrained to zero, generated from Prism (version 5, GraphPad Software, CA). Graphs show only the first 100 min of imaging to more clearly illustrate

changes in initial binding kinetics, though all time points were used to generate binding kinetic curves. Due to the low resolution of FMT, proximal tibia VOIs may also contain fluorescence of the distal femur. For this reason, this region is henceforth referred to as the knee region.

### *Micro-CT Analysis*

All animals were scanned by micro-CT prior to treatment to establish baseline bone parameters. Changes in bone mineral and structure resulting from OVX or PTH treatment were characterized from micro-CT assessment of skeletal changes *in vivo*. Anesthetized mice were placed in full-body holders and the tibiae aligned by visual inspection. Scans were made using a Scanco vivaCT 40 micro-CT (Brüttisellen, Switzerland) at an isotropic voxel size of 19  $\mu\text{m}$  (70 kVp, 114  $\mu\text{A}$ , 250 ms integration time, 1000 projections on 180° 2048 CCD detector array, cone-beam reconstruction with a radiation dose of approximately 520 mGy (CTDI<sub>air</sub>)). PTH-treated mice were additionally scanned by micro-CT after 14 days of intermittent PTH treatment to capture long-term bone changes. Three volumes of interest (VOIs) were selected, one for the vertebra, as well as one each for the epiphyseal and metaphyseal region of the proximal tibia (to exclude the growth plate region). Contours along the periosteal surfaces were drawn encompassing either 60 slices (1.05 mm) of the L1 vertebra, starting at the beginning of trabecular bone within the spinal body, 50 slices (0.875 mm) beginning at the proximal tip of the tibial epiphyseal trabecular bone, or 50 slices (0.875 mm) beginning just distal to the tibial growth plate, all extending in the distal direction. Baseline VOIs were transferred to the follow-up scans using an image registration approach to ensure analysis of consistent VOIs at each time point<sup>15</sup>. Bone mineral density (BMD) was calculated from the greyscale micro-CT images (Image Processing Language (IPL) v5.15, ScancoMedical, Brüttisellen, Switzerland) as the total bone mineral content within the contour divided by the contour volume. Localized bone formation and resorption was determined from the time-lapsed micro-CT images after registration using programs written in IPL for the registration, and Matlab (R2010b; Mathworks, Natick, MA, USA) for the quantification of bone turnover, following similar procedures as previously described<sup>127</sup>. Briefly, a three-color image was produced from the overlaid follow-up and baseline images after a threshold (23% of maximal greyscale value) was applied. From this image, the volume of formed, resorbed and quiescent bone

could be determined. The contact surfaces between the colored regions were used to calculate the formed and resorbed surface area.

#### *Soft Tissue-Blood Pool Correlation*

VOIs were placed over soft tissue regions in the abdomen and the corresponding fluorescence quantified. Kinetic curves for the soft tissue analysis were generated in Prism using one-phase exponential decay curves, with the non-specific binding at infinite times (NS) values constrained to  $>0$ . A standard curve was generated by direct addition of known concentrations of OsteoSense750 to serum collected from non-injected mice and subsequently scanned by the Odyssey fluorescent scanner. For comparison of soft tissue fluorescence (assessed by FMT) and serum bisphosphonate levels, mice were imaged by FMT 1, 15, 30, 45 and 60 min after injection, followed by immediate blood collection from the tail vein. Whole blood was separated at 3000 g for 10 min and serum isolated. Serum was scanned on the Odyssey fluorescent scanner and compared to standard curve fluorescent readings to determine bisphosphonate concentrations.

#### *Statistical Analysis*

All statistical analyses were conducted using Prism. Binding rate constants (k) and plateau values were calculated for curves from the line of best fit for each mouse using the formula:  $Y = Y_0 + (\text{Plateau} - Y_0)(1 - \exp^{-kx})$ , where Y=fluorescence at time x,  $Y_0$ =the fluorescence at time 0, and x=time in min. The plateau, reflecting the maximum binding fluorescence expected as time approaches infinity, and the rate constant, reflecting the rate at which the curve approaches its plateau value, were multiplied to generate a plateau-weighted (Pw) rate constant for each mouse representing overall curve characteristics. For soft tissue analysis,  $Y_0$  (fluorescent signal at time zero), NS (fluorescent signal as time approaches infinity) and K (clearance rate) values were calculated for curves from the line of best fit for each mouse using the formula:  $Y = (Y_0 - \text{NS})^{-kx} + \text{NS}$ . Comparison between groups was made using two-sample *t*-tests using the Welch-Satterthwaite method to avoid the assumption of equal variances. Comparison between knee and spine values within the same mouse was made using paired *t*-tests. Time-lapse micro-CT statistics were calculated using a two-way ANOVA. Interaction between binding kinetic and time-lapse micro-CT parameters were assessed by the probability of the slope of



the linear correlation being equal to zero using Prism. P values of <0.05 were considered to be statistically significant.  $K_{\text{Bone}}$  was determined using a modified Patlak's method as previously described<sup>92</sup>. In short, average  $K_{\text{Bone}}$  values were determined by calculating changes in area-under-the-plasma-clearance-curve (AUC) and whole-body retention (WBR) values generated for each mouse between each FMT imaging time point. Plasma concentrations and bone uptake (BU) values at each time point were determined by the formulas:

$$[plasma] = \frac{\text{soft tissue fluorescence (pmol)}}{\text{injected fluorescence (pmol)} \times \text{VOI volume (ml)}}$$
$$BU = \frac{\text{bone VOI fluorescence (pmol)} \times \text{mass of mouse (kg)}}{\text{injected fluorescence (pmol)} \times \text{VOI volume (ml)}}$$

## Results

### *Vertebrae bisphosphonate uptake kinetics are altered in ovariectomized and PTH-treated mice*

Average fluorescence of the L1 and L2 vertebrae was quantified from injected mice and subjected to nonlinear regression analysis (Figure 23A). Vertebral fluorescence showed significant reductions in binding plateaus, rate constants and Pw rate constants after short-term OVX when compared to control groups, with further significant reductions in long-term OVX mice (Figure 23B-D), while PTH-treated mice showed significant increases in binding plateau, rate constant and Pw rate constant values compared to untreated OVX controls.

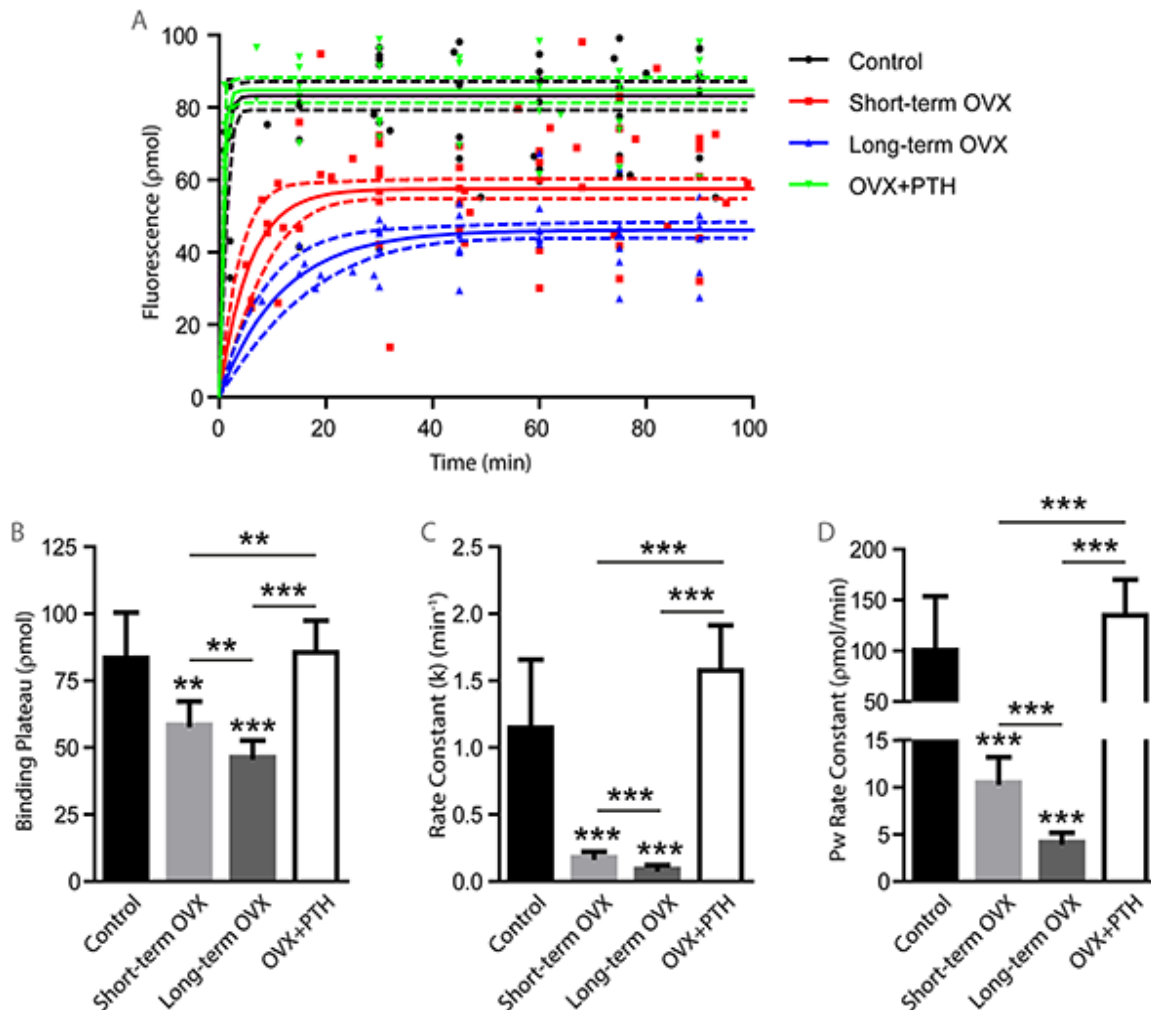


**Figure 23 Ovariectomy and treatment with PTH results in significantly altered binding kinetic parameters of fluorescently-conjugated bisphosphonate.** Time resolved bone binding pattern of fluorescently-labeled bisphosphonate in L1 and L2 (A). Long-term ovariectomized mice showed significantly reduced binding plateaus (B), rate constants (C) and plateau-weighted (Pw) rate constants (D) compared to short-term OVX mice, which in turn showed significant reductions in all parameters compared to control mice, while treatment of mice with PTH for 3 days resulted in values comparable to control mice and binding kinetic parameters significantly greater than OVX mice. Dotted lines represent 95% confidence interval of fitted curve. Graphs represent average values  $\pm$  SD. (\*\* $p < 0.01$ , \*\*\* $p < 0.001$ ) (n=9)

*Fluorescent bisphosphonate binding kinetics reveal differential changes in uptake parameters in the knee and spine*

To examine region-specific differences in uptake, changes in fluorescent bisphosphonate kinetic parameters obtained for the knee (as previously published<sup>142</sup>) and spine for each group were compared. Overall, changes in kinetic parameters were similar for both the knee and spine in response to OVX. No significant differences in percent change in plateau values were observed between short and long-term OVX, relative to control, for either the knee or the spine (Figure 24A). In contrast, while both the spine and the knee showed significant reductions in the rate constant, the changes observed in the knee were slightly but significantly greater than those observed in the spine after long-term OVX (Figure 24B). Both the knee and the spine showed reductions in the Pw rate constant, with significantly greater reductions after long-term OVX as compared to short-term (Figure 24C), but no significant differences were observed between regions. In response to PTH treatment of OVX mice, clear differences were observed in the rate constant and plateau values between the knee and spine regions. The spine showed a significantly greater increase in the binding plateau, while the knee showed a significantly greater increase in rate constant values in OVX mice treated with PTH, relative to untreated OVX controls (Figure 24D and E). Overall, no significant changes in the Pw rate constants were observed between the knee and the spine in response to PTH treatment (figure 24F).

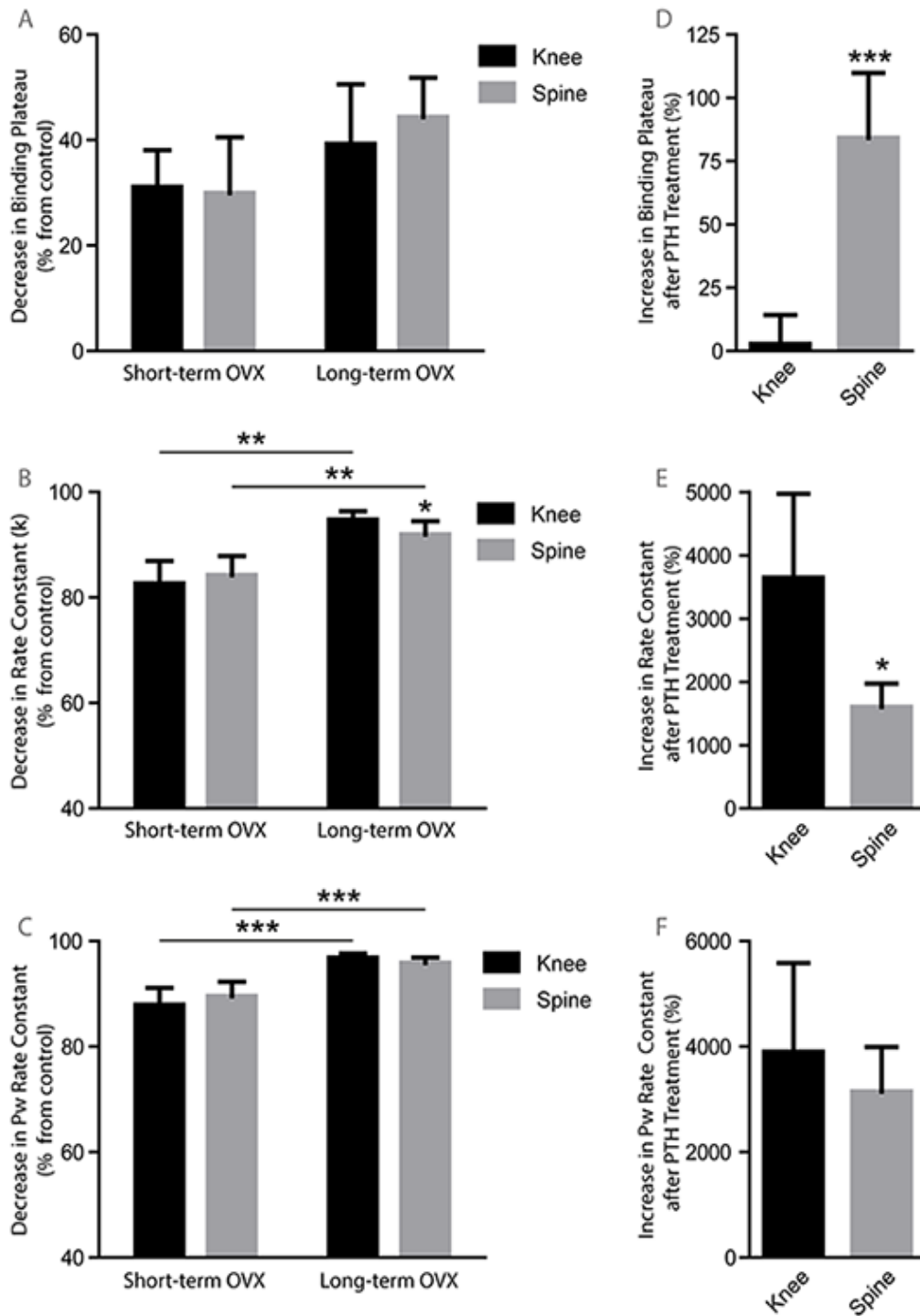
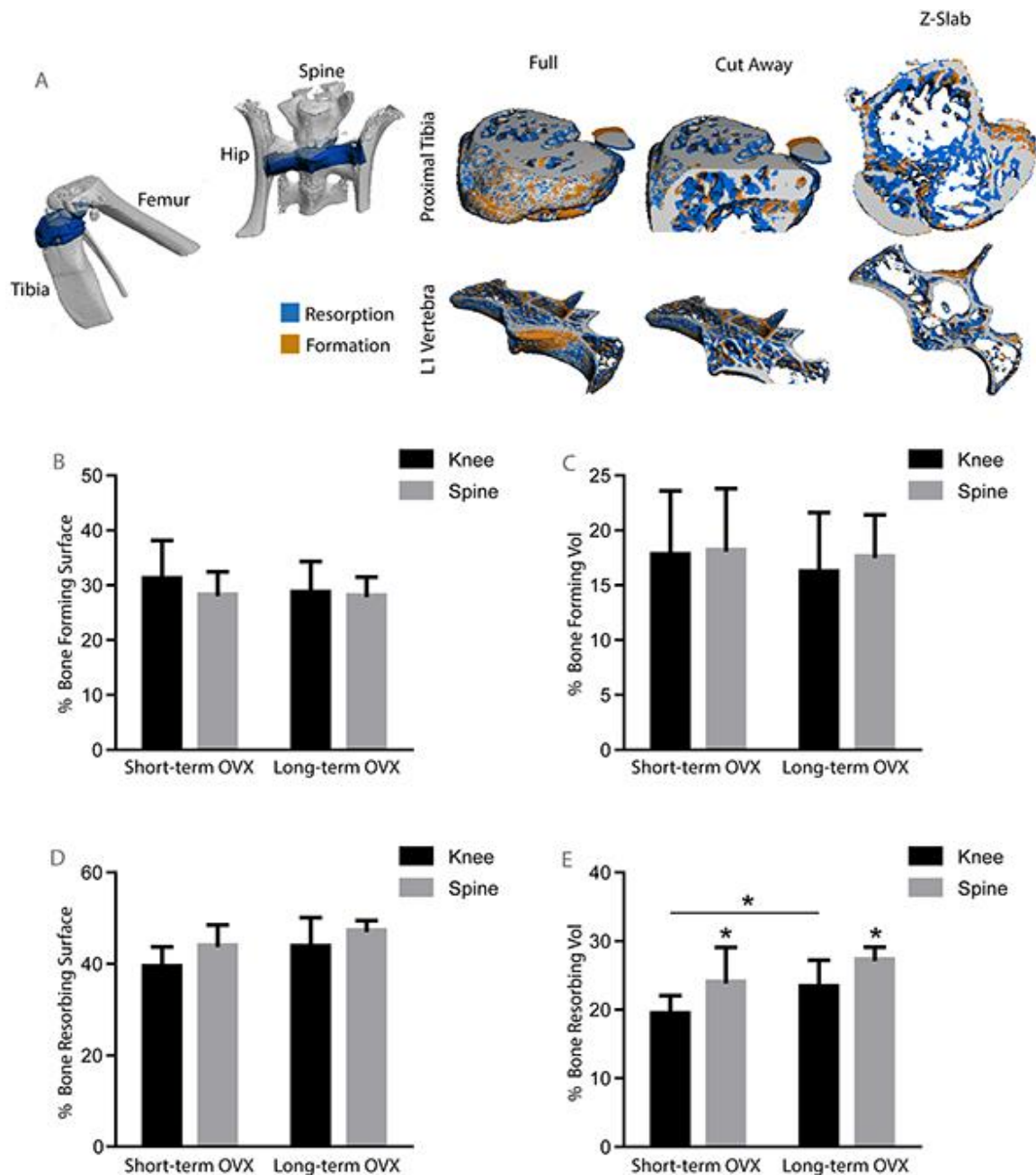


Figure 24 **Spine and knee regions show differential changes in bisphosphonate binding kinetics in response to ovariectomy and PTH treatment.** Analyzing changes in binding kinetic parameters in response to ovariectomy, both the knee and spine showed no significant differences in the change between short and long-term OVX (A), but did show a significant increase in rate constant values (B). Both regions showed significant changes in Pw rate constant values between short and long-term OVX mice (C). In response to PTH treatment in OVX mice, the spinal region showed significantly greater changes in plateau binding values (D), while the knee region showed significantly greater changes in rate constant values (E), relative to untreated OVX controls. Pw rate constant values showed no significant differences between the knee and spine region after PTH treatment (F). Dotted lines represent 95% confidence interval. Graphs represent average values  $\pm$  SD. (\* $p < 0.05$ , \*\* $p < 0.01$ , \*\*\* $p < 0.001$ ) (n=9)

To delineate the biological significance of the observed changes in binding plateau and rate constant values, micro-CT analyses were conducted to monitor changes in BMD, bone microstructure and turnover in the knee and spine. Bone loss expected as a result of OVX was confirmed by BMD assessment which showed significantly reduced values in both the spine and knee after long-term OVX (data not shown) and serum marker analyses<sup>142</sup>. Baseline and follow-up scans were overlaid to ensure analyses of similar regions and to visualize regions of bone formation and resorption which occurred between imaging time points and pre-OVX baseline scan (Figure 25A). Images were used to quantify bone forming and resorbing surfaces (Figure 25B and D) and volumes (Figure 25C and E). Time-lapse micro-CT showed a trend towards increased resorbing surfaces ( $p=0.0683$ ) and significantly greater resorbed bone volume in the tibia between short-term and long-term OVX. Relative to the tibia, the spine showed a trend towards an increased percent resorbing surface after short-term ( $p=0.0926$ ) and long-term ( $p=0.0771$ ) OVX, as well as significantly greater resorbed bone volume after short-term and long-term OVX. A two-way ANOVA was conducted to determine overall effects of skeletal site and length of OVX on time-lapse micro-CT parameters (Table S3). Neither the skeletal site (tibia vs spine), nor the duration of OVX (day 3 vs day 14) had a statistical impact on bone forming surfaces or volumes. In contrast, resorbing surfaces and volumes both showed a significant dependence on both the skeletal site assessed, as well as the duration of OVX.



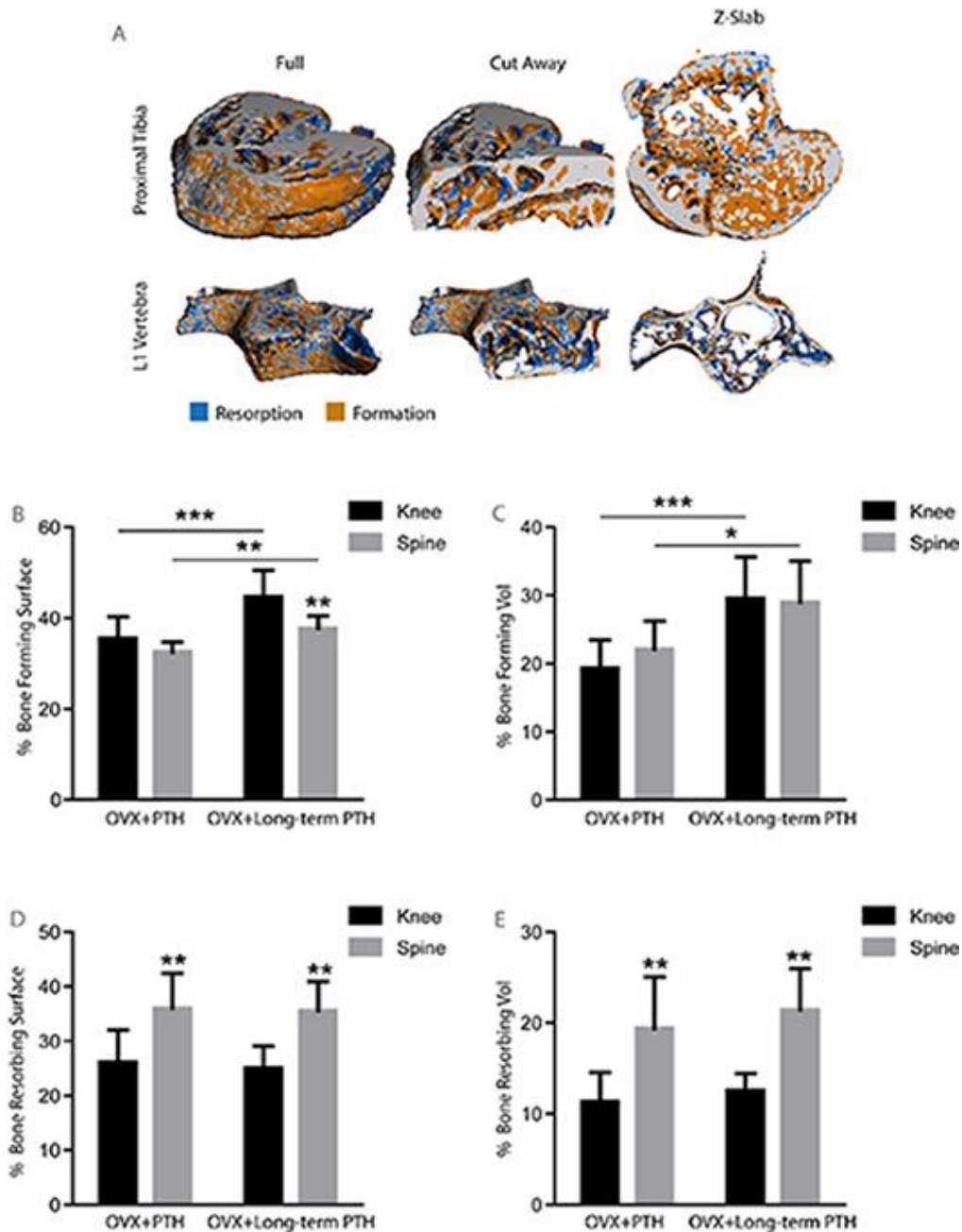
**Figure 25 Bone loss associated with ovariectomy preferentially affects the spine.** (A) *In vivo* micro-CT was used to analyze changes in bone microstructure in the L1 vertebrae and the tibia. Color-coded subtraction images show regions of bone formation (orange) and bone resorption (blue). Time-lapse micro-CT was used to quantify bone forming surfaces and volumes (B and C), as well as resorbing bone surfaces and volumes (D and E) at each time point relative to its baseline scan prior to OVX. The spine contained consistent levels of bone resorbing volumes after both short-term and long-term OVX, significantly greater than resorbing volumes observed in the tibia, while the tibia showed a significant increase in resorbing bone volume from short-term to long-term OVX. Two-way ANOVA analyses (Table S1) revealed that, although neither skeletal site nor duration of OVX significantly affected bone forming surfaces or volume, both bone region and length of OVX significantly affected bone resorption surfaces and volume. Graphs represent average values  $\pm$  SD. (\* $p < 0.05$ ) ( $n=9$ )

Table S3 Two-way ANOVA comparison of time-lapse micro-CT parameters from short-term and long-term OVX mice.

	Skeletal Site	Duration of OVX	Interaction
% Bone Forming Surface	ns	ns	ns
% Bone Forming Vol	ns	ns	ns
% Bone Resorbing Surface	0.0237	0.0279	ns
% Bone Resorbing Vol	0.0014	0.0059	ns



Micro-CT analyses were next conducted on mice treated with PTH. Because BMD values failed to show any significant changes after 3 days of PTH treatment, an additional follow-up scan was taken after 14 days of PTH treatment, which showed a significant increase in knee BMD (data not shown) and significantly increased bone metabolic serum markers<sup>142</sup> and likely represents changes in bone structure which would result from the day 3 metabolic bone statuses. Baseline and follow-up scans were overlaid to ensure analyses of similar regions and to visualize regions of localized bone formation and resorption in the vertebral and tibial VOIs (Figure 26A) and to quantify bone forming and resorbing surfaces (Figure 26B and D) and volumes (Figure 26C and E) which occurred relative to pre-treatment baseline scan. Both the tibia and spine showed significantly greater bone forming surfaces and volumes between early and long-term PTH treatment, with the tibia containing significantly greater forming surfaces than the spine after long-term PTH treatment. In contrast, the spine contained significantly greater bone resorbing surfaces and volumes than the tibia after both early and long-term PTH treatment. Two-way ANOVA analyses of time-lapse micro-CT parameters revealed that both the skeletal site and the duration of PTH treatment (day 3 vs day 14) significantly affected the bone forming surfaces, while only the length of PTH treatment affected bone formation volumes (Table S4).



**Figure 26 Treatment with PTH results in significant changes in bone microstructure.** *In vivo* micro-CT of the L1 vertebra and the knee over 14 days of PTH treatment (A). Time-lapse micro-CT was used to quantify bone forming surfaces and volumes (B and C), as well as resorbing bone surfaces and volumes (D and E) at each time point relative to its baseline scan before commencement of PTH treatment. Both the tibia and spine showed significant increases in bone forming surfaces and forming volumes after prolonged PTH treatment, with the tibia containing significantly greater bone forming surfaces than the spine after long-term PTH treatment. In contrast, the spine showed significantly greater levels of bone resorbing surfaces and volumes compared to the tibia. Two-way ANOVA analyses (Table S2) revealed that while only duration of PTH treatment affected bone formation volumes, both skeletal site and treatment length significantly affected bone forming surfaces. In regards to bone resorption, only skeletal site, and not duration of PTH treatment, was found to significantly affect resorbing volumes or surfaces. Graphs represent average values  $\pm$  SD. (\* $p < 0.05$ , \*\* $p < 0.01$ , \*\*\* $p < 0.0001$ ) (n=9)

Table S4 Two-way ANOVA comparison of time-lapse micro-CT parameters from OVX+PTH and OVX+long-term PTH-treated mice.

	Skeletal Site	Duration of PTH	Interaction
% Bone Forming Surface	0.0043	0.0001	ns
% Bone Forming Vol	ns	<0.0001	ns
% Bone Resorbing Surface	<0.0001	ns	ns
% Bone Resorbing Vol	<0.0001	ns	ns

*Binding kinetic parameters correlate with changes in bone formation and resorption*

In order to determine which aspects of bone formation and resorption are reflected in each bisphosphonate binding kinetic parameter, correlation studies were conducted between rate constant, plateau and Pw rate constant values determined by FMT and time-lapse micro-CT-derived bone forming and resorbing surfaces (Figure 27A and C) and volumes (Figure 27B and D), and their interaction assessed (Table 3). Percent forming surfaces, assessed by time-lapse micro-CT, showed significant correlations with rate constant and Pw rate constant values, assessed by FMT binding kinetics, while percent forming and resorbing bone volumes significantly correlated with plateau values.

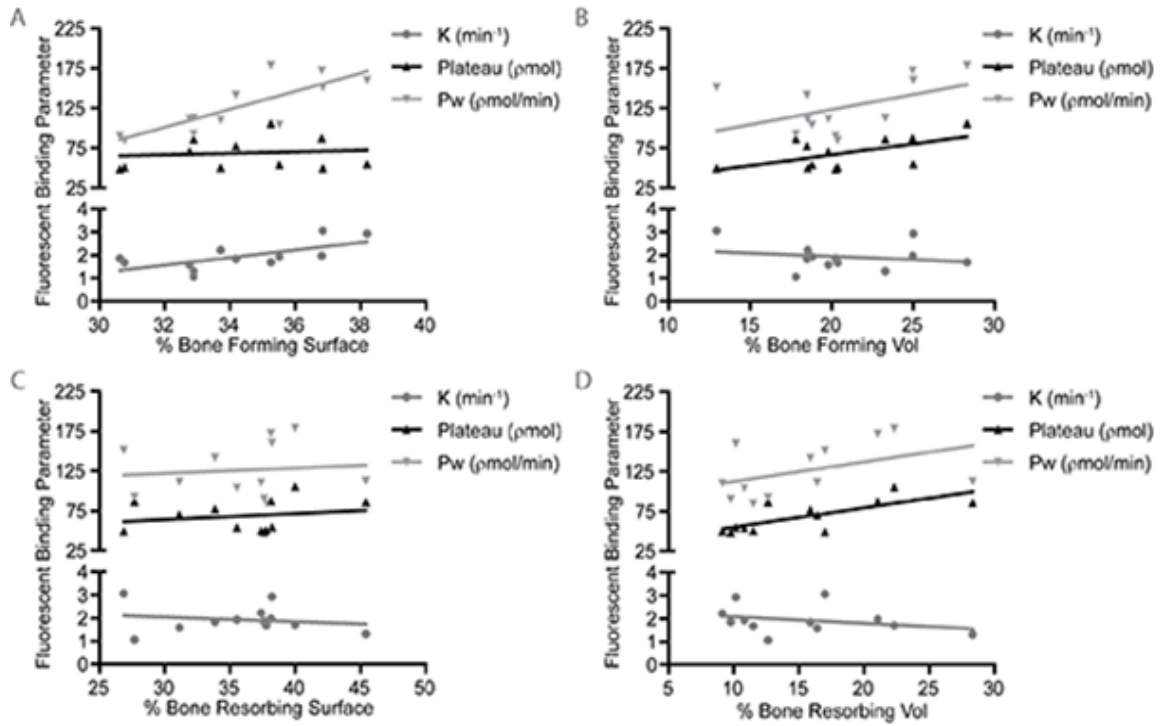


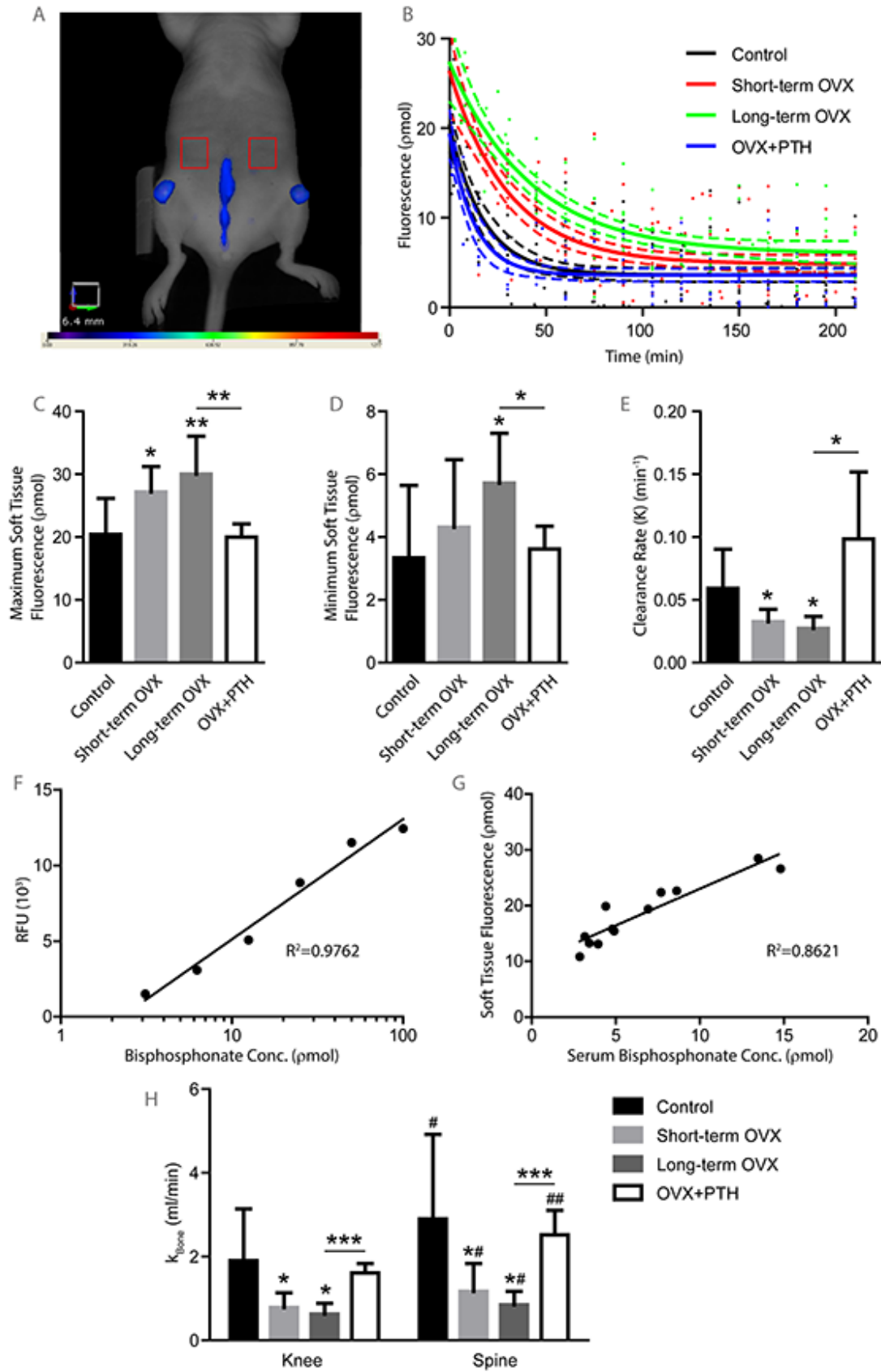
Figure 27 **Linear correlations between binding kinetic and time-lapse micro-CT parameters.** Binding kinetic parameters, assessed by *in vivo* FMT, for both the spine and knee regions, was subjected to linear regression analyses with % forming (A) and resorbing (C) surfaces and % forming (B) and resorbing (D) volumes as assessed by time-lapse micro-CT.

Table 3 **Rate constant values reflect changes in forming surfaces while plateau values reflect changes in bone formation and resorption volumes.** Linear correlations between binding kinetic and time-lapse micro-CT parameters shown in Figure 27 were assessed for their interaction. Values represent: Significance of the linear correlation/Probability that slopes are equal to zero. ns = not significant.

	Rate Constant (k)	Plateau	Pw Rate Constant
% Forming Surface	0.05/0.0174	ns/ns	0.01/0.0014
% Resorbing Surface	ns/ns	ns/ns	ns/ns
% Forming Volume	ns/ns	0.05/0.0430	ns/ns
% Resorbing Volume	ns/ns	0.01/0.0066	ns/ns

*Soft tissue fluorescence of the abdominal region correlates with serum levels of bisphosphonate*

To assess the blood pool levels of bisphosphonate available for binding over time, abdominal soft tissue fluorescence was measured (Figure 28A) and subjected to nonlinear regression analysis (Figure 28B). Both short and long-term OVX mice showed significantly greater maximum tissue fluorescence than control mice, while treatment with PTH significantly reduced maximum fluorescence back to levels comparable with control mice (Figure 28C). Ovariectomy also resulted in increased minimum fluorescence values with long-term OVX mice having significantly greater values than that of control mice. Treatment with PTH resulted in a significant decrease in minimum fluorescence values to levels consistent with control mice (Figure 28D). Both short and long-term ovariectomy resulted in significantly decreased soft tissue clearance from control mice, while PTH treatment resulted in a significant increase in the clearance rate compared to untreated long-term OVX (Figure 28E). A standard curve (Figure 28F) was used to calculate serum level bisphosphonates in imaged mice and compared to soft tissue fluorescence detected by FMT. A strong correlation ( $R^2=0.8621$ ) was found between bisphosphonate concentrations, determined by FMT soft tissue fluorescence, and *ex vivo* serum analysis (figure 28G). Using a modified Patlak's method, ovariectomized mice showed significantly reduced  $K_{\text{Bone}}$  values as compared to control mice in both the knee and spine regions, while PTH-treated mice showed significantly increased  $K_{\text{Bone}}$  values from untreated OVX controls (Figure 28H). Analyses also show significantly greater  $K_{\text{Bone}}$  values in the spine for each test group relative to the corresponding knee values.





**Figure 28 Abdominal soft tissue fluorescence correlates with serum bisphosphonate levels and shows altered clearance in OVX and PTH-treated mice.** Soft tissue fluorescence of reconstructed FMT images was quantified in regions devoid of bone (A) and subjected to nonlinear regression analysis (B). OVX resulted in significantly increased maximum (C) and minimum (D) soft tissue fluorescence compared to control mice, while treatment with PTH significantly reduced maximum and minimum fluorescence compared to untreated OVX controls. OVX also resulted in significantly decreased clearance rates of soft tissue fluorescence while treatment with PTH significantly increased the clearance rate of soft tissue fluorescence relative to untreated OVX controls. (F) A standard concentration curve of fluorescent bisphosphonates in serum was generated and used to quantify serum levels of bisphosphonate in intravenously injected mice. Fluorescence in the soft tissue region, determined by FMT imaging, and serum levels of fluorescent bisphosphonate show a strong correlation between soft tissue fluorescence and actual serum levels of bisphosphonate (G). Using a modified Patlak's method (H) analysis shows significant reductions in  $K_{\text{Bone}}$  values in response to OVX and significant increases in response to PTH treatment for both the knee and spine regions (\*). Analyses also show significantly greater  $K_{\text{Bone}}$  values for the spine relative to knee values for each group (#). Dotted lines represent 95% confidence interval. Graphs represent average values  $\pm$  SD. (\*, # $p < 0.05$ , \*\*, ## $p < 0.01$ , \*\*\* $p < 0.001$ ) (n=9)

## Discussion

In this study, we demonstrate that fluorescent bisphosphonates show consistent patterns of binding at both the vertebra and long bones in response to OVX or PTH treatment. Furthermore, we show that changes in binding kinetic parameters were found to mirror later changes observed by micro-CT methods. These binding kinetic parameters reflect the site-specific, variations observed in response to changes in metabolic status. We have additionally shown that soft tissue fluorescence, as assessed by *in vivo* FMT, correlates with serum levels of free bisphosphonate and can be used as a tool to monitor the changes in blood pool levels of bisphosphonates over time. Combining our uptake parameters of both the knee and spine regions with our soft tissue blood pool measure, we have generated  $K_{\text{Bone}}$  values for each mouse using a modified Patlak's method. Values obtained from this method show significant reductions in bisphosphonate uptake by the bone in response to ovariectomy and significant increases in bone uptake after PTH treatment.

As has been previously described for the knee region, short-term ovariectomized mice showed significantly reduced plateau, rate constant and Pw rate constant values compared to control mice, with further significant reductions observed in all parameters after long-term OVX in the spine. Conversely, treatment with PTH was found to significantly increase all binding parameters compared to untreated controls. Based on micro-CT morphometry, combined with the observed changes in binding kinetics of the spine and knee region in response to OVX and PTH treatment, bone surface and metabolic status plays an important role in both plateau and rate constant binding parameters. In response to treatment with PTH, we observed a preferential increase in rate constant within the knee and binding plateau within the spine. This corresponded to preferential increases in bone forming surfaces in the knee and elevated levels of bone resorption surfaces and volumes in the spine. This data suggests a relationship between rate constant and plateau values and changes in metabolic activity which ultimately gives rise to bone loss/apposition. Though rate constant and plateau values are interdependent, correlation studies with time-lapse micro-CT, which assesses localized changes in bone microstructure<sup>74, 82</sup>, support a preferential interaction between bone apposition surfaces and rate constant values, as well as bone loss and apposition volumes and plateau values. The fact that binding kinetics in the knee and spine differ in response to PTH treatment suggest that this kinetic monitoring

has the ability to distinguish between these metabolically distinct sites with a high degree of sensitivity. It is important to note that, because micro-CT provides only a snap shot of bone structure, time-lapse micro-CT analyses may underestimate the amount of bone forming volumes and surfaces in regions where new bone formation occurs over top of resorbed areas, but has not deposited sufficient mineral to overcome the mineral lost by previous resorption. Histological confirmation will be required to correlate metabolically actively forming and resorbing surfaces with bisphosphonate uptake. Nevertheless, micro-CT has previously been shown to correlate with dynamic histomorphometry in mice<sup>127</sup>.

Previous works have demonstrated a preferential uptake of bisphosphonates by newly mineralized bone, and by active remodeling surfaces compared to quiescent bone surfaces<sup>113, 142</sup>. Taken together, we propose a hierarchical model of bone bisphosphonate uptake from high uptake, newly mineralized bone, to medium uptake, newly exposed/resorbing bone, to low uptake, quiescent bone surfaces. Using these criteria, treatment with PTH results in increased high uptake bone surface within the knee region, resulting in rapid uptake shortly after injection while the spine shows increased accumulation of both high and medium uptake bone, resulting in increased uptake rates and plateau values. While the amount of high uptake, newly mineralized bone is dependent on the osteoblast activity, the amount of newly exposed mineral will be dependent on the osteoclasts and will be affected both by the number of osteoclasts as well as the depth of the resorbing pits. Though the preferential uptake of bisphosphonates by newly deposited minerals has previous been suggested to reflect the presence of amorphous, higher affinity calcium phosphate present in newly forming bone as compared to the lower affinity crystalline minerals present in fully mineralized bone<sup>42, 142</sup>, both quiescent and resorbed surfaces are comprised of fully mineralized bone. Reduced exposure and/or binding of the bone mineral, potentially limited by bone lining cells or secreted extracellular matrix components present on quiescent bone surfaces but not on resorbing surfaces, may explain their differential uptake of bisphosphonates from the blood.

Finally, we have demonstrated that time-related reductions in bisphosphonate fluorescence from within the abdominal soft tissue shows significant reductions in both the extent and rate of

clearance in response to OVX and significantly greater clearance kinetics in PTH-treated mice compared to untreated controls. These results are consistent with the observed changes in bisphosphonate bone uptake in that decreased bone uptake, in the case of OVX, would result in delayed blood clearance while increased bone uptake, observed in PTH-treated mice, would result in increased blood pool clearance. We also show a strong correlation between soft tissue fluorescence assessed by *in vivo* FMT and serum levels of free bisphosphonate. Using soft tissue fluorescence as a blood pool correction, modified compartment model Patlak's calculations were conducted to assign quantitative values of bisphosphonate bone uptake. Results show that ovariectomy gives rise to significant reductions in  $K_{\text{Bone}}$  values while treatment with PTH shows significant increases in this parameter. Additionally, Patlak's calculations also showed significantly greater  $K_{\text{Bone}}$  values for the spine in each test group relative to corresponding values observed in the knee, similar to results observed in humans using  $^{18}\text{F}$ -fluoride PET comparing the vertebra to the humerus<sup>24</sup>. This has previously been explained by greater tracer delivery to the spine, accounted for by greater regional blood flow<sup>101</sup>. Because these values are derived from both blood and bone values,  $K_{\text{Bone}}$  values reflect the accumulation of bisphosphonates on the bone adjusted for the clearance of available unbound probe from the blood and thus,  $K_{\text{Bone}}$  values should better approximate changes in bone metabolism. In our models of relatively short term OVX or treatment with PTH, minimal changes in body weight, renal function or blood flow are expected to occur, minimizing the overall benefit received with this modified multi-compartment analysis. However, while the resolution of FMT does not permit the evaluation of site-specific blood flow, this general blood pool correction factor should prove useful in mouse models in which significant changes in body mass or renal function occur, such as the case in tumor models and some therapeutic treatments, and help overcome some bias in bone binding kinetics resulting from the uptake of bisphosphonates by other skeletal sites as has previously been observed in treated patients<sup>6</sup>.

Previous works have suggested competing perspectives on the effects of PTH treatment on spine and tibia bone mineral changes<sup>63, 161</sup>. It is possible that because of the site of injection and the dosing administered in this study, bone changes in the spine reflect more a continuous PTH-dosing model in which the anabolic effects are replaced with significant up regulation in bone remodeling

with no net bone mineral increase<sup>86</sup>. Other works have also suggested that different skeletal sites may be comprised of functionally distinct cell populations which respond at different rates and to different extents to anabolic therapy<sup>102</sup>. This idea is supported by the fact that, while both the knee and spine regions show relatively similar increases in bone forming surfaces and volumes, relative to OVX controls, the knee shows substantially greater reductions in bone resorbing volumes and surfaces than were observed in the spine. As a result, the overall bone metabolic activity (bone formation and resorption) is greater in the spine than the knee. This is consistent with micro-CT and  $K_{\text{Bone}}$  values in which the spine shows significantly greater bone turnover (forming and resorbing bone volume) and greater uptake of bisphosphonate relative to the knee region. It has also been noted that PTH treatment tends to enhance bone formation at sites of stress<sup>108</sup> and this effect may be mediated through sclerostin<sup>100</sup>. Nude mice used in this study are also T cell-deficient, which have previously been shown to play a role in stimulating both osteoclastogenesis and osteoblast differentiation<sup>17, 96, 106, 153</sup>. It would be of great interest to determine which, if any, of these factors contribute to the differential responses observed to PTH treatment between the knee and the spine in this study and other studies published in mice, rats and humans. It is also possible that, because kinetic analyses were done after a relatively short time period after the beginning of PTH treatment, the knee region, and predominantly the actively-modeling trabecular regions distal to the growth plate, are more rapidly responsive and thus, show more significant changes in BMD values relative to the spine.

Overall, these methods show great utility in as *in vivo* tools for assessing metabolic activity in a range of potential models. We were able to show bone metabolism, as assessed by binding kinetics, varies between skeletal sites. We also provide evidence that these differences may be due to changes in bone surface properties, as illustrated by correlation with time-lapse micro-CT analyses. Both methods were also able to distinguish differential responses to bone anabolic treatment suggesting utility in monitoring site-specific responses to novel therapeutic interventions. With the addition of a blood pool correction and multi-compartment analyses, the binding kinetics assay now accounts for biases introduced by off-site uptake (both soft tissue and other, non-measured skeletal sites) as well as conditions which may result in delay clearance of free bisphosphonates from the blood pool (i.e. renal impairment).

## **Acknowledgements**

The authors are grateful to Dr. Olga Will for her assistance in conducting all animal experiments. Financial support was provided by the Deutsche Forschungsgemeinschaft (DFG) through the Forschergruppe 1586 SKELMET and by the research grant from the state of Schleswig-Holstein and the European Union ERDF-European Regional Development Fund (MOIN CC, Zukunftsprogramm Wirtschaft). Authors' roles: Study design: RJT, GMC, CCG and ST. Study conduct: RJT, GMC and MM. Data collection: RJT and MM. Data analysis: RJT and GMC. Data interpretation: RJT, GMC and CCG. Drafting manuscript: RJT. Revising manuscript content: RJT, GMC, MM, CCG and ST. Approval of final version of manuscript: RJT, GMC, CCG and ST. ST takes responsibility for the integrity of the data analysis.

### 3. Discussion and future directions

In the above works, the utility of bisphosphonates as targeting molecules for use in the development of novel therapeutics and imaging biomarkers was evaluated. In the case of drug targeting, we demonstrate the utility of the drug conjugate 5-FdU-alendronate as an effective therapeutic in the treatment of osteolytic bone metastases resulting in decreased frequency and size of metastatic lesions and increased inhibition of osteoclast activity without effecting new bone formation. We have also shown that 5-FdU-ale can be administered at high doses relative to alendronate alone without any toxic effects. This data supports both the further development of 5-FdU-ale as a potential anti-bone lesion therapeutic, possibly replacing the standard bisphosphonate adjuvant therapy given to breast cancer patients, as well as the development of other drug conjugates between bisphosphonates and anti-tumor or anti-metabolite drugs. It would also be of great interest to explore the use of these new therapeutics in the context of other bone diseases such as osteoporosis, where current long-term treatments depress new bone formation as well as resorption, and in prostate cancer and Paget's disease, where initial osteoclast activity plays a critical role but later stage disease can be primarily osteosclerotic in nature.

Using *in vivo* binding kinetics, we have now demonstrated that high affinity bisphosphonates show varying degrees of bone uptake depending on the metabolic activity of the bone, with newly deposited minerals showing greater uptake than regions of newly exposed minerals associated with bone resorption, which in turn shows greater uptake than quiescent bone surfaces. As a result, monitoring binding kinetics provides a site-specific, instantaneous marker of the bones current metabolic status. These correlations between binding kinetic parameters and bone status were also confirmed by time-lapse micro-CT where skeletal regions with increased actively mineralizing bone surfaces showed primarily increased binding rate constants, while skeletal regions showing upregulated bone resorption responded primarily with increased binding plateau values. This ability to identify regions of high bone metabolic activity was additionally applied in the context of osteolytic breast cancer bone lesions. Mice containing MDA-MB-231 were identified by bioluminescent detection as described above in chapter 2.2. Mice were injected with a fluorescently-labeled bisphosphonate and kinetic analyses were performed as described in chapter 2.3. Binding kinetic

parameters were determined for individual limbs containing bioluminescent tumor signal. Rate constants and binding plateau values were determined and correlated with tumor size, determined by bioluminescent signal area (Figure 29). Both the rate constant and plateau values showed good correlation with estimated tumor size ( $R^2=0.7938$  and  $0.7309$  respectively). These results suggest that, as the tumor size increases, rate constant values also increase. This is consistent with previous results which suggested that metabolically active bone shows a more rapid uptake of bisphosphonates. In contrast to rate constant values, binding plateau values appear to decrease as tumor size increases. This result is not surprising considering the amount of bone resorbed and most likely reflects the significant decrease in bone available for binding resulting from these large osteolytic lesions. This data suggests that binding kinetics may serve as a useful imaging biomarker for the detection of bone lesions and possibly serve as a means to distinguish metastatic from benign lesions. Further work is required to characterize the binding of bisphosphonates to bone in a highly osteolytic tumor environment. Specifically, regions of rapid bisphosphonate uptake will be compared to micro-CT analyses to identify regions of bone formation and resorption from baseline scans, along with corresponding histological analyses which will verify regions identified as resorbing or forming by micro-CT are associated with increased levels of osteoclasts or osteoblasts, respectively. This will allow us to quantify bisphosphonate binding in regions of formation, resorption and quiescence.



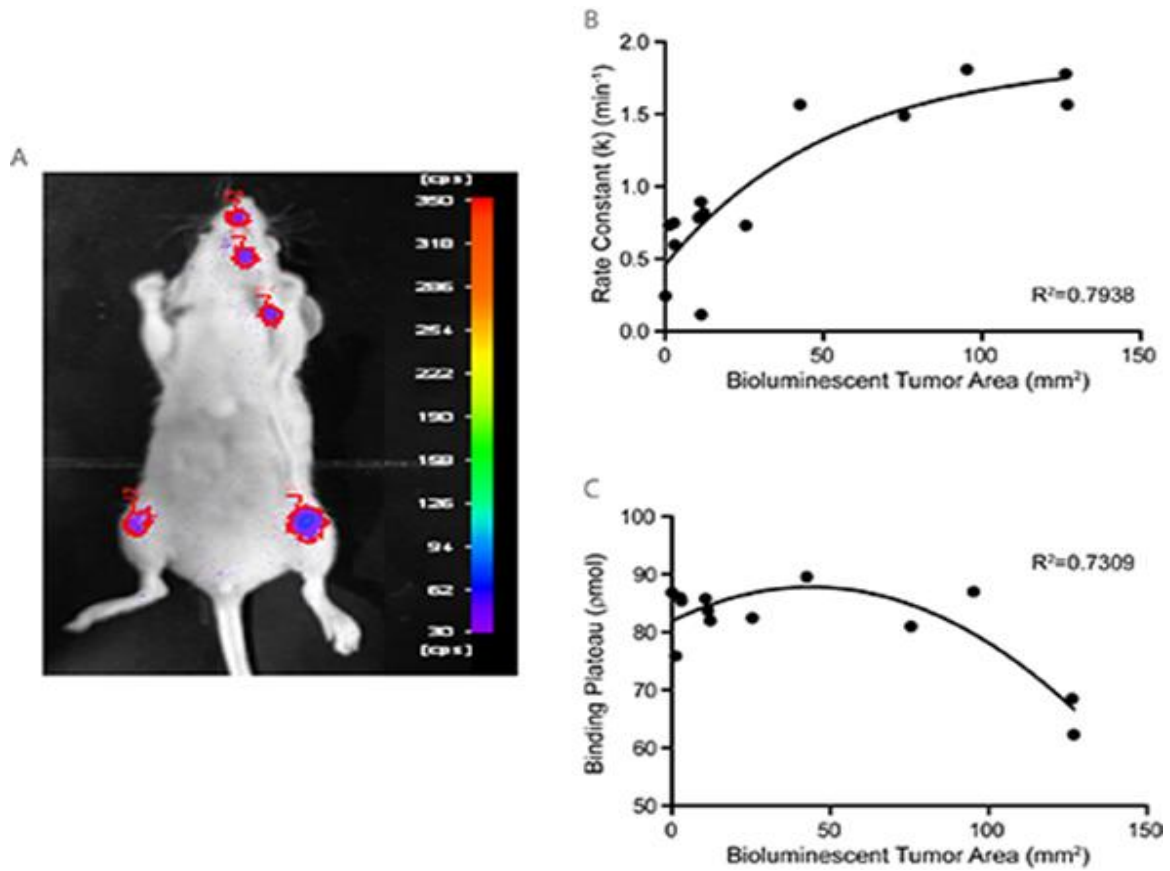


Figure 29 **Binding kinetic parameters correlate with tumor progression.** Mice were injected with the breast cancer cell line MDA-MB231 and imaged weekly for bioluminescent detection of bone metastases formation (A). Mice were injected with a fluorescently-labeled bisphosphonate and binding kinetic assessments for individual tumor-burdened limbs were assessed. Tumor area, assessed by bioluminescence, showed good correlations with both the rate constant ( $R^2=0.7938$ ) and plateau ( $R^2=0.7309$ ) values, assessed by FMT.

One additional topic which warrants further investigation is the differences in bisphosphonate binding characteristics associated with their varying bone affinities. Previous work has illustrated preferential binding of high affinity bisphosphonates to regions of newly mineralized bone<sup>142</sup> while low affinity bisphosphonates appear primarily in resorbing pits<sup>113</sup>. Due to a lack of histological confirmation, it still remains unclear whether this preferential binding of low affinity bisphosphonates to resorbing pits is due to newly exposed minerals as the result of osteoclast activity, or whether these resorbing pits are actually the sites of osteoblast activity depositing fresh, high uptake minerals to replace previously resorbed bone<sup>68</sup>. In any case, this differential binding pattern could prove useful in the preferential assessment and targeting of resorbing and forming bone. This may have great implications in the choice of bisphosphonate used to develop new conjugate drugs which will preferentially target osteolytic or osteosclerotic bone lesions and may also have utility in identifying mixed bone lesions in which both excessive bone loss and gain occurs, but fails to show any significant change in overall bone volume making identification of these lesions by traditional radiographic approaches difficult.

## 4. Conclusions

Bisphosphonates show a very high affinity for the bone and, as such, serve as a useful tool in the targeting of conjugated therapeutics. Here, data is presented on the novel conjugate drug 5-FdU-ale which shows no significant signs of toxicity and increased efficacy in the treatment of breast cancer bone metastases *in vivo*. Additionally, mice treated with 5-FdU-ale showed significant inhibition of osteoclasts while maintaining normal osteoblast function. This resulted in significantly greater bone volume and mineral assessments than mice treated with either alendronate or 5-FdU. With the addition of fluorescent dyes, bisphosphonates can also be used to provide a site-specific marker for the current metabolic state of the bone. Here, we provide evidence supporting the use of bisphosphonate binding kinetics in the monitoring of systemic or localized bone loss and the monitoring of the bone response to anabolic stimuli. These binding kinetic assays have great utility in assessing changes in bone metabolism at a very early stage before any structural changes are observed and thus, may prove useful in the early evaluation of novel therapeutics in the context of either excessive bone loss or gain. With further work incorporating the use of both high and low affinity bisphosphonates, the utility and sensitivity of binding kinetics is likely to prove a useful tool for both the bone monitoring of osteolytic, osteosclerotic and mixed bone lesions and may also guide the development of novel bisphosphonate conjugate therapeutics.

## 5. Additional published works

Fritsche H\*, Heilmann T\*, **Tower RJ\***, Hauser C, von Au A, El-Sheikh D, Campbell GM, Alp G, Schewe D, Hübner S, Tiwari S, Kownatzki D, Boretius S, Adam D, Jonat W, Becker T, Gluer CC, Zöller M, Kalthoff H, Schem C, Trauzold A. 2015. TRAIL-R2 promotes skeletal metastases in a breast cancer xenograft mouse model. *Oncotarget*, *accepted*

Dotterweich J, Ebert R, Kraus S, **Tower RJ**, Jakob F, Schütze N. 2014. Mesenchymal stem cell contact promotes *CCNI* splicing and transcription in myeloma cells. *Cell Commun Signal* 12(36)

Ranta TM, Suojanen J, Penate-Medina O, Will O, **Tower RJ**, Glüer CC, Kairemo K, Gahmberg CG, Koivunen E, Sorsa T, Saris PEJ and Reunanen J. 2014. *In vivo* targeting of activated leukocytes by B2-integrin binding peptide. *Mol Diagn Ther* 18:39-44

## 6. References

- 1 N. Al Nakouzi, O. Bawa, A. Le Pape, S. Lerondel, C. Gaudin, P. Opolon, P. Gonin, K. Fizazi, and A. Chauchereau, 'The Igr-Cap1 Xenograft Model Recapitulates Mixed Osteolytic/Blastic Bone Lesions Observed in Metastatic Prostate Cancer', *Neoplasia*, 14 (2012), 376-87.
- 2 M. H. Barcellos-Hoff, D. Lyden, and T. C. Wang, 'The Evolution of the Cancer Niche During Multistage Carcinogenesis', *Nat Rev Cancer*, 13 (2013), 511-8.
- 3 F. G. Basso, A. P. Turrioni, J. Hebling, and C. A. de Souza Costa, 'Effects of Zoledronic Acid on Odontoblast-Like Cells', *Arch Oral Biol*, 58 (2013), 467-73.
- 4 F. Berger, Y. P. Lee, A. M. Loening, A. Chatziioannou, S. J. Freedland, R. Leahy, J. R. Lieberman, A. S. Belldegrun, C. L. Sawyers, and S. S. Gambhir, 'Whole-Body Skeletal Imaging in Mice Utilizing Micropet: Optimization of Reproducibility and Applications in Animal Models of Bone Disease', *Eur J Nucl Med Mol Imaging*, 29 (2002), 1225-36.
- 5 G. M. Blake, S. J. Park-Holohan, G. J. Cook, and I. Fogelman, 'Quantitative Studies of Bone with the Use of 18f-Fluoride and 99mTc-Methylene Diphosphonate', *Semin Nucl Med*, 31 (2001), 28-49.
- 6 G. M. Blake, M. Siddique, M. L. Frost, A. E. Moore, and I. Fogelman, 'Radionuclide Studies of Bone Metabolism: Do Bone Uptake and Bone Plasma Clearance Provide Equivalent Measurements of Bone Turnover?', *Bone*, 49 (2011), 537-42.
- 7 G. M. Blake, M. Siddique, T. Puri, M. L. Frost, A. E. Moore, G. J. Cook, and I. Fogelman, 'A Semipopulation Input Function for Quantifying Static and Dynamic 18f-Fluoride Pet Scans', *Nucl Med Commun*, 33 (2012), 881-8.
- 8 G. Boivin, and P. J. Meunier, 'The Degree of Mineralization of Bone Tissue Measured by Computerized Quantitative Contact Microradiography', *Calcif Tissue Int*, 70 (2002), 503-11.
- 9 M. L. Bouxsein, 'Technology Insight: Noninvasive Assessment of Bone Strength in Osteoporosis', *Nat Clin Pract Rheumatol*, 4 (2008), 310-8.
- 10 B. Brodsky, and A. V. Persikov, 'Molecular Structure of the Collagen Triple Helix', *Adv Protein Chem*, 70 (2005), 301-39.
- 11 P. R. Buenzli, P. Pivonka, and D. W. Smith, 'Bone Refilling in Cortical Basic Multicellular Units: Insights into Tetracycline Double Labelling from a Computational Model', *Biomech Model Mechanobiol* (2013).
- 12 H. R. Buie, G. M. Campbell, R. J. Klinck, J. A. MacNeil, and S. K. Boyd, 'Automatic Segmentation of Cortical and Trabecular Compartments Based on a Dual Threshold Technique for in Vivo Micro-Ct Bone Analysis', *Bone*, 41 (2007), 505-15.
- 13 C. Busch, U. Drews, S. R. Eisele, C. Garbe, and M. Oppitz, 'Noggin Blocks Invasive Growth of Murine B16-F1 Melanoma Cells in the Optic Cup of the Chick Embryo', *Int J Cancer*, 122 (2008), 526-33.
- 14 J. Caetano-Lopes, H. Canhao, and J. E. Fonseca, 'Osteoblasts and Bone Formation', *Acta Reumatol Port*, 32 (2007), 103-10.
- 15 G. M. Campbell, S. Tiwari, F. Grundmann, N. Purcz, C. Schem, and C. C. Gluer, 'Three-Dimensional Image Registration Improves the Long-Term Precision of in Vivo Micro-Computed Tomographic Measurements in Anabolic and Catabolic Mouse Models', *Calcif Tissue Int*, 94 (2014), 282-92.
- 16 D. R. Carter, and W. C. Hayes, 'The Compressive Behavior of Bone as a Two-Phase Porous Structure', *J Bone Joint Surg Am*, 59 (1977), 954-62.
- 17 S. Cenci, M. N. Weitzmann, C. Roggia, N. Namba, D. Novack, J. Woodring, and R. Pacifici, 'Estrogen Deficiency Induces Bone Loss by Enhancing T-Cell Production of Tnf-Alpha', *J Clin Invest*, 106 (2000), 1229-37.
- 18 Y. C. Chen, D. M. Sosnoski, and A. M. Mastro, 'Breast Cancer Metastasis to the Bone: Mechanisms of Bone Loss', *Breast Cancer Res*, 12 (2010), 215.
- 19 E. S. Christenson, X. Jiang, R. Kagan, and P. Schnatz, 'Osteoporosis Management in Post-Menopausal Women', *Minerva Ginecol*, 64 (2012), 181-94.

- 20 B. Clarke, 'Normal Bone Anatomy and Physiology', *Clin J Am Soc Nephrol*, 3 Suppl 3 (2008), S131-9.
- 21 R. E. Coleman, 'Skeletal Complications of Malignancy', *Cancer*, 80 (1997), 1588-94.
- 22 R. E. Coleman, and R. D. Rubens, 'The Clinical Course of Bone Metastases from Breast Cancer', *Br J Cancer*, 55 (1987), 61-6.
- 23 P. Collin-Osdoby, 'Role of Vascular Endothelial Cells in Bone Biology', *J Cell Biochem*, 55 (1994), 304-9.
- 24 G. J. Cook, M. A. Lodge, G. M. Blake, P. K. Marsden, and I. Fogelman, 'Differences in Skeletal Kinetics between Vertebral and Humeral Bone Measured by <sup>18</sup>F-Fluoride Positron Emission Tomography in Postmenopausal Women', *J Bone Miner Res*, 15 (2000), 763-9.
- 25 F. P. Coxon, K. Thompson, A. J. Roelofs, F. H. Ebetino, and M. J. Rogers, 'Visualizing Mineral Binding and Uptake of Bisphosphonate by Osteoclasts and Non-Resorbing Cells', *Bone*, 42 (2008), 848-60.
- 26 P. V. Danenberg, C. Heidelberger, M. A. Mulkins, and A. R. Peterson, 'The Incorporation of 5-Fluoro-2'-Deoxyuridine into DNA of Mammalian Tumor Cells', *Biochem Biophys Res Commun*, 102 (1981), 654-8.
- 27 F. Daubine, C. Le Gall, J. Gasser, J. Green, and P. Clezardin, 'Antitumor Effects of Clinical Dosing Regimens of Bisphosphonates in Experimental Breast Cancer Bone Metastasis', *J Natl Cancer Inst*, 99 (2007), 322-30.
- 28 P. D. Delmas, 'Biochemical Markers of Bone Turnover', *J Bone Miner Res*, 8 Suppl 2 (1993), S549-55.
- 29 N. Dirckx, M. Van Hul, and C. Maes, 'Osteoblast Recruitment to Sites of Bone Formation in Skeletal Development, Homeostasis, and Regeneration', *Birth Defects Res C Embryo Today*, 99 (2013), 170-91.
- 30 M. T. Drake, B. L. Clarke, and S. Khosla, 'Bisphosphonates: Mechanism of Action and Role in Clinical Practice', *Mayo Clin Proc*, 83 (2008), 1032-45.
- 31 J. E. Dunford, M. J. Rogers, F. H. Ebetino, R. J. Phipps, and F. P. Coxon, 'Inhibition of Protein Prenylation by Bisphosphonates Causes Sustained Activation of Rac, Cdc42, and Rho Gtpases', *J Bone Miner Res*, 21 (2006), 684-94.
- 32 J. E. Dunford, K. Thompson, F. P. Coxon, S. P. Luckman, F. M. Hahn, C. D. Poulter, F. H. Ebetino, and M. J. Rogers, 'Structure-Activity Relationships for Inhibition of Farnesyl Diphosphate Synthase in Vitro and Inhibition of Bone Resorption in Vivo by Nitrogen-Containing Bisphosphonates', *J Pharmacol Exp Ther*, 296 (2001), 235-42.
- 33 Marco Eijken, Sigrid Swagemakers, Marijke Koedam, Cobie Steenbergen, Pieter Derkx, André G. Uitterlinden, Peter J. van der Spek, Jenny A. Visser, Frank H. de Jong, Huibert A. P. Pols, and Johannes P. T. M. van Leeuwen, 'The Activin a-Follistatin System: Potent Regulator of Human Extracellular Matrix Mineralization', *The FASEB Journal*, 21 (2007), 2949-60.
- 34 A. A. El-Mabhouh, P. N. Nation, J. T. Abele, T. Riauka, E. Postema, A. J. McEwan, and J. R. Mercer, 'A Conjugate of Gemcitabine with Bisphosphonate (Gem/Bp) Shows Potential as a Targeted Bone-Specific Therapeutic Agent in an Animal Model of Human Breast Cancer Bone Metastases', *Oncol Res*, 19 (2011), 287-95.
- 35 E. F. Eriksen, D. W. Axelrod, and F. Melsen, 'Bone Histomorphometry', (New York: Raven Press, 1994), pp. 1-12.
- 36 Sturtz GA Fabulet O, 'Synthesis of Gem-Bisphosphonic Doxorubicinconjugates', *Phosphorus Sulfur Silicon Relat Elem.*, 101 (1995), 225-34.
- 37 S. Fechner, C. Busch, M. Oppitz, U. Drews, and M. Meyer-Wittkopf, 'The Chick Embryo as a Model for Intrauterine Ultrasound-Guided Heart Intervention', *Ultrasound Obstet Gynecol*, 31 (2008), 277-83.
- 38 J. E. Fisher, M. J. Rogers, J. M. Halasy, S. P. Luckman, D. E. Hughes, P. J. Masarachia, G. Wesolowski, R. G. Russell, G. A. Rodan, and A. A. Reszka, 'Alendronate Mechanism of Action: Geranylgeraniol, an Intermediate in the Mevalonate Pathway, Prevents Inhibition of Osteoclast Formation, Bone Resorption, and Kinase Activation in Vitro', *Proc Natl Acad Sci U S A*, 96 (1999), 133-8.

- 39 K. Fizazi, A. Lipton, X. Mariette, J. J. Body, Y. Rahim, J. R. Gralow, G. Gao, L. Wu, W. Sohn, and S. Jun, 'Randomized Phase II Trial of Denosumab in Patients with Bone Metastases from Prostate Cancer, Breast Cancer, or Other Neoplasms after Intravenous Bisphosphonates', *J Clin Oncol*, 27 (2009), 1564-71.
- 40 H. Fleisch, 'Bisphosphonates. Pharmacology and Use in the Treatment of Tumour-Induced Hypercalcaemic and Metastatic Bone Disease', *Drugs*, 42 (1991), 919-44.
- 41 I. Fogelman, R. G. Bessent, J. G. Turner, D. L. Citrin, I. T. Boyle, and W. R. Greig, 'The Use of Whole-Body Retention of Tc-99m Diphosphonate in the Diagnosis of Metabolic Bone Disease', *J Nucl Med*, 19 (1978), 270-5.
- 42 M. D. Francis, D. L. Ferguson, A. J. Tofe, J. A. Bevan, and S. E. Michaels, 'Comparative Evaluation of Three Diphosphonates: In Vitro Adsorption (C- 14 Labeled) and in Vivo Osteogenic Uptake (Tc-99m Complexed)', *J Nucl Med*, 21 (1980), 1185-9.
- 43 P. Fratzl, 'Bone Fracture: When the Cracks Begin to Show', *Nat Mater*, 7 (2008), 610-2.
- 44 C. A. Frolik, E. C. Black, R. L. Cain, J. H. Satterwhite, P. L. Brown-Augsburger, M. Sato, and J. M. Hock, 'Anabolic and Catabolic Bone Effects of Human Parathyroid Hormone (1-34) Are Predicted by Duration of Hormone Exposure', *Bone*, 33 (2003), 372-9.
- 45 M. L. Frost, M. Siddique, G. M. Blake, A. E. Moore, P. J. Schleyer, J. T. Dunn, E. J. Somer, P. K. Marsden, R. Eastell, and I. Fogelman, 'Differential Effects of Teriparatide on Regional Bone Formation Using (18)F-Fluoride Positron Emission Tomography', *J Bone Miner Res*, 26 (2011), 1002-11.
- 46 D. L. Galson, and G. D. Roodman, 'Pathobiology of Paget's Disease of Bone', *J Bone Metab*, 21 (2014), 85-98.
- 47 H. K. Genant, K. Engelke, and S. Prevrhal, 'Advanced Ct Bone Imaging in Osteoporosis', *Rheumatology (Oxford)*, 47 Suppl 4 (2008), iv9-16.
- 48 L. J. Gibson, 'The Mechanical Behaviour of Cancellous Bone', *J Biomech*, 18 (1985), 317-28.
- 49 M. Gnant, 'Intravenous Bisphosphonates for Breast Cancer: Impact on Patient Outcomes and Scientific Concepts', *Breast Dis*, 33 (2011), 71-81.
- 50 E. E. Graves, D. Yessayan, G. Turner, R. Weissleder, and V. Ntziachristos, 'Validation of in Vivo Fluorochrome Concentrations Measured Using Fluorescence Molecular Tomography', *J Biomed Opt*, 10 (2005), 44019.
- 51 J. R. Green, 'Antitumor Effects of Bisphosphonates', *Cancer*, 97 (2003), 840-7.
- 52 T. A. Guise, W. M. Kozlow, A. Heras-Herzig, S. S. Padalecki, J. J. Yin, and J. M. Chirgwin, 'Molecular Mechanisms of Breast Cancer Metastases to Bone', *Clin Breast Cancer*, 5 Suppl (2005), S46-53.
- 53 T. A. Guise, and G. R. Mundy, 'Cancer and Bone', *Endocr Rev*, 19 (1998), 18-54.
- 54 H. S. Gupta, J. Seto, W. Wagermaier, P. Zaslansky, P. Boesecke, and P. Fratzl, 'Cooperative Deformation of Mineral and Collagen in Bone at the Nanoscale', *Proc Natl Acad Sci U S A*, 103 (2006), 17741-6.
- 55 S. E. Halpern, P. L. Hagan, D. M. Chauncey, and P. Ayers, 'The Effect of Parathyroid Hormone on Technetium-99m Pyrophosphate Distribution in Rats', *Eur J Nucl Med*, 5 (1980), 515-9.
- 56 K. Harigaya, and H. Handa, 'Generation of Functional Clonal Cell Lines from Human Bone Marrow Stroma', *Proc Natl Acad Sci U S A*, 82 (1985), 3477-80.
- 57 K. Hashimoto, K. Morishige, K. Sawada, M. Tahara, S. Shimizu, S. Ogata, M. Sakata, K. Tasaka, and T. Kimura, 'Alendronate Suppresses Tumor Angiogenesis by Inhibiting Rho Activation of Endothelial Cells', *Biochem Biophys Res Commun*, 354 (2007), 478-84.
- 58 B. E. Hillner, J. N. Ingle, J. R. Berenson, N. A. Janjan, K. S. Albain, A. Lipton, G. Yee, J. S. Biermann, R. T. Chlebowski, and D. G. Pfister, 'American Society of Clinical Oncology Guideline on the Role of Bisphosphonates in Breast Cancer. American Society of Clinical Oncology Bisphosphonates Expert Panel', *J Clin Oncol*, 18 (2000), 1378-91.
- 59 A. B. Hodsman, D. C. Bauer, D. W. Dempster, L. Dian, D. A. Hanley, S. T. Harris, D. L. Kendler, M. R. McClung, P. D. Miller, W. P. Olszynski, E. Orwoll, and C. K. Yuen, 'Parathyroid Hormone and Teriparatide for the Treatment of Osteoporosis: A Review of the Evidence and Suggested Guidelines for Its Use', *Endocr Rev*, 26 (2005), 688-703.

- 60 L. C. Hofbauer, S. Khosla, C. R. Dunstan, D. L. Lacey, W. J. Boyle, and B. L. Riggs, 'The Roles of Osteoprotegerin and Osteoprotegerin Ligand in the Paracrine Regulation of Bone Resorption', *J Bone Miner Res*, 15 (2000), 2-12.
- 61 F. Hosain, R. P. Spencer, H. M. Couthon, and G. L. Sturtz, 'Targeted Delivery of Antineoplastic Agent to Bone: Biodistribution Studies of Technetium-99m-Labeled Gem-Bisphosphonate Conjugate of Methotrexate', *J Nucl Med*, 37 (1996), 105-7.
- 62 W. K. Hsu, M. S. Virk, B. T. Feeley, D. B. Stout, A. F. Chatziioannou, and J. R. Lieberman, 'Characterization of Osteolytic, Osteoblastic, and Mixed Lesions in a Prostate Cancer Mouse Model Using <sup>18</sup>F-Fdg and <sup>18</sup>F-Fluoride Pet/Ct', *J Nucl Med*, 49 (2008), 414-21.
- 63 A. Iida-Klein, H. Zhou, S. S. Lu, L. R. Levine, M. Ducayen-Knowles, D. W. Dempster, J. Nieves, and R. Lindsay, 'Anabolic Action of Parathyroid Hormone Is Skeletal Site Specific at the Tissue and Cellular Levels in Mice', *J Bone Miner Res*, 17 (2002), 808-16.
- 64 M. Ito, M. Chokki, Y. Ogino, Y. Satomi, Y. Azuma, T. Ohta, and M. Kiyoki, 'Comparison of Cytotoxic Effects of Bisphosphonates in Vitro and in Vivo', *Calcif Tissue Int*, 63 (1998), 143-7.
- 65 I. Jager, and P. Fratzl, 'Mineralized Collagen Fibrils: A Mechanical Model with a Staggered Arrangement of Mineral Particles', *Biophys J*, 79 (2000), 1737-46.
- 66 R. L. Jilka, 'Molecular and Cellular Mechanisms of the Anabolic Effect of Intermittent Pth', *Bone*, 40 (2007), 1434-46.
- 67 O. Johnell, and J. A. Kanis, 'An Estimate of the Worldwide Prevalence and Disability Associated with Osteoporotic Fractures', *Osteoporos Int*, 17 (2006), 1726-33.
- 68 B. B. Kalpakcioglu, S. Morshed, K. Engelke, and H. K. Genant, 'Advanced Imaging of Bone Macrostructure and Microstructure in Bone Fragility and Fracture Repair', *J Bone Joint Surg Am*, 90 Suppl 1 (2008), 68-78.
- 69 J. A. Kanis, O. Johnell, A. Oden, I. Sembo, I. Redlund-Johnell, A. Dawson, C. De Laet, and B. Jonsson, 'Long-Term Risk of Osteoporotic Fracture in Malmo', *Osteoporos Int*, 11 (2000), 669-74.
- 70 K. L. Kavanagh, K. Guo, J. E. Dunford, X. Wu, S. Knapp, F. H. Ebetino, M. J. Rogers, R. G. Russell, and U. Oppermann, 'The Molecular Mechanism of Nitrogen-Containing Bisphosphonates as Antiosteoporosis Drugs', *Proc Natl Acad Sci U S A*, 103 (2006), 7829-34.
- 71 K. M. Kozloff, L. I. Volakis, J. C. Marini, and M. S. Caird, 'Near-Infrared Fluorescent Probe Traces Bisphosphonate Delivery and Retention in Vivo', *J Bone Miner Res*, 25 (2010), 1748-58.
- 72 K. M. Kozloff, R. Weissleder, and U. Mahmood, 'Noninvasive Optical Detection of Bone Mineral', *J Bone Miner Res*, 22 (2007), 1208-16.
- 73 W. Kozlow, and T. A. Guise, 'Breast Cancer Metastasis to Bone: Mechanisms of Osteolysis and Implications for Therapy', *J Mammary Gland Biol Neoplasia*, 10 (2005), 169-80.
- 74 E. Kristensen, B. Hallgrimsson, D. W. Morck, and S. K. Boyd, 'Timing of Growth Hormone Treatment Affects Trabecular Bone Microarchitecture and Mineralization in Growth Hormone Deficient Mice', *Bone*, 47 (2010), 295-300.
- 75 J. Kular, J. Tickner, S. M. Chim, and J. Xu, 'An Overview of the Regulation of Bone Remodelling at the Cellular Level', *Clin Biochem*, 45 (2012), 863-73.
- 76 F. M. Lambers, F. Stuker, C. Weigt, G. Kuhn, K. Koch, F. A. Schulte, J. Ripoll, M. Rudin, and R. Muller, 'Longitudinal in Vivo Imaging of Bone Formation and Resorption Using Fluorescence Molecular Tomography', *Bone*, 52 (2013), 587-95.
- 77 C. T. Leu, E. Luegmayr, L. P. Freedman, G. A. Rodan, and A. A. Reszka, 'Relative Binding Affinities of Bisphosphonates for Human Bone and Relationship to Antiresorptive Efficacy', *Bone*, 38 (2006), 628-36.
- 78 U. A. Liberman, S. R. Weiss, J. Broll, H. W. Minne, H. Quan, N. H. Bell, J. Rodriguez-Portales, R. W. Downs, Jr., J. Dequeker, and M. Favus, 'Effect of Oral Alendronate on Bone Mineral Density and the Incidence of Fractures in Postmenopausal Osteoporosis. The Alendronate Phase Iii Osteoporosis Treatment Study Group', *N Engl J Med*, 333 (1995), 1437-43.
- 79 A. Lipton, J. A. Chapman, L. Demers, L. E. Shepherd, L. Han, C. F. Wilson, K. I. Pritchard, K. E. Litzel, S. M. Ali, and M. Pollak, 'Elevated Bone Turnover Predicts for Bone Metastasis in Postmenopausal Breast Cancer: Results of Ncic Ctg Ma.14', *J Clin Oncol*, 29 (2011), 3605-10.



- 80 Q. Liu, Q. Wan, R. Yang, H. Zhou, and Z. Li, 'Effects of Intermittent Versus Continuous Parathyroid Hormone Administration on Condylar Chondrocyte Proliferation and Differentiation', *Biochem Biophys Res Commun*, 424 (2012), 182-8.
- 81 D. B. Longley, D. P. Harkin, and P. G. Johnston, '5-Fluorouracil: Mechanisms of Action and Clinical Strategies', *Nat Rev Cancer*, 3 (2003), 330-8.
- 82 C. Lukas, D. Ruffoni, F. M. Lambers, F. A. Schulte, G. Kuhn, P. Kollmannsberger, R. Weinkamer, and R. Muller, 'Mineralization Kinetics in Murine Trabecular Bone Quantified by Time-Lapsed in Vivo Micro-Computed Tomography', *Bone*, 56 (2013), 55-60.
- 83 E. J. Mackie, L. Tatarczuch, and M. Mirams, 'The Skeleton: A Multi-Functional Complex Organ: The Growth Plate Chondrocyte and Endochondral Ossification', *J Endocrinol*, 211 (2011), 109-21.
- 84 S. C. Manolagas, 'Birth and Death of Bone Cells: Basic Regulatory Mechanisms and Implications for the Pathogenesis and Treatment of Osteoporosis', *Endocr Rev*, 21 (2000), 115-37.
- 85 A. Martin, J. Aguirre, A. Sarasa-Renedo, D. Tsoukatou, A. Garofalakis, H. Meyer, C. Mamalaki, J. Ripoll, and A. M. Planas, 'Imaging Changes in Lymphoid Organs in Vivo after Brain Ischemia with Three-Dimensional Fluorescence Molecular Tomography in Transgenic Mice Expressing Green Fluorescent Protein in T Lymphocytes', *Mol Imaging*, 7 (2008), 157-67.
- 86 S. J. Marx, 'Hyperparathyroid and Hypoparathyroid Disorders', *N Engl J Med*, 343 (2000), 1863-75.
- 87 M. McClung, S. T. Harris, P. D. Miller, D. C. Bauer, K. S. Davison, L. Dian, D. A. Hanley, D. L. Kendler, C. K. Yuen, and E. M. Lewiecki, 'Bisphosphonate Therapy for Osteoporosis: Benefits, Risks, and Drug Holiday', *Am J Med*, 126 (2013), 13-20.
- 88 C. H. McCollough, A. N. Primak, N. Braun, J. Kofler, L. Yu, and J. Christner, 'Strategies for Reducing Radiation Dose in Ct', *Radiol Clin North Am*, 47 (2009), 27-40.
- 89 J. A. Meganck, K. M. Kozloff, M. M. Thornton, S. M. Broski, and S. A. Goldstein, 'Beam Hardening Artifacts in Micro-Computed Tomography Scanning Can Be Reduced by X-Ray Beam Filtration and the Resulting Images Can Be Used to Accurately Measure Bmd', *Bone*, 45 (2009), 1104-16.
- 90 L. J. Melton, 3rd, E. A. Chrischilles, C. Cooper, A. W. Lane, and B. L. Riggs, 'Perspective. How Many Women Have Osteoporosis?', *J Bone Miner Res*, 7 (1992), 1005-10.
- 91 H. Monkkonen, S. Auriola, P. Lehenkari, M. Kellinsalmi, I. E. Hassinen, J. Vepsalainen, and J. Monkkonen, 'A New Endogenous Atp Analog (Apppi) Inhibits the Mitochondrial Adenine Nucleotide Translocase (Ant) and Is Responsible for the Apoptosis Induced by Nitrogen-Containing Bisphosphonates', *Br J Pharmacol*, 147 (2006), 437-45.
- 92 A. E. Moore, G. M. Blake, and I. Fogelman, 'Quantitative Measurements of Bone Remodeling Using 99mTc-Methylene Diphosphonate Bone Scans and Blood Sampling', *J Nucl Med*, 49 (2008), 375-82.
- 93 H. Nakatake, H. Ekimoto, M. Aso, A. Ogawa, A. Yamaguchi, and H. Suemune, 'Dialkyl Bisphosphonate Platinum(II) Complex as a Potential Drug for Metastatic Bone Tumor', *Chem Pharm Bull (Tokyo)*, 59 (2011), 710-3.
- 94 V. Ntziachristos, C. H. Tung, C. Bremer, and R. Weissleder, 'Fluorescence Molecular Tomography Resolves Protease Activity in Vivo', *Nat Med*, 8 (2002), 757-60.
- 95 R. Pacifici, 'Estrogen, Cytokines, and Pathogenesis of Postmenopausal Osteoporosis', *J Bone Miner Res*, 11 (1996), 1043-51.
- 96 ———, 'Role of T Cells in Ovariectomy Induced Bone Loss--Revisited', *J Bone Miner Res*, 27 (2012), 231-9.
- 97 S. J. Park-Holohan, G. M. Blake, and I. Fogelman, 'Quantitative Studies of Bone Using (18)F-Fluoride and (99m)Tc-Methylene Diphosphonate: Evaluation of Renal and Whole-Blood Kinetics', *Nucl Med Commun*, 22 (2001), 1037-44.
- 98 M. A. Perazella, and G. S. Markowitz, 'Bisphosphonate Nephrotoxicity', *Kidney Int*, 74 (2008), 1385-93.

- 99 P. Pogoda, M. Priemel, J. M. Rueger, and M. Amling, 'Bone Remodeling: New Aspects of a Key Process That Controls Skeletal Maintenance and Repair', *Osteoporos Int*, 16 Suppl 2 (2005), S18-24.
- 100 K. E. Poole, and J. Reeve, 'Parathyroid Hormone - a Bone Anabolic and Catabolic Agent', *Curr Opin Pharmacol*, 5 (2005), 612-7.
- 101 T. Puri, M. L. Frost, K. M. Curran, M. Siddique, A. E. Moore, G. J. Cook, P. K. Marsden, I. Fogelman, and G. M. Blake, 'Differences in Regional Bone Metabolism at the Spine and Hip: A Quantitative Study Using (18)F-Fluoride Positron Emission Tomography', *Osteoporos Int*, 24 (2013), 633-9.
- 102 S. C. Rawlinson, I. J. McKay, M. Ghuman, C. Wellmann, P. Ryan, S. Prajaneh, G. Zaman, F. J. Hughes, and V. J. Kingsmill, 'Adult Rat Bones Maintain Distinct Regionalized Expression of Markers Associated with Their Development', *PLoS One*, 4 (2009), e8358.
- 103 J. Reeve, P. J. Meunier, J. A. Parsons, M. Bernat, O. L. Bijvoet, P. Courpron, C. Edouard, L. Klenerman, R. M. Neer, J. C. Renier, D. Slovik, F. J. Vismans, and J. T. Potts, Jr., 'Anabolic Effect of Human Parathyroid Hormone Fragment on Trabecular Bone in Involutional Osteoporosis: A Multicentre Trial', *Br Med J*, 280 (1980), 1340-4.
- 104 M. M. Reinholz, S. P. Zinnen, A. C. Dueck, D. Dingli, G. G. Reinholz, L. A. Jonart, K. A. Kitzmann, A. K. Bruzek, V. Negron, A. K. Abdalla, B. K. Arendt, A. J. Croatt, L. Sanchez-Perez, D. P. Sebesta, H. Lonnberg, T. Yoneda, K. A. Nath, D. F. Jelinek, S. J. Russell, J. N. Ingle, T. C. Spelsberg, H. B. Dixon, A. Karpeisky, and W. L. Lingle, 'A Promising Approach for Treatment of Tumor-Induced Bone Diseases: Utilizing Bisphosphonate Derivatives of Nucleoside Antimetabolites', *Bone*, 47 (2010), 12-22.
- 105 J. Y. Rho, L. Kuhn-Spearing, and P. Zioupos, 'Mechanical Properties and the Hierarchical Structure of Bone', *Med Eng Phys*, 20 (1998), 92-102.
- 106 L. Rifas, S. Arackal, and M. N. Weitzmann, 'Inflammatory T Cells Rapidly Induce Differentiation of Human Bone Marrow Stromal Cells into Mature Osteoblasts', *J Cell Biochem*, 88 (2003), 650-9.
- 107 B. L. Riggs, 'The Mechanisms of Estrogen Regulation of Bone Resorption', *J Clin Invest*, 106 (2000), 1203-4.
- 108 M. D. Roberts, T. J. Santner, and R. T. Hart, 'Local Bone Formation Due to Combined Mechanical Loading and Intermittent Hpth-(1-34) Treatment and Its Correlation to Mechanical Signal Distributions', *J Biomech*, 42 (2009), 2431-8.
- 109 B. Roche, A. Vanden-Bossche, M. Normand, L. Malaval, L. Vico, and M. H. Lafage-Proust, 'Validated Laser Doppler Protocol for Measurement of Mouse Bone Blood Perfusion - Response to Age or Ovariectomy Differs with Genetic Background', *Bone*, 55 (2013), 418-26.
- 110 G. A. Rodan, and T. J. Martin, 'Therapeutic Approaches to Bone Diseases', *Science*, 289 (2000), 1508-14.
- 111 A. J. Roelofs, F. P. Coxon, F. H. Ebetino, M. W. Lundy, Z. J. Henneman, G. H. Nancollas, S. Sun, K. M. Blazewska, J. L. Bala, B. A. Kashemirov, A. B. Khalid, C. E. McKenna, and M. J. Rogers, 'Fluorescent Risedronate Analogues Reveal Bisphosphonate Uptake by Bone Marrow Monocytes and Localization around Osteocytes in Vivo', *J Bone Miner Res*, 25 (2010), 606-16.
- 112 A. J. Roelofs, M. Jauhainen, H. Monkkonen, M. J. Rogers, J. Monkkonen, and K. Thompson, 'Peripheral Blood Monocytes Are Responsible for Gammadelta T Cell Activation Induced by Zoledronic Acid through Accumulation of Ipp/Dmapp', *Br J Haematol*, 144 (2009), 245-50.
- 113 A. J. Roelofs, C. A. Stewart, S. Sun, K. M. Blazewska, B. A. Kashemirov, C. E. McKenna, R. G. Russell, M. J. Rogers, M. W. Lundy, F. H. Ebetino, and F. P. Coxon, 'Influence of Bone Affinity on the Skeletal Distribution of Fluorescently Labeled Bisphosphonates in Vivo', *J Bone Miner Res*, 27 (2012), 835-47.
- 114 M. J. Rogers, R. J. Brown, V. Hodkin, G. M. Blackburn, R. G. Russell, and D. J. Watts, 'Bisphosphonates Are Incorporated into Adenine Nucleotides by Human Aminoacyl-Trna Synthetase Enzymes', *Biochem Biophys Res Commun*, 224 (1996), 863-9.
- 115 G. D. Roodman, 'Biology of Osteoclast Activation in Cancer', *J Clin Oncol*, 19 (2001), 3562-71.

- 116 ———, 'Genes Associate with Abnormal Bone Cell Activity in Bone Metastasis', *Cancer Metastasis Rev*, 31 (2012), 569-78.
- 117 G. D. Roodman, and J. J. Windle, 'Paget Disease of Bone', *J Clin Invest*, 115 (2005), 200-8.
- 118 C. J. Rosen, and J. P. Bilezikian, 'Clinical Review 123: Anabolic Therapy for Osteoporosis', *J Clin Endocrinol Metab*, 86 (2001), 957-64.
- 119 R. G. Russell, 'Bisphosphonates: From Bench to Bedside', *Ann N Y Acad Sci*, 1068 (2006), 367-401.
- 120 R. G. Russell, P. I. Croucher, and M. J. Rogers, 'Bisphosphonates: Pharmacology, Mechanisms of Action and Clinical Uses', *Osteoporos Int*, 9 Suppl 2 (1999), S66-80.
- 121 F. Saad, D. M. Gleason, R. Murray, S. Tchekmedyian, P. Venner, L. Lacombe, J. L. Chin, J. J. Vinholes, J. A. Goas, and B. Chen, 'A Randomized, Placebo-Controlled Trial of Zoledronic Acid in Patients with Hormone-Refractory Metastatic Prostate Carcinoma', *J Natl Cancer Inst*, 94 (2002), 1458-68.
- 122 J. Sceneay, M. J. Smyth, and A. Moller, 'The Pre-Metastatic Niche: Finding Common Ground', *Cancer Metastasis Rev*, 32 (2013), 449-64.
- 123 C. Schem, D. Bauerschlag, S. Bender, A. C. Lorenzen, D. Loermann, S. Hamann, F. Rosel, H. Kalthoff, C. C. Gluer, W. Jonat, and S. Tiwari, 'Preclinical Evaluation of Sunitinib as a Single Agent in the Prophylactic Setting in a Mouse Model of Bone Metastases', *BMC Cancer*, 13 (2013), 32.
- 124 H. Schott, D. Goltz, T. C. Schott, C. Jauch, and R. A. Schwendener, 'N(4)-[Alkyl-(Hydroxyphosphono)Phosphonate]-Cytidine-New Drugs Covalently Linking Antimetabolites (5-Fdu, Arau or Azt) with Bone-Targeting Bisphosphonates (Alendronate or Pamidronate)', *Bioorg Med Chem*, 19 (2011), 3520-6.
- 125 S. Schott, H. Niessner, T. Sinnberg, S. Venturelli, A. Berger, K. Ikenberg, J. Villanueva, F. Meier, C. Garbe, and C. Busch, 'Cytotoxicity of New Duplex Drugs Linking 3'-C-Ethynylcytidine and 5-Fluor-2'-Deoxyuridine against Human Melanoma Cells', *Int J Cancer*, 131 (2012), 2165-74.
- 126 S. Schott, M. Wallwiener, B. Kootz, H. Seeger, T. Fehm, and H. Neubauer, 'Cytotoxicity of the New Antimetabolite-Bisphosphonate (5-Fdu-Alendronate) in Comparison to Standard Therapeutics on Breast and Ovarian Cancer Cell Lines in the Atp Tumor Chemosensitivity Assay', *Invest New Drugs*, 30 (2012), 1750-5.
- 127 F. A. Schulte, F. M. Lambers, G. Kuhn, and R. Muller, 'In Vivo Micro-Computed Tomography Allows Direct Three-Dimensional Quantification of Both Bone Formation and Bone Resorption Parameters Using Time-Lapsed Imaging', *Bone*, 48 (2011), 433-42.
- 128 SciFighting, 'How Kickboxers Get Stronger Bones'2014] [Accessed September 4 2014].
- 129 E. Seeman, and P. D. Delmas, 'Bone Quality--the Material and Structural Basis of Bone Strength and Fragility', *N Engl J Med*, 354 (2006), 2250-61.
- 130 M. J. Seibel, 'Biochemical Markers of Bone Turnover: Part I: Biochemistry and Variability', *Clin Biochem Rev*, 26 (2005), 97-122.
- 131 K. Shimozuma, H. Sonoo, M. Fukunaga, K. Ichihara, T. Aoyama, and K. Tanaka, 'Biochemical Markers of Bone Turnover in Breast Cancer Patients with Bone Metastases: A Preliminary Report', *Jpn J Clin Oncol*, 29 (1999), 16-22.
- 132 M. Siddique, G. M. Blake, M. L. Frost, A. E. Moore, T. Puri, P. K. Marsden, and I. Fogelman, 'Estimation of Regional Bone Metabolism from Whole-Body 18f-Fluoride Pet Static Images', *Eur J Nucl Med Mol Imaging*, 39 (2012), 337-43.
- 133 N. A. Sims, and T. J. Martin, 'Coupling the Activities of Bone Formation and Resorption: A Multitude of Signals within the Basic Multicellular Unit', *Bonekey Rep*, 3 (2014), 481.
- 134 T. J. Snoeks, A. Khmelinskii, B. P. Lelieveldt, E. L. Kaijzel, and C. W. Lowik, 'Optical Advances in Skeletal Imaging Applied to Bone Metastases', *Bone*, 48 (2011), 106-14.
- 135 W. R. Stewart, R. H. Gelberman, J. M. Harrelson, and H. F. Seigler, 'Skeletal Metastases of Melanoma', *J Bone Joint Surg Am*, 60 (1978), 645-9.
- 136 G. Sturtz, G. Appéré, K. Bristol, O. Fodstad, G. Schwartzmann, and H. R. Hendriks, 'A Study of the Delivery-Targeting Concept Applied to Antineoplastic Drugs Active on Human Osteosarcoma. I. Synthesis and Biological Activity in Nude Mice Carrying Human

- Osteosarcoma Xenografts of Gem-Bisphosphonic Methotrexate Analogues', *European Journal of Medicinal Chemistry*, 27 (1992), 825-33.
- 137 T. Suda, N. Takahashi, N. Udagawa, E. Jimi, M. T. Gillespie, and T. J. Martin, 'Modulation of Osteoclast Differentiation and Function by the New Members of the Tumor Necrosis Factor Receptor and Ligand Families', *Endocr Rev*, 20 (1999), 345-57.
- 138 L. J. Suva, C. Washam, R. W. Nicholas, and R. J. Griffin, 'Bone Metastasis: Mechanisms and Therapeutic Opportunities', *Nat Rev Endocrinol*, 7 (2011), 208-18.
- 139 R. S. Taichman, 'Blood and Bone: Two Tissues Whose Fates Are Intertwined to Create the Hematopoietic Stem-Cell Niche', *Blood*, 105 (2005), 2631-9.
- 140 S. L. Teitelbaum, 'Bone Resorption by Osteoclasts', *Science*, 289 (2000), 1504-8.
- 141 R. L. Theriault, and R. L. Theriault, 'Biology of Bone Metastases', *Cancer Control*, 19 (2012), 92-101.
- 142 R. J. Tower, G. M. Campbell, M. Muller, O. Will, C. C. Gluer, and S. Tiwari, 'Binding Kinetics of a Fluorescently Labeled Bisphosphonate as a Tool for Dynamic Monitoring of Bone Mineral Deposition in Vivo', *J Bone Miner Res*, 29 (2014), 1993-2003.
- 143 M. Tzaphlidou, 'Bone Architecture: Collagen Structure and Calcium/Phosphorus Maps', *J Biol Phys*, 34 (2008), 39-49.
- 144 T. E. Uveges, K. M. Kozloff, J. M. Ty, F. Ledgard, C. L. Raggio, G. Gronowicz, S. A. Goldstein, and J. C. Marini, 'Alendronate Treatment of the Brl Osteogenesis Imperfecta Mouse Improves Femoral Geometry and Load Response before Fracture but Decreases Predicted Material Properties and Has Detrimental Effects on Osteoblasts and Bone Formation', *J Bone Miner Res*, 24 (2009), 849-59.
- 145 A. Valachis, N. P. Polyzos, R. E. Coleman, M. Gnant, H. Eidtmann, A. M. Brufsky, R. Aft, A. J. Tevaarwerk, K. Swenson, P. Lind, and D. Mauri, 'Adjuvant Therapy with Zoledronic Acid in Patients with Breast Cancer: A Systematic Review and Meta-Analysis', *Oncologist*, 18 (2013), 353-61.
- 146 S. Vallet, S. Mukherjee, N. Vaghela, T. Hideshima, M. Fulciniti, S. Pozzi, L. Santo, D. Cirstea, K. Patel, A. R. Sohani, A. Guimaraes, W. Xie, D. Chauhan, J. A. Schoonmaker, E. Attar, M. Churchill, E. Weller, N. Munshi, J. S. Seehra, R. Weissleder, K. C. Anderson, D. T. Scadden, and N. Raje, 'Activin a Promotes Multiple Myeloma-Induced Osteolysis and Is a Promising Target for Myeloma Bone Disease', *Proc Natl Acad Sci U S A*, 107 (2010), 5124-9.
- 147 Sonia Vallet, Siddhartha Mukherjee, Nileshwari Vaghela, Teru Hideshima, Mariateresa Fulciniti, Samantha Pozzi, Loredana Santo, Diana Cirstea, Kishan Patel, Aliyah R. Sohani, Alex Guimaraes, Wanling Xie, Dharminder Chauhan, Jesse A. Schoonmaker, Eyal Attar, Michael Churchill, Edie Weller, Nikhil Munshi, Jasbir S. Seehra, Ralph Weissleder, Kenneth C. Anderson, David T. Scadden, and Noopur Raje, 'Activin a Promotes Multiple Myeloma-Induced Osteolysis and Is a Promising Target for Myeloma Bone Disease', *Proceedings of the National Academy of Sciences*, 107 (2010), 5124-29.
- 148 C. H. Van Poznak, S. Temin, G. C. Yee, N. A. Janjan, W. E. Barlow, J. S. Biermann, L. D. Bosserman, C. Geoghegan, B. E. Hillner, R. L. Theriault, D. S. Zuckerman, and J. H. Von Roenn, 'American Society of Clinical Oncology Executive Summary of the Clinical Practice Guideline Update on the Role of Bone-Modifying Agents in Metastatic Breast Cancer', *J Clin Oncol*, 29 (2011), 1221-7.
- 149 K. N. Weilbaecher, T. A. Guise, and L. K. McCauley, 'Cancer to Bone: A Fatal Attraction', *Nat Rev Cancer*, 11 (2011), 411-25.
- 150 J. Weinreich, T. C. Schott, I. Konigsrainer, M. Kuper, A. Konigsrainer, and H. Schott, 'Cytostatic Activity of a 5-Fluoro-2'-Deoxyuridine-Alendronate Conjugate against Gastric Adenocarcinoma and Non-Malignant Intestinal and Fibroblast Cell Lines', *Anticancer Res*, 32 (2012), 4299-305.
- 151 A. Wetterwald, G. van der Pluijm, I. Que, B. Sijmons, J. Buijs, M. Karperien, C. W. Lowik, E. Gautschi, G. N. Thalmann, and M. G. Cecchini, 'Optical Imaging of Cancer Metastasis to Bone Marrow: A Mouse Model of Minimal Residual Disease', *Am J Pathol*, 160 (2002), 1143-53.

- 152 F. Wingen, H. Sterz, H. Blum, H. Möller, W. Pittermann, B. L. Pool, H. J. Sinn, H. Spring, and D. Schmähel, 'Synthesis, Antitumor Activity, Distribution and Toxicity of 4-[4-[Bis(2-Chloroethyl)Amino]Phenyl]-1-Hydroxybutane-1,1-Bisphosphonic Acid (Bad), a New Lost Derivative with Increased Accumulation in Rat Osteosarcoma', *J Cancer Res Clin Oncol*, 111 (1986), 209-19.
- 153 S. E. Wythe, V. Nicolaidou, and N. J. Horwood, 'Cells of the Immune System Orchestrate Changes in Bone Cell Function', *Calcif Tissue Int*, 94 (2014), 98-111.
- 154 T. Yamaza, Y. Miura, Y. M. Bi, Y. Z. Liu, K. Akiyama, W. Sonoyama, V. Patel, S. Gutkind, M. Young, S. Gronthos, A. Le, C. Y. Wang, W. J. Chen, and S. T. Shi, 'Pharmacologic Stem Cell Based Intervention as a New Approach to Osteoporosis Treatment in Rodents', *PLoS One*, 3 (2008).
- 155 H. Yi, H. J. Cho, S. M. Cho, K. Jo, J. A. Park, S. H. Lee, B. J. Chang, J. S. Kim, and H. C. Shin, 'Effect of 5-Fu and Mtx on the Expression of Drug-Resistance Related Cancer Stem Cell Markers in Non-Small Cell Lung Cancer Cells', *Korean J Physiol Pharmacol*, 16 (2012), 11-6.
- 156 T. Yoshimasu, Y. Kokawa, S. Oura, I. Hirai, R. Sasaki, H. Tanino, T. Sakurai, and Y. Okamura, 'Time Course of Carcinoembryonic Antigen after Resection of Lung Cancer: A Predictor of Recurrence', *Cancer Science*, 94 (2003), 741-44.
- 157 A. Zaheer, R. E. Lenkinski, A. Mahmood, A. G. Jones, L. C. Cantley, and J. V. Frangioni, 'In Vivo near-Infrared Fluorescence Imaging of Osteoblastic Activity', *Nat Biotechnol*, 19 (2001), 1148-54.
- 158 A. J. Zajac, and P. E. Phillips, 'Paget's Disease of Bone: Clinical Features and Treatment', *Clin Exp Rheumatol*, 3 (1985), 75-88.
- 159 R. M. Zebaze, A. Ghasem-Zadeh, A. Bohte, S. Iuliano-Burns, M. Mirams, R. I. Price, E. J. Mackie, and E. Seeman, 'Intracortical Remodelling and Porosity in the Distal Radius and Post-Mortem Femurs of Women: A Cross-Sectional Study', *Lancet*, 375 (2010), 1729-36.
- 160 Y. Zhang, J. P. Bressler, J. Neal, B. Lal, H. E. Bhang, J. Laterra, and M. G. Pomper, 'Abcg2/Bcrp Expression Modulates D-Luciferin Based Bioluminescence Imaging', *Cancer Res*, 67 (2007), 9389-97.
- 161 H. Zhou, A. Iida-Klein, S. S. Lu, M. Ducayen-Knowles, L. R. Levine, D. W. Dempster, and R. Lindsay, 'Anabolic Action of Parathyroid Hormone on Cortical and Cancellous Bone Differs between Axial and Appendicular Skeletal Sites in Mice', *Bone*, 32 (2003), 513-20.